NON-INTRUSIVE CHARACTERIZATION OF PROPERTIES OF HYDROGELS

by

UDAY CHIPPADA

A dissertation submitted to the

Graduate School-New Brunswick

Rutgers, The State University of New Jersey

in partial fulfillment of the requirements

for the degree of

Doctor of Philosophy

Graduate Program in Mechanical and Aerospace Engineering

written under the direction of

Professor Noshir A. Langrana

and approved by

_____

_____

_____

_____

_____

New Brunswick, New Jersey

January 2010

ABSTRACT OF THE DISSERTATION

Non-Intrusive Characterization of Properties of Soft Hydrogels

By UDAY CHIPPADA

Dissertation Director:

Dr. Noshir A. Langrana

Besides biological and chemical cues, cellular behavior has been found to be affected by mechanical cues such as traction forces, surface topology and in particular mechanical properties of the substrate. In previous studies involving hydrogel substrates, mechanical characterization was performed assuming Poisson's ratio to be equal to one-half. However, this might not be true in all cases and might alter the calculation of stiffness of hydrogels.

The present study mainly focuses on characterizing the Young's modulus (E), shear modulus (G) and Poisson's ratio (v) of soft hydrogels using a non-intrusive technique. For this purpose, an apparatus referred to as the "four magnet setup", which allows the determination of local gel elastic properties, was developed. Closed form equations involving E, G and v of the hydrogel were derived and finite element analysis was employed to validate the equations. Linear elastic properties of bis-gels and DNA gels were obtained using the apparatus and verified using rheometry and bead experiments. This is the first report in literature in which the mechanical properties consisting of E, G and v were simultaneously obtained for soft hydrogels.

A DNA gel design space involving parameters such as crosslinker concentration, side-chain concentration and lengths of DNA strands was systematically developed and the mechanical properties were evaluated using bead experiments. It was found that stiffness of DNA gels can be modulated over a wide range by modifying the various design parameters.

Addition of DNA crosslinks generates force and alters the mechanical properties, which has implications for cell and tissue culture substrate design. Two techniques have been developed to characterize the force actuating potential of DNA gels. It was found that the force generated was proportional to the elastic modulus of the gel. Also, at higher temperatures the stiffness of the gels decreased and the amount of force generated also decreased. A comparison of the force generated in both methods showed that either method can be successfully employed. The force was found to be in the range of values reported in the literature for axonal growth in spinal cord neurons.

Acknowledgements

The completion of a doctoral dissertation is a great achievement for me and could not have been possible without the help and support from many individuals. First and foremost, I wish to express my deepest gratitude and sincere thanks to my advisor, Dr. Noshir Langrana, for his unselfish commitment of time, conscientious advice, sincere effort, and constant support and encouragement throughout my Ph.D. program. Dr. Langrana's mentoring, supervision and guidance and the opportunities provided to me in the lab have greatly helped in making this work possible. His enthusiasm and passion have taught me how to truly appreciate science and engineering. I am also deeply grateful to Dr. Bernard Yurke for the guidance offered in performing many experiments and the insight provided in understanding the research topics. I am also grateful to him for his valuable comments on the manuscripts written over the course of the past 3 years and for his immense help in deriving the various equations presented in this work. Special thanks go to Dr. Rene Schloss for her invaluable comments and suggestions during the group meetings. I would also like to thank Professors Alberto Cuitino, George Weng and David Shreiber, the committee members, for taking the time to read the thesis and for their review and constructive critiques on the proposal and the dissertation. I would also like to extend thanks to Dr. Dajun Zhang, who was my advisor for the first two years of my Ph.D. program, for exposing me to the biological aspects of mechanical engineering which greatly enhanced my interest in the present study.

Dedication

Dedicated to my parents

For their deep love, support and encouragement

Table of Contents

List of Illustrations

List of Tables

CHAPTER 1   Introduction

1.1   Biomaterials Background

Biological systems are complex and the design and development of biomaterials for therapies poses a major challenge to professionals in the field of biomedical engineering. Biomaterials science has come a long way from its empirical beginnings, with a consistent growth and playing an integral part in modern medicine. A biomaterial is commonly defined as "a nonviable material used in a medical device, intended to interact with biological systems"[31]. Removing the words "used in a medical device" allows this definition to include a wider range of applications where we interface synthetic materials and modified natural materials with biology. The biomaterials field encompasses aspects of physics, medicine, biology, chemistry, engineering and material science[26]. Until the mid-1970s, biomaterials were purely used for providing structural and mechanical integrity in the body[7]. However, the establishment of biomaterials science has brought forth numerous applications including therapeutic devices, drug delivery systems, diagnostic examinations and tissue engineering scaffolds. Biomaterials science was boosted by the establishment of tissue engineering in the mid-1980s by Y.C. Fung[30]. Tissue engineering involved the replacement of organ function and living tissue with synthetic substitutes and needed the design of materials with different bioactive properties to be used for substrates. This became the major driving force in the development of new classes of biomaterials.

Biomaterials are primarily classified into three categories, namely metals, ceramics and polymers. Metallic biomaterials are typically used in orthopedic applications especially for bone and dental replacements. They have excellent mechanical strength and resistance to fracture which makes them the right choice for the load bearing medical applications. In addition, metals exhibit biocompatibility, or the ability to reside in the body without inducing significant immune responses or toxicity. Some examples of metallic biomaterials include stainless steel, titanium alloys, cobalt alloys and noble metals. Metallic biomaterials are usually limited in their use owing to non-degradability and stiffness mismatch with respect to tissues and bones.

Ceramic biomaterials on the other hand are non-metallic, inorganic materials primarily classified as bioinert, bioactive and bioresorbable[3,15,22]. Bioinert refers to any material that once placed in the human body has minimal interaction with its surrounding tissue, for e.g., alumina and zirconia. In contrast, bioactive refers to materials which upon placing in the human body will interact with the surrounding bone and in some cases, even soft tissues. Examples of bioactive ceramic materials are synthetic hydroxyapatite, glass ceramic and Bioglass®. Bioresorbable refers to any materials that upon placement within the human body start to dissolve and are slowly replaced by advancing tissue, such as bone. Examples of bioresorbable materials include tricalcium phosphate, gypsum and calcium carbonate.

The third kind of biomaterials known as polymers (derived from the Greek words *poly* meaning "many" and *meros* meaning "parts"). Polymers comprise the largest and most diverse class of biomaterials with varying mechanical and physical properties and varying levels of chemical reactivity and degradation[10,14,16,28]. Polymeric biomaterials

find application in a large number of disciplines such as orthopedics, dentistry, ophthalmology, neurosurgery, facial surgery, gastroenterology and cardiology. Based on their source of availability, polymers are widely classified as natural and synthetic. Natural polymers are polymerized through enzymatic processes by living organisms, while in synthetic polymers, polymerization is carried out by either condensation (step-reaction) or addition (chain-reaction) mechanisms[1,9]. There are many other ways in which polymers can be classified. For example, based on lifetime, polymers are classified as biodegradable and non-biodegradable. Similarly based on the type of structure, they can be classified as linear chain, crosslinked or three-dimensional. Alternatively, it is also possible to consider the relative molecular weight or the degree of polymerization. A classification of polymers based on their origin is presented in Figure 1-1.
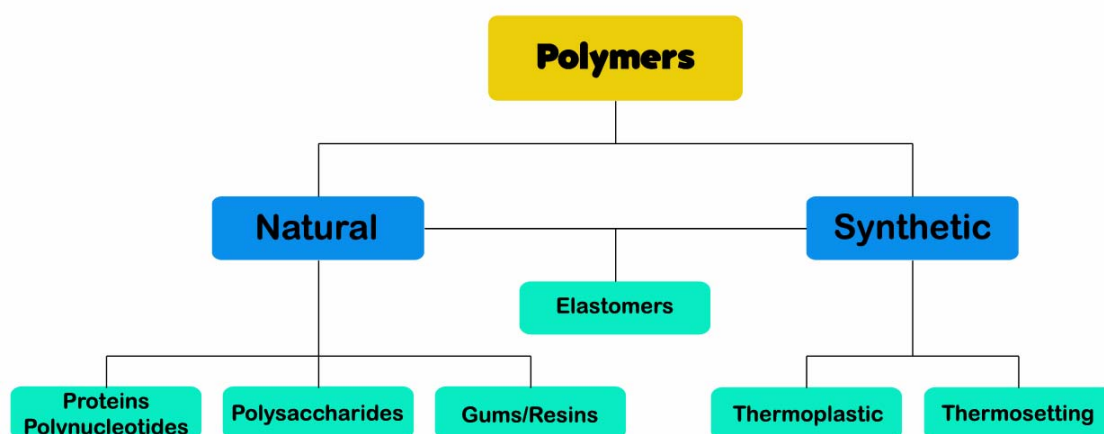
Figure 1-1. Classification of polymers based on their origin.

The original use of polymers was primarily in experimental surgical studies, centered on replacements for connective tissues. Nylon sutures were reported in the early 1940s, while use of poly (methylmethacrylite) PMMA, Dacron polyester and polyvinyl

chloride were reported in the mid-1940s[2,17]. Although these polymers still remain as the essential components in clinical medicine, a host of new applications emerged with the advances in the sciences of cell biology and developmental biology. The inception of tissue engineering brought regenerative medicine to the fore along with a myriad of other applications. Presently, polymers are being used to assist regeneration of three-dimensional tissue and organ structures, as controlled drug delivery systems, and for gene therapy. Polymeric biomaterials, such as hydrogels, serve as tissue engineering templates or scaffolds by mimicking the natural support structures used by the human body to guide the behavior and development of cells within tissues. Table 1-1 shows some general examples of biomaterials applications.

Table 1-1. Examples of biomaterials applications

Orthopedic prosthesis	Knee joint Hip joint Fracture fixation
General surgery	Sutures Staples Adhesives Blood substitutes
Plastics and reconstructive implants	Breast augmentation or reconstruction Maxillofacial reconstruction Penile implant
Controlled drug delivery	Coating for tablets Transdermal systems Microcapsules Implants
Extracorporeal	Oxygenators Dialyzers Plasmapheresis
Cardiovascular implants	Heart valves Vascular grafts Pacemakers Stents

1.2   Tissue Engineering

Every year, millions of people suffer from loss of an organ or tissue due to accidents or diseases. Over 8 million surgical procedures involving tissue or organ transplantation are performed every year in the US to treat these patients with an expense of many billions of dollars. However donor shortage has led to an exciting and revolutionary strategy, called tissue engineering, to treat these patients. Tissue engineering is an interdisciplinary field that applies the principles of engineering and life sciences towards the development of biological substitutes that aid in tissue or whole organ[21] function. Recent progress has been made in this area where investigators have attempted to engineer biological, cell-based tissues *in vitro* to restore, maintain and improve the tissue function. Many of these strategies have focused on manipulation of the cell environment and on understanding the interface between cells and the bio-scaffolds. Cells can integrate and respond to numerous external cues including chemical and biological information as well as the physical properties of their extracellular matrix (ECM)[11,13,29]. Among the critical extracellular cues, the effects of physical stimuli such as surface topology, traction force, mechanical strain and in particular, the mechanical properties have been identified to affect cellular behavior in a cell-type specific manner[8,12,25,27,33]. The mechanical properties (tensile, shear and bulk moduli) of polymeric biomaterials are significantly lower when compared to the metallic or ceramic biomaterials. Various factors, such as molecular weight, residual monomer, crosslinking, backbone stiffness and copolymerization involving alternating, random, block or graft molecules can affect the strength of polymers[32]. Polymers span a wide range of stiffness

ranging from soft elastomers to rigid materials. These versatile mechanical properties resulted in the widespread use and rapid growth of polymeric biomaterials.

1.3   Motivation for the Present Study

The present study is aimed at comprehensively characterizing the properties of soft, elastic, polymeric hydrogels in a non-destructive fashion. An apparatus was developed, that allows the determination of the local gel elasticity, by measuring the response of embedded micron-sized magnetic needles to externally applied magnetic fields. This microscope-based four magnet apparatus can apply both force and torque on the microneedles, and the corresponding displacements and rotations of the microneedles can be measured. Determination of these four parameters allowed us to calculate the linear elasticity parameters, namely the Young's modulus, shear modulus and Poisson's ratio. Classical linear elasticity theory was employed to derive the force-displacement and torque-rotation relations necessary to process the measurement data. Two specific hydrogels namely bis-crosslinked polyacrylamide gels and DNA-crosslinked polyacrylamide gels were utilized, and their local and global properties were characterized.

The technique for measuring gel stiffness presented here was developed to meet the needs of our ongoing studies on the suitability of various hydrogels for tissue culture applications. Prior work in our group involved using DNA in hydrogels to create new classes of active materials whose bulk mechanical properties could be controlled dynamically through the application of crosslinker strands[23,24]. Two methods to alter the stiffness of the gel were utilized. In the first application, the stiffness of the gels was

increased by increasing the amount of crosslinker. In the second application, using principles similar to those employed in DNA-based motors[34], the stiffness of the gels was decreased. This provides an example that, by using end-modified DNA oligonucleotides incorporated in polyacrylamide gels, one has access to a greater range of options in the construction of active and biomimetic polyacrylamide gels.

Our ongoing research primarily focuses on understanding tissue-scaffold and cell-biomaterial interfacial events and on facilitating the design of implantable bio-scaffolds for various tissue engineering applications including spinal cord injury repair, liver tissue engineering and stem cell engineering. Among others, the effects of gel/substrate stiffness on the growth and proliferation of cells was extensively investigated. L929 and GFP fibroblasts and neurons were able to sense the mechanical stiffness changes on bis-crosslinked and on static and dynamic DNA-crosslinked polyacrylamide hydrogels. For example, fibroblasts responded by altering morphology, focal adhesion and cytoskeletal structures while neurons responded largely by adjusting neurite outgrowth and adhesion properties[18-20]. Similarly, the aspect ratio of differentiated and undifferentiated stem cells after 2 days in culture, and differentiated stem cell proliferation were found to be significantly higher on rigid 20% polyacrylamide gels than on more compliant 5% substrates. It was also found that on soft gels, although differentiated cells proliferate less, they are able to sustain hepatic function much better over time. This study has been extended to alginate microcapsules, and from the mechanical and physical characterization of the alginate crosslinking network, it was determined that 2.2% alginate micro-encapsulation can be optimally adapted to both hepatocytes and neuronal differentiation from embryonic stem cells. Presently, effects of stiffness and charge of

chitosan-alginate based polyelectrolyte complexes on the differentiation of mouse embryonic stem cells into bone cells, are also being investigated.

Use of traditional methods like compression or indentation for measuring mechanical properties will be very restrictive on the microliter-sized hydrogel samples that are presently being used as substrates for tissue engineering in our laboratory. Such methods are also of limited usefulness when stiffness varies with position and time within the gel. This latter shortcoming is of particular concern in our studies where the stiffness of the gel is modulated as a function of time through the application of DNA strands. These shortcomings can be overcome by the techniques of embedding micron-sized needles and beads in the hydrogels and deflecting them non-intrusively by an externally applied magnetic force as described in the present study. In addition to this, most of the studies involving hydrogels assume the value of Poisson's ratio to be equal to one-half, which may not be true in all cases. An error in the measurement of Poisson's ratio could affect the calculation of the stiffness of hydrogels by as much as 10-20%. Thus, a method to simultaneously determine the elastic modulus and the Poisson's ratio was essential to fully characterize the mechanical properties of soft hydrogels.

1.4   Dissertation Organization

Following this chapter, a background of hydrogels and their use in tissue culture is presented in Chapter 2. A brief introduction of the theory of elasticity is also presented. The microscope-based four magnet setup is discussed in detail in Chapter 3 and the equations for converting the applied magnetic fields into the corresponding force or

torque is presented. This work appeared in one of the articles published in the *ASME Journal of Biomechanical Engineering*[4].

In Chapter 4, analytical solutions for the translation and rotation of a cylindrical rod embedded in a soft elastic medium are presented. Equations for Young's modulus, shear modulus and Poisson's ratio involving the force-displacement and the torque-rotation data are derived. Finite element simulations for a cylindrical rod embedded in an elastic medium are also performed as a validation for the analytical equations. This work has been published in the *Journal of Applied Physics*[5].

Results of experimental determination of the local and global mechanical properties of bis-crosslinked polyacrylamide gels as a function of monomer and crosslinker content are presented in Chapter 5, while similar results for DNA crosslinked polyacrylamide gels are presented in Chapter 6. This work was submitted to the *Journal of Materials Research*[6] and has been accepted for publication.

In Chapter 7, the concept of force generation using DNA gels is discussed along with results of the experiments conducted in support of this theory. Chapter 8 concludes the dissertation with the summary, limitations and future applications of the work presented.

References

1.   Billmeyer FW. Textbook of polymer science; 1984.
2.   Blaine G. The use of plastics in surgery. Lancet. 1946;251(2):525-8.
3.   Boretos JW. Advances in bioceramics. Advances in Ceramic Materials. 1987;2(1):15.
4.   Chippada U, Yurke B, Georges PC, Langrana NA. A Nonintrusive Method of Measuring the Local Mechanical Properties of Soft Hydrogels Using Magnetic Microneedles. Journal of Biomechanical Engineering. 2009;131:021014.
5.   Chippada U, Yurke B, Langrana NA. Complete Mechanical Characterization of Soft Media Using Non-Spherical Rods. Journal of Applied Physics. 2009;106(6).
6.   Chippada U, Yurke B, Langrana NA. Simultaneous Determination of Young's Modulus, Shear Modulus and Poisson's Ratio of Soft Hydrogels. Journal of Materials Research. 2009;(under review).
7.   Dillow AK, Lowman AM. Biomimetic materials and design: biointerfacial strategies, tissue engineering, and targeted drug delivery: CRC; 2002.
8.   Discher DE, Janmey P, Wang Y. Tissue cells feel and respond to the stiffness of their substrate. Volume 310: American Association for the Advancement of Science, 2005:1139-43.
9.   Flory PJ. Principles of polymer chemistry: Cornell Univ Pr; 1953.
10.   Freed LE, Vunjak-Novakovic G, Biron RJ, et al. Biodegradable polymer scaffolds for tissue engineering. Nature Biotechnology. 1994;12(7):689-93.
11.   Geiger B. Cell biology: encounters in space. Science. 2001;294(5547):1661.
12.   Georges PC, Janmey PA. Cell type-specific response to growth on soft materials. Volume 98: Am Physiological Soc, 2005:1547-53.
13.   Griffith LG, Swartz MA. Capturing complex 3D tissue physiology in vitro. Nature Reviews Molecular Cell Biology. 2006;7(3):211-24.
14.   Gunatillake PA, Adhikari R. Biodegradable synthetic polymers for tissue engineering. Eur Cell Mater. 2003;5(1).
15.   Hench LL. Bioceramics: from concept to clinic. Journal of the American Ceramic Society. 1991;74(7):1487-510.
16.   Hutmacher DW. Scaffolds in tissue engineering bone and cartilage. Biomaterials. 2000;21(24):2529-43.
17.   Ingraham FD, Alexander Jr E, Matson DD. Synthetic plastic materials in surgery. N Engl J Med. 1947;236:362-8.
18.   Jiang FX, Yurke B, Firestein BL, Langrana NA. Neurite outgrowth on a DNA crosslinked hydrogel with tunable stiffnesses. Annals of Biomedical Engineering. 2008;36(9):1565-79.
19.   Jiang FX, Yurke B, Schloss R, Firestein BL, Langrana NA. The relationship between fibroblast growth and the dynamic stiffnesses of a DNA crosslinked hydrogel. Biomaterials. 2009;In Press(doi:10.1016/j.biomaterials.2009.10.050).

20. Jiang FX, Georges PC, Li B, et al. Cell growth in response to mechanical stiffness is affected by neuron-astroglia interactions. The Open Neuroscience Journal. 2007;1(1):7-14.

21. Langer R, Vacanti JP. Tissue engineering. Science. 1993;260(5110):920-6.

22. LeGeros RZ. Calcium phosphate materials in restorative dentistry: a review. Advances in dental research. 1988;2(1):164-80.

23. Lin DC, Yurke B, Langrana NA. Inducing reversible stiffness changes in DNA-crosslinked gels. Journal of Materials Research. 2005;20(6):1456-64.

24. Lin DC, Yurke B, Langrana NA. Mechanical properties of a reversible, DNA-crosslinked polyacrylamide hydrogel. Journal of Biomechanical Engineering. 2004;126:104.

25. Lo CM, Wang HB, Dembo M, Wang Y. Cell movement is guided by the rigidity of the substrate. Biophysical journal. 2000;79(1):144-52.

26. Park DH, Borlongan CV, Eve DJ, Sanberg PR. The emerging field of cell and tissue engineering. Medical science monitor: international medical journal of experimental and clinical research. 2008;14(11).

27. Pelham RJ, Wang Y. Cell locomotion and focal adhesions are regulated by substrate flexibility. Volume 94: National Acad Sciences, 1997:13661-5.

28. Peter SJ, Miller MJ, Yasko AW, Yaszemski MJ, Mikos AG. Polymer concepts in tissue engineering. Journal of biomedical materials research. 1998;43(4):422-7.

29. Stegemann JP, Hong H, Nerem RM. Mechanical, biochemical, and extracellular matrix effects on vascular smooth muscle cell phenotype. Volume 98: Am Physiological Soc, 2005:2321-7.

30. Viola J, Lal B, Grad O. The emergence of tissue engineering as a research field. National Science Foundation Arlington, VA, USA. 2003:9–14.

31. Williams DF. Definitions in biomaterials: Elsevier Amsterdam; 1987.

32. Wise DL. Encyclopedic handbook of biomaterials and bioengineering: Marcel Dekker; 1995.

33. Yeung T, Georges PC, Flanagan LA, et al. Effects of substrate stiffness on cell morphology, cytoskeletal structure, and adhesion. Cell motility and the cytoskeleton. 2005;60(1):24-34.

34. Yurke B, Lin DC, Langrana NA. Use of DNA Nanodevices in Modulating the Mechanical Properties of Polyacrylamide Gels. Lecture Notes in Computer Science. 2006;3892:417.

CHAPTER 2   Hydrogels and their Properties

2.1   Polymer Gels

A polymer gel is a solvent-containing network in which adequate amount of crosslinks exist to link all polymer chains to other chains at multiple points. Polymer gels are a novel state of matter, as they have both solid and liquid-like properties. After chemical or physical crosslinking, the individual polymer chains lose their identity and become part of a large three-dimensional interconnected network. The combination of the elastic and fluid properties makes them good candidates for applications in numerous fields ranging from pharmaceuticals, biotechnology, agriculture, food processing and electronics.

Polymer gels can be classified as natural and synthetic gels. Natural polymer gels, such as alginate and collagen, are naturally occurring and are used in tissue engineering applications owing to their biocompatibility. But, they have many disadvantages like batch to batch variations, potential transplant rejection or adverse host response[3]. Synthetic gels on the other hand, are relatively abundant, easy to characterize and reproducible. The majority of synthetic polymer gels are formed by the covalent cross-linking of linear or branched macromolecules using multi-functional cross-linking agents[18]. Such gels are networks with infinite molecular weight and consequently they swell rather than dissolve, when immersed in a solvent. Currently, considerable interest and activity exists in the application of synthetic polymers, particularly hydrogels, for medical and biomedical applications.

2.2   Hydrogels

Researchers, over the years, have defined hydrogels in many different ways. The most common of these is that, hydrogel is a water-swollen, crosslinked polymeric network produced by the simple reaction of one or more monomers or by hydrogen bonds and strong van der Waals interactions between chains[37]. Another definition is that, it is a polymeric material which exhibits the ability to swell and retain a significant fraction of water within its structure, but will not dissolve in water[40]. Simply put, hydrogels are polymer gels in which the solvent is water[26,48]. Hydrogels have received considerable attention in the past 30 years, due to their exceptional promise in biomaterial applications. They have a strong resemblance to living soft tissue due to their relatively high water content and soft, rubbery consistency. Hydrogels have existed in nature since the evolution of life. Bacterial biofilms, hydrated living tissues and extracellular matrix components are some examples. A variety of naturally occurring polymers such as collagen, alginate, agarose and gelatin were also explored in early human history. However, the modern history of hydrogels as a class of materials designed for medical use, dates back to the late 1950s. Poly(2-hydroxyethyl methacrylate) commonly known as P-HEMA was the first synthetic hydrogel to be synthesized in 1936 by DuPont scientists[35], but it was not until 1960, that Wichterle and Lim[54] established the importance of P-HEMA hydrogels as excellent candidates for contact lens applications. This innovation led to the contact lens industry and to the modern field of biomedical hydrogels. The commercial success of soft contact lenses generated enormous interest in hydrogels, and eventually led to the development of smart hydrogels, that can change their properties upon application of an external stimulus such as pH, temperature, ionic

strength, salt type, solvent, light or electric field[24,27,50]. The work of Lim and Sun[28] in 1980 demonstrated the successful use of calcium alginate microcapsules for cell encapsulation. This was followed by Yannas et al.[55], who incorporated natural polymers such as collagen into hydrogels for use in artificial burn dressings. Hydrogels began to be slowly exploited in various research fields such as biomaterials[39,60], agriculture[43], pharmaceutics[15,19,57], and biotechnology[7]. More recently, hydrogels have become especially attractive to the field of tissue engineering as matrices for repairing and regenerating a wide variety of tissues and organs.

2.3   Classification of Hydrogels

Hydrogels are mainly classified as natural or synthetic according to their origin. Table 2-1 lists some of the natural polymers and synthetic monomers from which hydrogels can be prepared. Hydrogels from natural polymers have been widely used for tissue engineering applications, but limitations such as wet physical properties and batch to batch variations, have motivated researchers to modify these polymers as well as to use synthetic polymers to prepare hydrogels, in the past couple of decades.

Hydrogels can also be classified as physical or chemical gels based on their crosslinking. Chemical gels are usually covalently-crosslinked networks produced by crosslinking of water-soluble polymers or by conversion of hydrophobic polymers to hydrophilic polymers to form a network. These gels are permanent or thermoset, meaning the bonds do not break at elevated temperatures and hence do not reform at lower temperatures. The crosslinker used in chemically crosslinked gels is often toxic. This means the crosslinker needs to be removed prior to use in biological systems, which

might alter the gel integrity. As a result, physically crosslinked gels are gaining much attention. Physical gels are held together by molecular entanglements or secondary forces including ionic interactions[11], hydrogen bonds[29,30,36], crystallization[49], hydrophobic interactions[16] and protein interactions[5]. These gels are thermoreversible and demonstrate a transition from solid to liquid, at a characteristic temperature. There are many other means of classifying hydrogels.

2.4 Synthesis of Hydrogels

Hydrogels are usually prepared by swelling crosslinked structures in an aqueous medium such as water or alcohols like methanol, ethanol or benzyl alcohol. The crosslinked structures contain either chemical or physical crosslinks. In chemically crosslinked gels, covalent bonds are present between different polymer chains, while physical interactions such as ionic interactions or hydrogen bonding exist between the polymer chains. Table 2-2 gives a list of a number of ways of classifying hydrogels.

Table 2-1. Natural and synthetic monomers that can be used for hydrogel preparation

Natural Polymers	Synthetic Monomers
	Hydroxyethylmethacrylate (HEMA)
Chitosan	N-(2-Hydroxy propyl)methacrylate (HPMA)
Alginate	N-Vinyl-2-pyrrolidone (NVP)
Fibrin	N-isopropylacrylamide (NIPAMM)
Collagen	Vinyl acetate (VAc)
Gelatin	Acryolic acid (AA)
Hyaluronic acid	Methacrylic acid (MAA)
Dextran	Polyethylene glycol acrylate/methacrylate (IPEGA/PEGMA)
	Polyethylene glycol diacrylate/dimethacrylate (PEGDA/PEGDMA)

Table 2-2. Classification of hydrogels

Classification	Contents
Source	Natural Synthetic
Component	Homopolymer Copolymer Multipolymer
Preparation method	Simultaneous polymerization Crosslink of polymer
Electric charge	Nonion Anion Cation Zwitter ion
Physical structure	Amorphous Semicrystalline Hydrogen bonded
Crosslink	Covalent bond Intermolecular force
Functions	Biodegradable Stimuli responsive Superabsorbant
Physical appearance	Matrix Film Microsphere

2.4.1   Chemical Crosslinking

Chemical crosslinking can be achieved by radical polymerization, chemical reaction of complementary groups, photopolymerization or by crosslinking using enzymes. Radical polymerization involves the crosslinking of low molecular weight monomers in the presence of crosslinking agents. For example, poly(2-hydroxyethyl methacrylate) or pHEMA is obtained by the polymerization of HEMA in the presence of a suitable crosslinker such as EGD[53]. Other examples include dextran dissolved in water with glycidylacrylate, which has been investigated for the delivery of drugs, proteins and

imaging agents[33]. Figure 2-1 shows chemical crosslinking by copolymerization of a monomer with a crosslinking agent to synthesize a hydrogel.
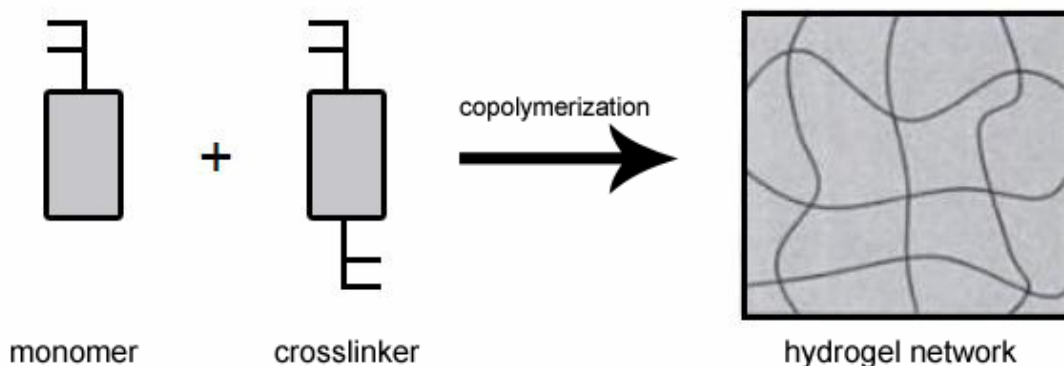
Figure 2-1. Copolymerization of monomer to form synthetic hydrogel

The solubility properties of water-soluble polymers are due to the presence of functional groups (mainly OH, COOH and NH_2). Covalent linkages between polymer chains can be established by the reaction of such functional groups, if they have complementary reactivity. The crosslinking can be achieved by crosslinking with aldehydes, for example, poly(vinyl alcohol) can be crosslinked using glutaraldehyde[6,38]. However this needs drastic conditions like low pH, high temperature or adding methanol as a quencher. Crosslinking of gelatin using polyaldehydes by partial oxidation was also reported previously[10] and the resulting hydrogels were used in wound treatment and te delivery of epidermal growth factor. Crosslinking can also be achieved by addition reactions such as reacting bis (or higher) functional crosslinking agents with functional groups of water-soluble polymers. The addition reactions are usually carried out in organic solvents because water can also react with the crosslinking agent. The

crosslinking agents used in these reactions are usually toxic and need to be extracted from the hydrogels, to remove any traces of unreacted crosslinker, before use in biological applications.

Another technique that is commonly used for chemically crosslinking gels is high energy irradiation or photopolymerization. Photopolymerization is the use of visible or ultraviolet (UV) light to interact with light-sensitive compounds called photo-initiators to create free radicals that can initiate polymerization to form crosslinked hydrogels[46]. Photopolymerization has several advantages like fast curing rates, spatial and temporal control over polymerization, and minimal heat production[8]. The most important advantage however is the ability to create hydrogels *in situ* from aqueous precursors in a minimally invasive manner. Examples of hydrogels prepared by photopolymerization include PEG acrylate derivatives[44], PEG methacrylate derivatives[20], polyvinyl alcohol (PVA) derivatives and modified polysaccharides such as hyaluronic acid[32] and dextran methacrylate[21]. Photopolymerized gels have been used as barriers following tissue injury to improve healing response, as scaffolds for cartilage regeneration, for cell encapsulation, and for localized drug delivery.

Covalent crosslinking of hydrogels is also achieved using high energy radiation like gamma irradiation[59] or electron irradiation[23,25,34]. Unlike photopolymerized hydrogels, irradiated hydrogels do not need a photoinitiator whose toxicity may be of issue in clinical applications. The high energy radiation directly creates free radicals which form intramolecular linkages as shown in Figure 2-2. Some examples of polymers that readily crosslink when irradiated include polyethylene, polypropylene, polystyrene,

polyacrylates, PEG, PVA and polyamides. Hydrogels prepared using this technique have been previously used as drug delivery systems[31] and for wound dressings[1,42,58].
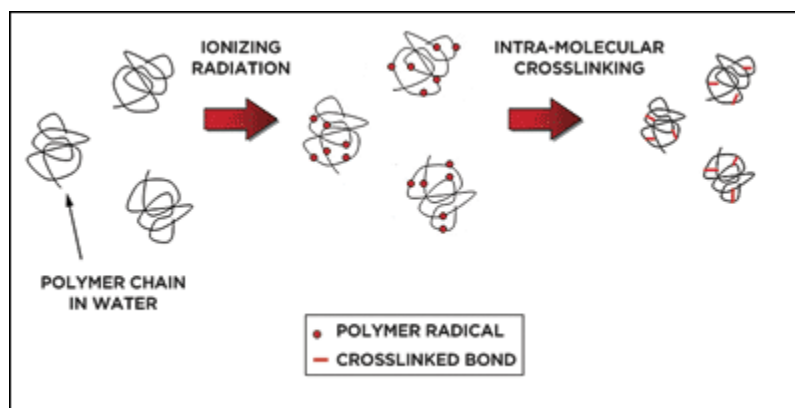
Figure 2-2. Intra-molecular crosslinking in hydrogels by irradiation

Another interesting technique, first pioneered by Sperinde et al.[47], is the use of enzymes to synthesize PEG-based hydrogels. In their work, a tetrahydroxy PEG was functionalized with glutaminyl groups (PEG-Q_a) and PEG networks were formed by adding transglutaminase to aqueous solutions of PEG-Q_a and poly(lysine-co-phenylalanine). The advantage of this method is that, the gel usually forms between 5 to 30 min under mild conditions, and since the gelation kinetics can be well controlled, these systems are very suitable as *in situ* gelling systems.

2.4.2 Physical Crosslinking

Chemical crosslinking uses crosslinking agents which are usually toxic and can affect the integrity of cells or proteins that need to be entrapped by the hydrogels. This has led to a great interest in physically crosslinked gels over the past few years. Physical

crosslinking can be achieved by ionic reactions, crystallization, protein interactions or through hydrogen bonds. Hydrogels involving ionic reactions are synthesized by forming ionic bridges between polymeric chains. Ionically crosslinked hydrogels can be classified into two groups based on the type of polymer, either anionic or cationic. Cationic polymers such as chitosan are positively charged and need to be reacted with negatively charged components (ions or molecules) for gelation to occur. The presence of the ionic bonds can be demonstrated by IR spectra, turbidimetric titration or vicosimetry. The advantage of ionic crosslinking is that it can be performed at both the room temperature as well as at the physiological temperature. Thus alginate gels which form by ionic reactions are used as matrix for encapsulation of living cells[14] and for the release of proteins[13]. Crystallization is another physical crosslinking mechanism through which a hydrogel can be synthesized. The hydrogel is usually formed due to the formation of crystallites which act as physical crosslinking sites in the network. Crystallization can occur in homopolymer systems such as PVA[56] and Dextran 6000[49] or by stereocomplex formation such as PLLA and PDLA[17].

Protein engineering is a very recent field in materials chemistry and has been used to synthesize new biomaterials for use in biological applications. The major advantage of employing proteins in hydrogels is that the physical and chemical properties of the gel can be precisely controlled by the proper design of the genetic code in synthetic DNA sequences and synthetic amino acids. Cappello et al.[4,5] prepared sequential block copolymers which are associated in the form of beta strands and sheets and undergo irreversible sol-to-gel transition with time under physiological conditions. Natural proteins can also be used to prepare hydrogels. Kopecek and coworkers[51,52] investigated

natural and engineered proteins which showed coiled-coil interactions and used them as crosslinkers for poly(N-(2-hydroxypropyl)methacrylamide) commonly known as PHPMA.

2.5   Properties of Hydrogels

For any material, the physical, chemical and mechanical properties play an important role in determining if it is suitable for a given application. However, for hydrogels, these properties are highly dependant on the environmental conditions as well. Thus, while determining the properties of a hydrogel, mimicking the *in situ* conditions becomes imperative. Hydrogels have a variety of properties including their absorption capacity, swelling behavior, permeability, surface properties, optical properties and mechanical properties which make them promising materials for a wide variety of applications. The characteristics of the polymer chains and the crosslinking structures in these aqueous solutions play an important role in the outcome of the properties of the hydrogel.

2.5.1   Swelling and Absorption Capacity

The polymer chains in a hydrogel interact with the solvent molecule (usually water) and tend to expand to the fully solvated state, while the crosslinked structure applies a retractive force to pull the chains inside. Equilibrium is achieved when these expanding and retracting forces counterbalance each other. Swelling ratio or water

content, given by Eq. 1 and Eq. 2, are generally used to describe the swelling behavior of hydrogels.

$$water\ content = \frac{weight\ of\ water}{weight\ of\ water + weight\ of\ gel} \times 100 \qquad \text{Eq. 1}$$

$$swelling\ ratio = \frac{weight\ of\ swollen\ gel}{weight\ of\ dry\ gel} \qquad \text{Eq. 2}$$

The swelling characteristics are crucial to the use of hydrogels in biomedical and pharmaceutical applications since the equilibrium swelling ratio influences the solute diffusion coefficient, surface wettability and mobility and the optical and mechanical properties of the hydrogel. The swelling properties are determined by many factors, including the type and composition of monomers, crosslinking density and other environmental factors such as temperature, pH and ionic strength.

2.5.2 Permeability of Hydrogels

Permeability is the ability of a hydrogel to transmit another substance such as fluids, cells or proteins. Developing hydrogel membranes and coatings of appropriate permeability characteristics is key to the success of a number of bioartificial organ transplantations. The permeability of a hydrogel to water and solutes can be adjusted over a wide range by varying the crosslinker concentration at synthesis or copolymerizing with more hydrophilic or hydrophobic monomers[12]. Some of the real life situations where permeability of hydrogels is critical are oxygen permeation for contact lens applications, nutrient and immunological biosubstance transport for immunoisolation and release of drugs and proteins for drug delivery systems.

2.5.3 Surface Properties of Hydrogels

Biocompatibility is the ability of a hydrogel to reside in the body without inducing significant immune response or toxicity. The important question in biocompatibility is how the hydrogel transduces its structural makeup to direct or influence the response of proteins, cells and organisms. This transduction occurs through the surface properties of the hydrogel, i.e. the body reads the surface structure and responds to it. The surface of a hydrogel can be rough, smooth or stepped; it can be composed of different chemistries or could be highly crystalline, disordered and inhomogeneous. Studies have been performed on the importance of roughness, wettability, surface mobility, chemical composition, crystallinity and heterogeneity, however significant research has not yet been performed on determining which parameters are of utmost importance in understanding biological responses to surfaces. Some of the techniques used for determining the surface property include electron spectroscopy[2,9,41], secondary ion mass spectrometry[45], scanning electron microscopy, Fourier transform infrared spectroscopy[22], scanning tunneling microscopy and atomic force microscopy. The information obtained using these methods can be used to monitor contamination, ensure surface reproducibility and explore the interaction of the hydrogels with living systems.

2.5.4 Mechanical Properties of Hydrogels

The mechanical properties of hydrogels depend on their composition and structure. Because of the high water content of fully swollen hydrogels, they normally have weak mechanical strengths. The mechanical properties of the hydrogel are affected by the comonomer composition, crosslinking density, polymerization conditions and degree of swelling. The mechanical strength of the hydrogel is often derived entirely from the crosslinks in the system, particularly in the swollen state where physical entanglements are almost nonexistent. The dependence of mechanical properties on crosslink density has been studied intensively by many researchers. However it should be noted that when the crosslinking density is altered, changes to properties other than strength also occur. For example, increasing the crosslinker concentration would make the polymer chains to come closer, thus reducing the diffusivity, release and swelling rates including the maximum degree of swelling. This would mean that these properties will need to be re-measured every time additional crosslinks are added.

The mechanical behavior of hydrogels is best understood by theories of elasticity and viscoelasticity. These theories are based on the time-independent and time-dependent recovery of the chain orientation and structure respectively. Elasticity theory assumes that when a stress is applied to the hydrogel the strain response is instantaneous. However for many biomaterials, including hydrogels and tissues, this is not a valid assumption. For example, if a weight is suspended from a specimen of ligament, the ligament continues to extend even though load is constant. Similarly, if the ligament is elongated to a fixed length, the load drops continuously with time. This is due to creep and stress relaxation respectively and these are the result of viscous flow in the material. Despite this liquid-

like behavior, hydrogels are functionally solids and are thus assumed to be perfectly elastic for the present study. In the next section a brief introduction to fundamentals of elastic theory is presented.

2.6   Theory of Elasticity

Elasticity is the physical property of a material by virtue of which it returns to its original shape after the force under which it deforms is removed. The applied force is usually referred to as stress, which is the force acting per unit cross-sectional area of the material, while the relative deformation is called as strain. The elastic regime is characterized by a linear relationship between stress and strain. The ratio of stress to strain is constant for a given material and is the defining mechanical property of the material. Based on whether the force applied is perpendicular or parallel to the area supporting it, the stresses and strains can be axial or shear. The proportionality constant obtained for the ratio of the axial stress to the axial strain is called as Young's modulus (represented by E) while the ratio of the shear stress to shear strain is referred to as shear modulus (represented by G). For a linearly, isotropic and homogenous material E and G are sufficient to completely characterize the mechanical properties of the material. However, most polymeric materials and tissue samples are anisotropic, meaning they have different properties in different directions. For example, bone, ligament and sutures are stiffer in the longitudinal direction as compared to the transverse direction. For such materials, on a macroscopic scale, more than two elastic constants are required to relate the stress and the strain properties. However, on a microscopic scale, polymers are comparatively isotropic and the elastic and shear modulus are adequate to fully

characterize their local mechanical properties. In the next chapter, construction of a microscope based four magnet device will be presented. This device can be non-intrusively utilized to fully characterize the local mechanical properties of hydrogels.

References

1.   Ajji Z, Othman I, Rosiak JM. Production of hydrogel wound dressings using gamma radiation. Nuclear Inst and Methods in Physics Research, B. 2005;229(3-4):375-80.

2.   Andrade JD. Surface and Interfacial Aspects of Biomedical Polymers. Vol. 1. Surface Chemistry and Physics. Plenum Press. 1985:470.

3.   Angelova N, Hunkeler D. Rationalizing the design of polymeric biomaterials. Environ Microbiol. 1999;64:4333-9.

4.   Cappello J, Crissman J, Dorman M, et al. Genetic engineering of structural protein polymers. Biotechnology Progress. 1990;6(3).

5.   Cappello J, Crissman JW, Crissman M, et al. In-situ self-assembling protein polymer gel systems for administration, delivery, and release of drugs. Journal of Controlled Release. 1998;53(1-3):105-17.

6.   Dai WS, Barbari TA. Hydrogel membranes with mesh size asymmetry based on the gradient crosslinking of poly (vinyl alcohol). Journal of Membrane Science. 1999;156(1):67-79.

7.   Daubresse C, Grandfils C, Jerome R, Teyssie P. Enzyme immobilization in nanoparticles produced by inverse microemulsion polymerization. Journal of Colloid and Interface Science. 1994;168(1):222-9.

8.   Decker C. UV-curing chemistry: past, present, and future. JCT, Journal of coatings technology. 1987;59(751):97-106.

9.   Dilks A. X-ray photoelectron spectroscopy for the investigation of polymeric materials. Electron Spectroscopy: Theory, Techniques, and Applications. 1981;4:277–359.

10.   Draye JP, Delaey B, Van de Voorde A, Van Den Bulcke A, Bogdanov B, Schacht E. In vitro release characteristics of bioactive molecules from dextran dialdehyde cross-linked gelatin hydrogel films. Biomaterials. 1998;19(1-3):99-107.

11.   Ganji F, Abdekhodaie MJ, Ramazani Sa A. Gelation time and degradation rate of chitosan-based injectable hydrogel. Journal of Sol-Gel Science and Technology. 2007;42(1):47-53.

12.   Gehrke SH, Lee PI. Hydrogels for drug delivery systems. Specialized Drug Delivery Systems. 1990:333-92.

13.   Gombotz WR, Wee SF. Protein release from alginate matrices. Advanced drug delivery reviews. 1998;31(3):267-85.

14.   Goosen MFA, O'Shea GM, Gharapetian HM, Chou S, Sun AM. Optimization of microencapsulation parameters: semipermeable microcapsules as a bioartificial pancreas. Biotechnology and bioengineering. 1985;27(2).

15.   Heller J. Polmers for controlled parenteral delivery of peptides and proteins. Advanced drug delivery reviews. 1993;10(2-3):163-204.

16.   Hennink WE, Van Nostrum CF. Novel crosslinking methods to design hydrogels. Advanced drug delivery reviews. 2002;54(1):13-36.

17.	Ikada Y, Jamshidi K, Tsuji H, Hyon SH. Stereocomplex formation between enantiomeric poly (lactides). Macromolecules. 1987;20(4):904-6.

18.	Kajiwara K, Ross-Murphy SB. Synthetic gels on the move. Nature. 1992;355(6357):208-9.

19.	Kamath KR, Park K. Biodegradable hydrogels in drug delivery. Advanced drug delivery reviews. 1993;11(1-2):59-84.

20.	Kim IS, Jeong YI, Kim SH. Self-assembled hydrogel nanoparticles composed of dextran and poly (ethylene glycol) macromer. International journal of pharmaceutics. 2000;205(1-2):109-16.

21.	Kim SH, Chu CC. Synthesis and characterization of dextran-methacrylate hydrogels and structural study by SEM. Journal of biomedical materials research. 2000;49(4).

22.	Koenig JL. Fourier transform infrared spectroscopy of polymers. Adv Polym Sci. 1983;54:87.

23.	Kofinas P, Athanassiou V, Merrill EW. Hydrogels prepared by electron irradiation of poly (ethylene oxide) in water solution: unexpected dependence of cross-link density and protein diffusion coefficients on initial PEO molecular weight. Biomaterials. 1996;17(15):1547-50.

24.	Kopecek J, Vacik J, Lim D. Permeability of membranes containing ionogenic groups. Journal of Polymer Science Part A-1: Polymer Chemistry. 1971;9(10).

25.	Krsko P, Sukhishvili S, Mansfield M, Clancy R, Libera M. Electron-beam surface-patterned poly (ethylene glycol) microhydrogels. Langmuir. 2003;19(14):5618-25.

26.	Kudela V. Hydrogels. Encyclopedia of polymer science and engineering. 1987;7.

27.	Kwon IC, Bae YH, Kim SW. Electrically credible polymer gel for controlled release of drugs. 1991.

28.	Lim F, Sun AM. Microencapsulated islets as bioartificial endocrine pancreas. Science. 1980;210(4472):908-10.

29.	Lin DC, Yurke B, Langrana NA. Inducing reversible stiffness changes in DNA-crosslinked gels. Journal of Materials Research. 2005;20(6):1456-64.

30.	Lin DC, Yurke B, Langrana NA. Mechanical properties of a reversible, DNA-crosslinked polyacrylamide hydrogel. Journal of biomechanical engineering. 2004;126:104.

31.	Lugao AB, Machado LDB, Miranda LF, Alvarez MR, Rosiak JM. Study of wound dressing structure and hydration/dehydration properties. Radiation physics and chemistry(1993). 1998;52(1-6):319-22.

32.	Matsuda T, Moghaddam MJ, Miwa H, Sakurai K, Ilda F. Photoinduced prevention of tissue adhesion. ASAIO Journal. 1992;38(3):M154.

33.	Mehvar R. Dextrans for targeted and sustained delivery of therapeutic and imaging agents. Journal of Controlled Release. 2000;69(1):1-25.

34.	Merrill EW, Dennison KA, Sung C. Partitioning and diffusion of solutes in hydrogels of poly (ethylene oxide). Biomaterials. 1993;14(15):1117-26.

35.	Nemours EIP. Methacrylate Resins. Industrial & Engineering Chemistry. 1936;28(10):1160-3.

36.   Oh KS, Han SK, Choi YW, Lee JH, Lee JY, Yuk SH. Hydrogen-bonded polymer gel and its application as a temperature-sensitive drug delivery system. Biomaterials. 2004;25(12):2393-8.

37.   Peppas NA. Hydrogels in medicine and pharmacy: CRC Press; 1986.

38.   Peppas NA, Benner Jr RE. Proposed method of intracordal injection and gelation of poly (vinyl alcohol) solution in vocal cords: polymer considerations. Biomaterials. 1980;1(3):158.

39.   Pulapura S, Kohn J. Trends in the development of bioresorbable polymers for medical applications. Journal of biomaterials applications. 1992;6(3):216.

40.   Ratner BD, Hoffman AS. Hydrogels for medical and related applications.1–33.

41.   Ratner BD, McElroy BJ. Electron spectroscopy for chemical analysis: applications in the biomedical sciences. Spectroscopy in the Biomedical Sciences. 1986:107–40.

42.   Razzak MT, Darwis D. Irradiation of polyvinyl alcohol and polyvinyl pyrrolidone blended hydrogel for wound dressing. Radiation Physics and Chemistry. 2001;62(1):107-13.

43.   Rehab A, Akelah A, Issa R, D'Antone S, Solaro R, Chiellini E. Controlled release of herbicides supported on polysaccharide based hydrogels. Journal of Bioactive and Compatible Polymers. 1991;6(1):52.

44.   Sawhney AS, Pathak CP, Hubbell JA. Bioerodible Hydrogels Based on Photopolymerized Poly (ethylene glycol)-co-poly (. alpha.-hydroxy acid) Diacrylate Macromers. Macromolecules. 1993;26(4):581-7.

45.   Schuetzle D, Riley TL, Devries JE, Prater TJ. Applications of high-performance mass spectrometry to the surface analysis of materials. Mass spectrometry reviews(Print). 1984;3(4):527-85.

46.   Scranton AB, Bowman CN, Peiffer RW. Photopolymerization: fundamentals and applications: American Chemical Society Washington DC; 1997.

47.   Sperinde JJ, Griffith LG. Synthesis and characterization of enzymatically-cross-linked poly (ethylene glycol) hydrogels. Macromolecules. 1997;30(18):5255-64.

48.   Sperling LH. Introduction to physical polymer science: Wiley-Interscience; 2006.

49.   Stenekes RJH, Talsma H, Hennink WE. Formation of dextran hydrogels by crystallization. Biomaterials. 2001;22(13):1891-8.

50.   Suzuki A, Tanaka T. Phase transition in polymer gels induced by visible light. 1990.

51.   Tang A, Wang C, Stewart RJ, Kope ek J. The coiled coils in the design of protein-based constructs: hybrid hydrogels and epitope displays. Journal of Controlled Release. 2001;72(1-3):57-70.

52.   Wang C, Kopec ek J, Stewart RJ. Hybrid hydrogels cross-linked by genetically engineered coiled-coil block proteins. Biomacromolecules. 2001;2(3):912-20.

53.   Wichterle O, Bartl P, Rosenberg M. Water-soluble methacrylates as embedding media for preparation of ultra-thin sections. 1960.

54.   Wichterle O, Lim D. Hydrophilic gels for biological use. 1960.

55.   Yannas IV, Lee E, Orgill DP, Skrabut EM, Murphy GF. Synthesis and characterization of a model extracellular matrix that induces partial regeneration of adult mammalian skin. Proceedings of the National Academy of Sciences. 1989;86(3):933-7.

56. Yokoyama F, Masada I, Shimamura K, Ikawa T, Monobe K. Morphology and structure of highly elastic poly (vinyl alcohol) hydrogel prepared by repeated freezing-and-melting. Colloid & Polymer Science. 1986;264(7):595-601.

57. Yoshida R, Sakai K, Okano T, Sakurai Y. Pulsatile drug delivery systems using hydrogels. Advanced drug delivery reviews. 1993;11(1-2):85-108.

58. Yoshii F, Zhanshan Y, Isobe K, Shinozaki K, Makuuchi K. Electron beam crosslinked PEO and PEO/PVA hydrogels for wound dressing. Radiation Physics and Chemistry. 1999;55(2):133-8.

59. Zhang L, Zhang W, Zhang Z, et al. Radiation effects on crystalline polymers. I: Gamma-radiation-induced crosslinking and structural characterization of polyethylene oxide. International journal of radiation applications and instrumentation Part C, Radiation physics and chemistry. 1992;40(6):501-5.

60. Zhang X, Goosen FA, Wyss SP, Pichora D. Biodegradable polymers for orthopedic applications. Polymer Reviews. 1993;33(1):81-102.

CHAPTER 3   The Four Magnet Manipulator

3.1   Significance of Mechanical Properties

Recent trends in tissue engineering research have brought afore a new and challenging focus from replacement to regeneration of the biological materials using biomaterials. The various properties of the biomaterial play a primary role in determining which application it can be used for. Tissue engineering approaches rely on two types of polymeric cell carriers. The first approach is the use of well established solid scaffolds such as poly(α-hydroxy esters)[29,51] that are designed as degradable sutures, bone regeneration or drug-releasing matrix materials. The second approach is the new and promising strategy relying on hydrophilic polymer networks, such as hydrogels. These tissue engineering applications generally require the use of a porous, bioresorbable scaffold which serves as a three-dimensional (3D) template for cell attachment and subsequent tissue formation. Due to their hydrated nature, hydrogels can better mimic the properties of the natural tissue and neural micro-environment that cells reside in. In addition, hydrogels contain pores and void spaces between the polymer chains, which provide many advantages including an increased supply of nutrients and oxygen for the cells. Pores within the network provide room for cells as well as for newly formed tissue after proliferation and expansion. Figure 3-1 shows the components and features of hydrogels used for tissue engineering applications[50].

Cell behavior is affected by external factors including cell-extracellular matrix (ECM) interactions and cell-cell crosstalk[8]. In addition to biological and chemical cues,

mechanical cues such as traction forces, surface topology and mechanical properties are an integral part of the cell-ECM interactions[12,33,41,43,44,53,54,58]. These cues need to be taken into consideration while using hydrogels as substrates for cell culture. Soft hydrogels have been used by many investigators as substrates for tissue engineering and mechanical manipulation of different cell types such as fibroblasts[33,53], macrophages[7], epithelial cells[43], embryonic stem cells[5,13,15,28] and neuronal cells[11,25] among many others. These mammalian cells are anchorage dependant and require a surface to which they can attach and grow. Hydrogels provide this growth template and assist in stabilizing cells. The mechanical stiffness of these substrates plays a crucial role in determining the biological function of the cells. It has been previously demonstrated that spinal cord neurons extend more primary dendrites and shorter axons on stiffer gels[24]. For the range of the stiffness of tens of Pascals to a few kiloPascals, neurite branching number was found to be significantly higher and astroglia are less adherent to the softer gels[17]. Apart from neurons, other cell types were also shown to be sensitive to the substrate compliance[9,26,42]. On the other hand, cells can alter the surrounding environment, for example by secreting ECM components so as to adhere, proliferate and locomote[34]. It was also found that cells induce the reorganization of ECM by exerting forces[23]. This force generation is a very important capability of cells in wound closure mediation[37] and tissue component alignment[20]. Previous researchers have also reported that cells react to reorganization of ECM resulting from tractions by other cells[22] and that cells incorporate feedback from ECM to adjust shape and function. Thus, when using hydrogels to mimic the functions of ECM, it is essential to characterize the mechanical properties of the hydrogels.
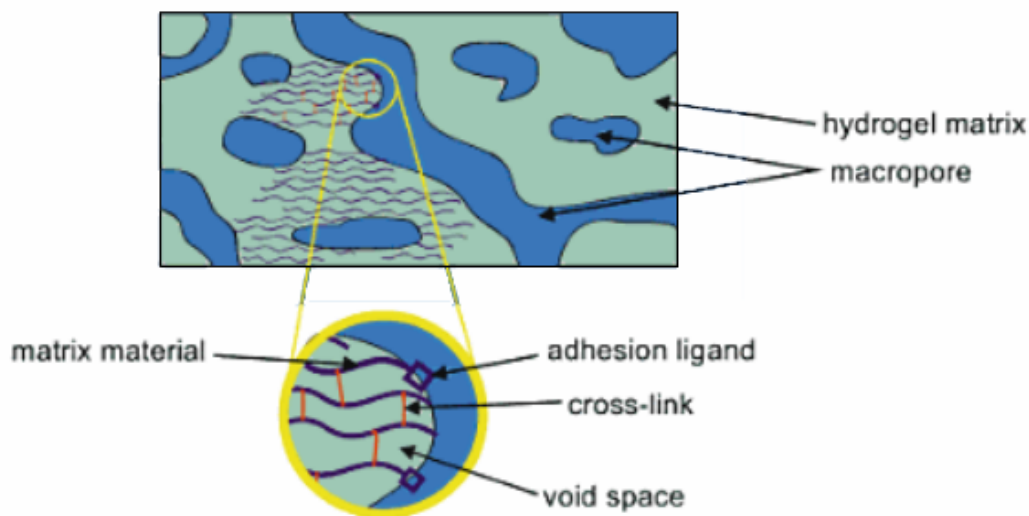
Figure 3-1. Components and features of hydrogels

3.2   Previous Work

Many experimental methods were previously employed to characterize the mechanical properties, mainly the Young's modulus of hydrogels. Common methods include simple tensile testing to determine the rubber elastic behavior or dynamic mechanical analysis in tension or shear to determine the viscoelastic properties. For most uniaxial tensile tests, the hydrogel samples are cut and prepared into dumb-bell shape, and placed between two clamps[4,54]. Tests are run at constant extension rates with varying loads until the sample reaches ultimate failure. The stress(σ)-strain(ε) behavior of the samples can be obtained from these tests and the slope of this data would provide the Young's modulus of the hydrogels. In addition (σ) versus ($\varepsilon - 1/\varepsilon^2$) can also be plotted, and using the rubber elasticity equations, the shear modulus (G) can be obtained from the

slope of the plot. Figure 3-2 compares the typical experimental stress-strain behavior of a crosslinked gel with the theoretical statistical thermodynamic predictions.
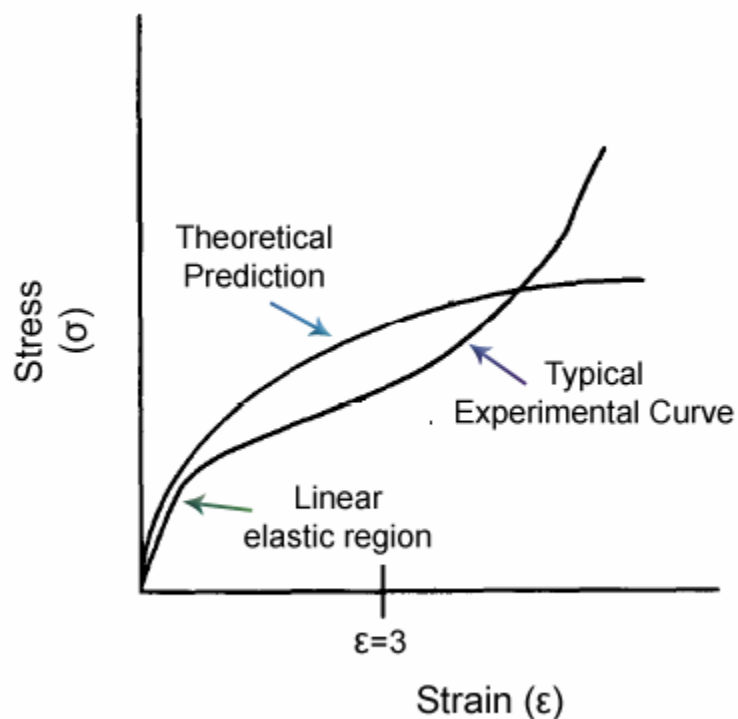
Figure 3-2. Experimental v/s theoretical stress-strain curve for hydrogels

Compression testing is similar to tensile testing, except that instead of pulling the sample, it is compressed. The hydrogels are usually prepared as round samples, and compression tests are performed to plot the stress-strain curves. Young's modulus of the hydrogels is the slope of these curves. Stammen and coworkers[49] utilized an electromechanical material testing machine to characterize the functional compressive and shear mechanical properties of novel PVA hydrogels. Confined and unconfined compression tests were also performed by other research groups to measure the

mechanical properties of poly(1-vinyl-2-pyrollidine)-gelatin IPN hydrogels[35], composite hydrogel matrices with bundles of polyethylene therephthalate (PET)[3] and DNA crosslinked polyacrylamide hydrogels[31]. In theory, the value of Young's modulus obtained from tensile and compression tests for a particular hydrogel must be the same, however it has been found that the values can differ[38]. This could be attributed to the difference in thickness of samples, which could lead to difference in diffusion of reactive species during polymerization.

In addition to tensile tests, Wong et al.[54] have utilized a micro-indentation technique based on the Hertz equation[48] (Eq. 3). This technique involves the placement of a stainless steel ball on the gel and the measurement of the deflection of the embedded fluorescent beads under the steel ball on the surface of the hydrogel.

$$E = \frac{3(1 - v^2)F}{4\delta^{3/2}r^{1/2}}$$
Eq. 3

where v is the Poisson's ratio (assumed to be 0.3), F is the buoyancy-corrected gravitational force, δ is the deflection and r is the radius of the bead. A major advantage of using the indentation technique is that mechanical properties of gradient gels[43], or gels with varying mechanical properties, can be obtained in a somewhat non-intrusive manner, although the sample is usually damaged during the test.

Another useful method is the manipulation of embedded spherical beads by an external force, such as a magnetic force. Lin et al.[32] have demonstrated the use of such a method for DNA crosslinked polyacrylamide hydrogels and have derived the equations[30] necessary for calculating the Young's modulus of hydrogels from the force applied and the displacement of the embedded beads. In brief, DNA gel prepared in a centrifuge tube was heated above its melting point and a 0.79 mm steel bead was positioned and

maintained in the center of the tube as the gel cooled and set. A calibrated electromagnet was used to apply force on the bead, as shown in Figure 3-3, and the deflection of the bead is measured as the force is increased. The deflections were taken to be elastic since the bead returned to its original position after the applied force was removed. The modulus of elasticity was then calculated using Eq. 4.

$$E = \frac{F}{2\pi\delta R}$$ Eq. 4

where F is the applied magnetic force, δ is the displacement and R is the radius of the bead.
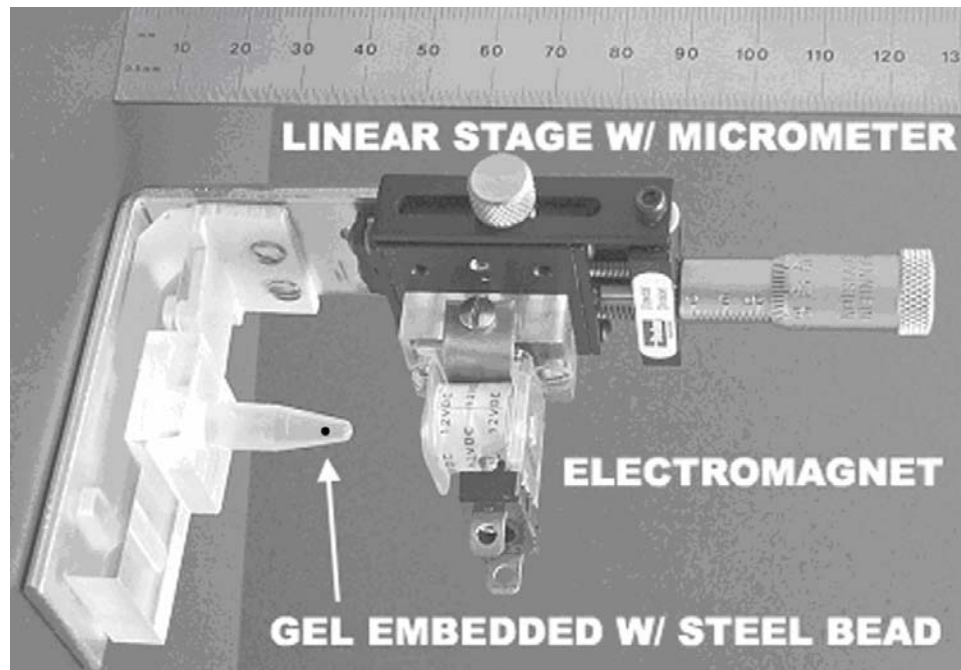
Figure 3-3. Test fixture for measuring Young's modulus using spherical beads

With the advancement of technology, more sophisticated methods such as atomic force microscopy (AFM)[21,36,45,46], optical tweezers[56,57], laser tracking microrheology[39,55],

magnetic bead microrheometry[6,40] and magnetic twisting cytometry[16,27,52] are being used to characterize the mechanical properties of hydrogels. However most of these techniques are either intrusive or destructive in nature. In addition, use of traditional methods like compression or indentation for measuring the mechanical properties of the gels will be of limited utility for microliter-sized samples that are mounted on a microscope with cells attached to the surface of the gels. Such methods are also of limited usefulness when stiffness varies with position and time within the gel. This latter shortcoming is of particular concern in our studies where the stiffness of the gel is modulated as a function of time through the application of DNA strands. Such application of DNA will result in time varying stiffness gradients. These shortcomings can be overcome by embedding micron-sized particles in the hydrogels that can be deflected non-intrusively using a magnetic manipulator, that will be discussed in the next section.

3.3   Design Requirements

Micron-sized particles embedded in stiff hydrogels need sufficient amount of force to visibly move them. In a previous study[32], a 15 µN force was needed to move magnetic beads of 400 µm radius embedded in 6 kPa modulus hydrogels by 1µm, which allowed the calculation of the global stiffness of the hydrogel. In the present study, we are interested in displacing micron-sized nickel needles (10x1x1 µm) in hydrogels, having stiffness of the same order of magnitude, and the primary concern is the range of forces needed to accomplish this task. Since the force acting on an object placed in the magnetic field is proportional to the volume and the magnetization of the object, the force needed to move 10x1x1 µm needles should be in the order of 0.1-100 nN.

Using the above information as a guide, a four-magnet manipulator was built which can apply nano-Newton forces on micron-size particles. In an initial study, using a single magnet (Figure 3-4), a field gradient of 200 Gauss/cm (0.02 T/m) was sufficient to move the microneedles embedded in 6 kPa hydrogels by 1 μm. Thus the four-magnet setup is designed to produce a maximum field gradient of 800 Gauss/cm and it can be further increased by increasing the number of windings in the electromagnets. Gosse et al.[19] have developed a magnetic tweezers setup with six electromagnets capable of creating field gradients, which generate forces ranging from 50 fN to 20 pN on super-para-magnetic beads. These beads were used as handles by displacing them in solution in different directions by changing the current running through the coils. Amblard and coworkers[2] built a similar manipulator for studying the local rheology and micromechanical properties of biological systems. Their system produced approximately 0.1 pN on 2.4 μm paramagnetic beads with a magnetic susceptibility of 10^{-2} SI. In its application, the magnetic manipulator presented in this study is very similar to these systems. The manipulator applies magnetic forces on the microneedles embedded in hydrogels which either displace or rotate, depending on whether a gradient or a uniform magnetic field is generated.
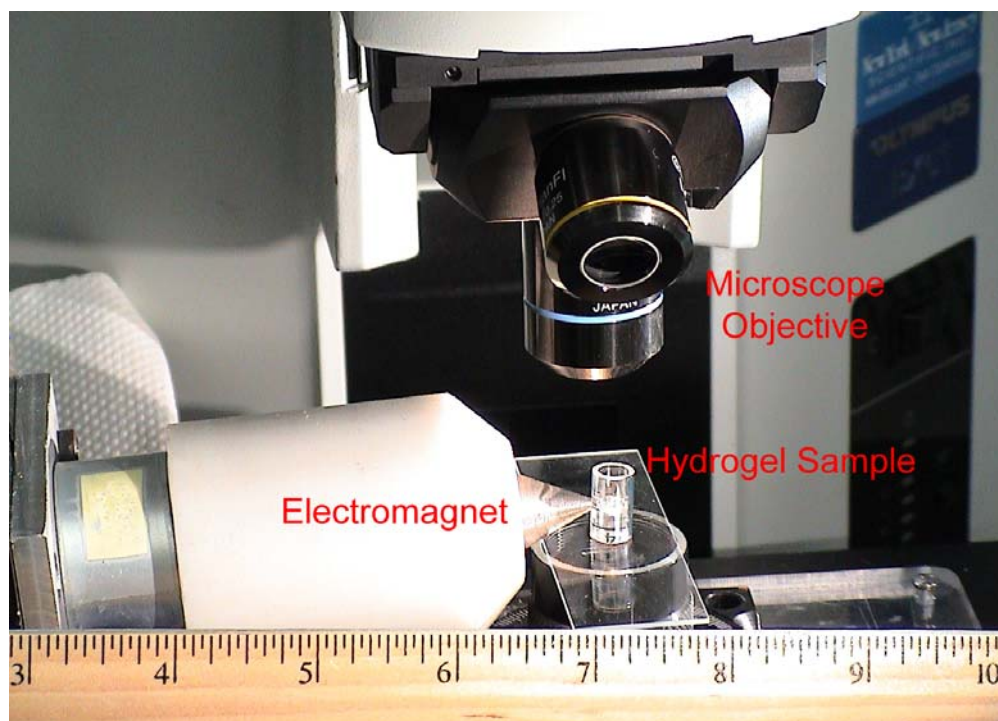
Figure 3-4. Single magnet setup mounted on microscope

3.4   Nickel Microneedles

100% pure nickel microneedles of different width and length combinations were fabricated at NJNC (New Jersey Nanotechnology Consortium LLC, a wholly owned subsidiary of Alcatel-Lucent). NJNC has designed 248 nm masks which were used to fabricate needles with a thickness of 1 micron and length of 10 microns. These were delivered on a 1cm x 1cm silicon chip and were released prior to use via a buffered hydrofluoric acid etch. There are approximately 3 million needles per chip which are collected in a vial containing distilled water. These needles tend to aggregate to form loose clusters. Figure 3-5 shows a scanning electron microscope image of such a cluster. Upon vigorous mixing, the clusters break into isolated needles which are then embedded in the hydrogels during gel preparation.
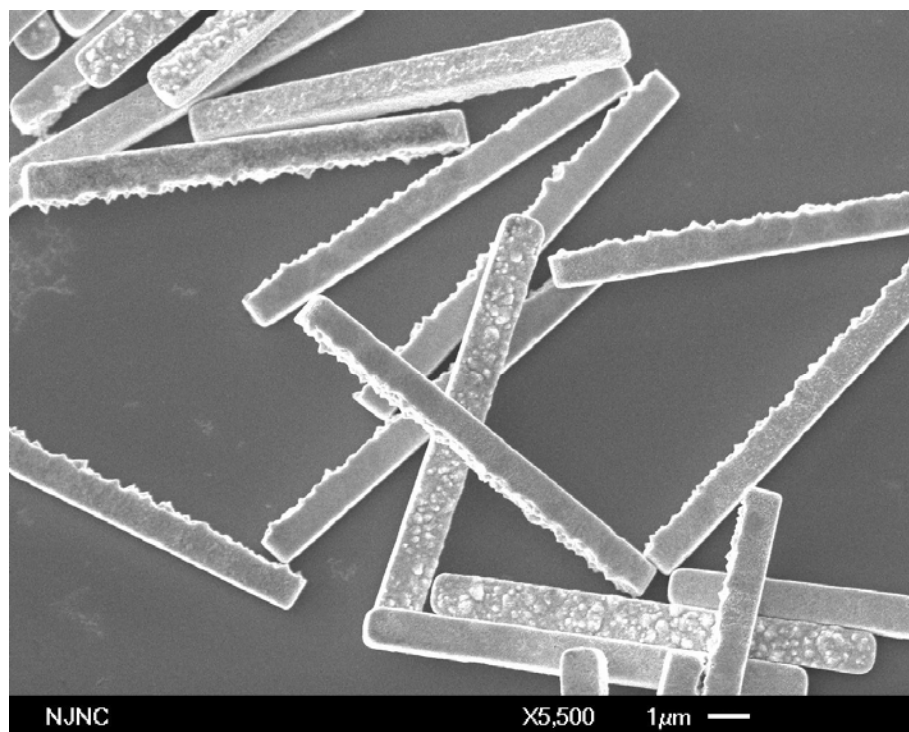
Figure 3-5. SEM images of nickel microneedles used in experiments

3.4.1 Biocompatibility of Nickel Microneedles

A potential drawback of this system when used in conjunction with cells could be the toxicity from the nickel particles placed in the hydrogels. Therefore we examined how the presence of nickel needles, embedded in a polyacrylamide gel substrate, affects the integrity of the actin cytoskeleton of neuronal cells cultured on the gels for five days. Acrylamide (7.5% w/v) and bis-acrylamide (0.3% w/v, Fisher Scientific) solutions were polymerized with ammonium persulfate and *N,N,N',N'*-tetramethyl-ethylene-diamine (TEMED) under a non-aqueous layer of toluene containing 0.5% acrylic acid *N*-hydroxy-succinimide (NHS) ester (Sigma-Aldrich, St Louis, MO) between two chemically modified coverslips as previously described[17]. The NHS incorporated at the surface of the gel was reacted with 0.2 mg/ml poly-D-lysine (Sigma-Aldrich, St Louis, MO) to produce

a uniform coating of adhesive ligand. Gels were then allowed to equilibrate overnight at 37°C in cell culture medium. Two cell types frequently used by our group, astrocytes and neurons, were cultured on these gels, fixed at five days in vitro (DIV), and stained with phalloidin for actin visualization. Neuronal and glial cells were derived from prenatal rat embryos and maintained in an incubator at 37°C and 5% CO_2. For cultures containing both neuronal and glial cells, cells were plated directly onto substrates. For astrocyte cultures, cells were maintained for 12 days in culture and shaken overnight to remove neurons. Cells were grown in an incubator at 37°C and 5% CO_2. Neurobasal medium (Gibco, Grand Island, NY) was supplemented with 2 mM l-glutamine, 50 μg/mL streptomycin, and 50 units/mL penicillin (and 10% fetal bovine serum for pure astrocyte cultures). At 5DIV, cultures were fixed with 4% paraformaldehyde at 37°C for 30 min. Samples were blocked and permeabilized in 5% bovine serum albumin and 0.2% Triton X-100 and stained with rhodamine-phalloidin (Molecular Probes, Eugene, OR).

Figure 3-6 shows images of cells grown on gels without needles (CONTROL) and with nickel needles (ASTRO/NEURON + Ni). Phase images of needles (white arrow) were pseudo-colored in white for ease of fluorescence visualization. A phase image (Figure 3-7) is also included to show how needles and cells appear without color manipulation. Nickel needles were generally out of focus from cells as they were embedded into the gels while cells grew only on the gel surface. Cells were found to grow both above and near where nickel needles are embedded in the gels. There was no difference in the actin cytoskeleton of neurons or astrocytes compared to the controls. Thus it can be concluded that the toxicity from the nickel needles does not affect the behavior of the cells when the needles are embedded in the hydrogels.
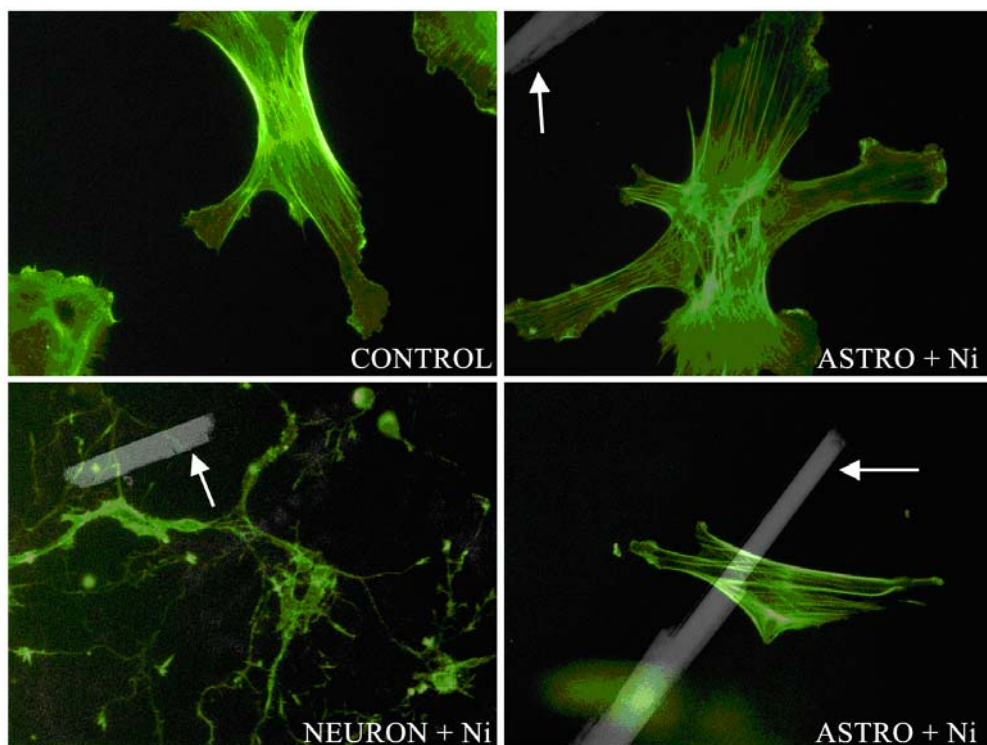
Figure 3-6. Nickel toxicity and biocompatibility study
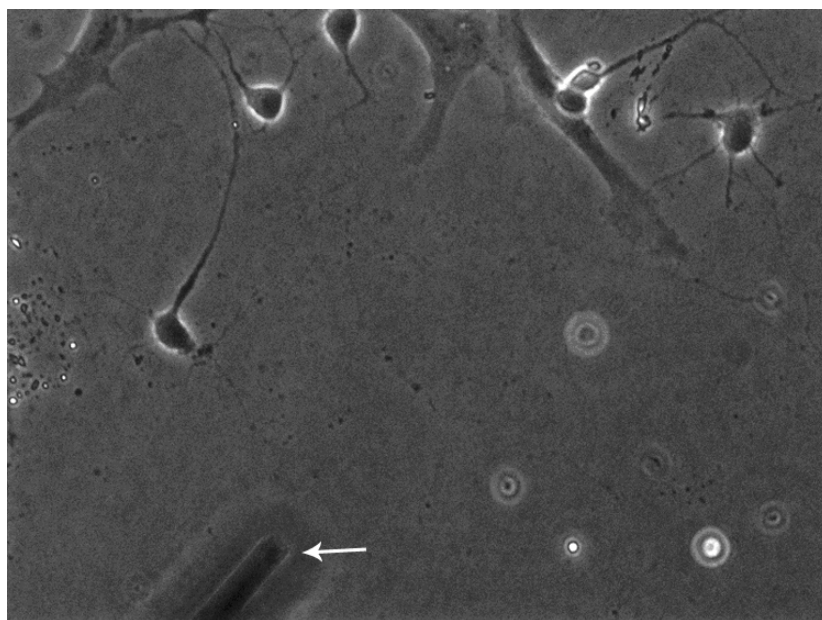
Figure 3-7. Phase image of the cells in conjunction with the needles

3.5   Construction of the Four Magnet Manipulator

Four electro-magnets, individually driven by a power supply, were placed at the four corners of a 12.5 x 12.5 cm square iron frame as shown in Figure 3-8. In order to bring the magnetic poles closer to the sample, soft magnetic pole pieces are placed at the center of each electromagnet. These pole pieces provide with a strong magnetic field and also keep the heat generating coils away from the sample. A cooling system consisting of pipes that carry water towards and away from the coils was also constructed to dissipate the heat quickly from the coils. A BK Precision 1791 high current linear power supply, capable of providing 10 amps regulated DC power with 640 Watt output (0-64V), in conjunction with PA01 power amplifiers (Amaci Electronics, Phoenix, AZ), was used to drive the electromagnets, and LM324 op-amps (Digikey Corp., MN) were used to regulate the power supplied. Figure 3-9 shows a schematic of the electric circuit for one of the electromagnets. The magnetic field generated is controlled by a feedback circuit developed in Labview which utilizes the Hall probes (UVA-PAH-5V500, Sensor Solutions Corp, Steamboat Springs, CO) attached to the face of each of the bottom pole pieces, to measure and adjust the current supplied to acquire the required field. The magnet manipulator is easily mounted on a microscope stage as shown in Figure 3-10. The soft magnetic pole pieces are adjusted to allow a 1 cm by 1 cm square region in which samples can be placed. A standard microscope slide is suspended between the four sets of pole pieces on which the hydrogel sample with needles embedded is positioned.

The magnitude of the magnetic field in the z-direction is expected to be small compared to the magnitude of the magnetic field in the x-y plane in the sample region. This is due to the symmetry of the pole pieces and due to the fact that the distance of the

magnetic support structure from the poles is large compared to the spacing between the poles. Similarly, the derivatives of the magnetic field with respect to z are expected to be small compared to the field derivatives with respect to x and y. These expectations were confirmed by measurement. In particular, with one pole set at 885.5 Gauss and the remaining poles set at 350 Gauss each, the field at the center in x, y and z directions was found to be 336, 336 and 14 Gauss respectively. Similarly the magnitude of the derivative of the magnetic field in the x-y plane along the direction of greatest change was found to be 60.68 Gauss/mm while gradient along the z-axis was found to be less than 5 Gauss/mm. Similar measurements were made over a range of magnetic fields applied at the poles and in all cases the z-direction fields at the center were found to be close to zero. Since, the torque generated by the z-component of the magnetic field is small compared to the torque generated by the magnetic field within the x-y plane, and since the magnitude of the force generated by the field derivatives in the z-direction is small compared to the magnitude of the force generated by field derivatives in the x-y plane, we have neglected these in the data analysis.
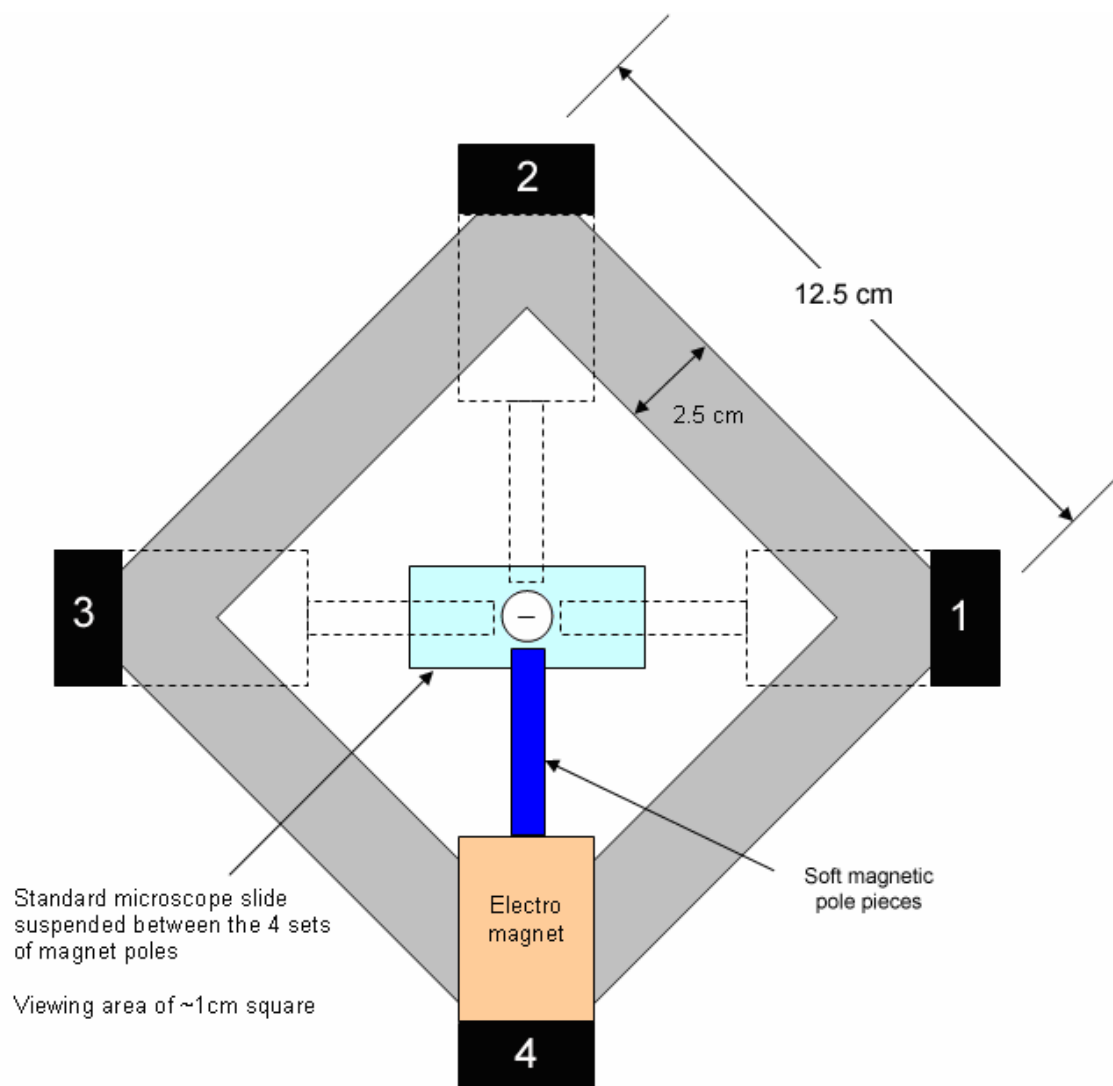
Figure 3-8. Schematic of the four magnet manipulator
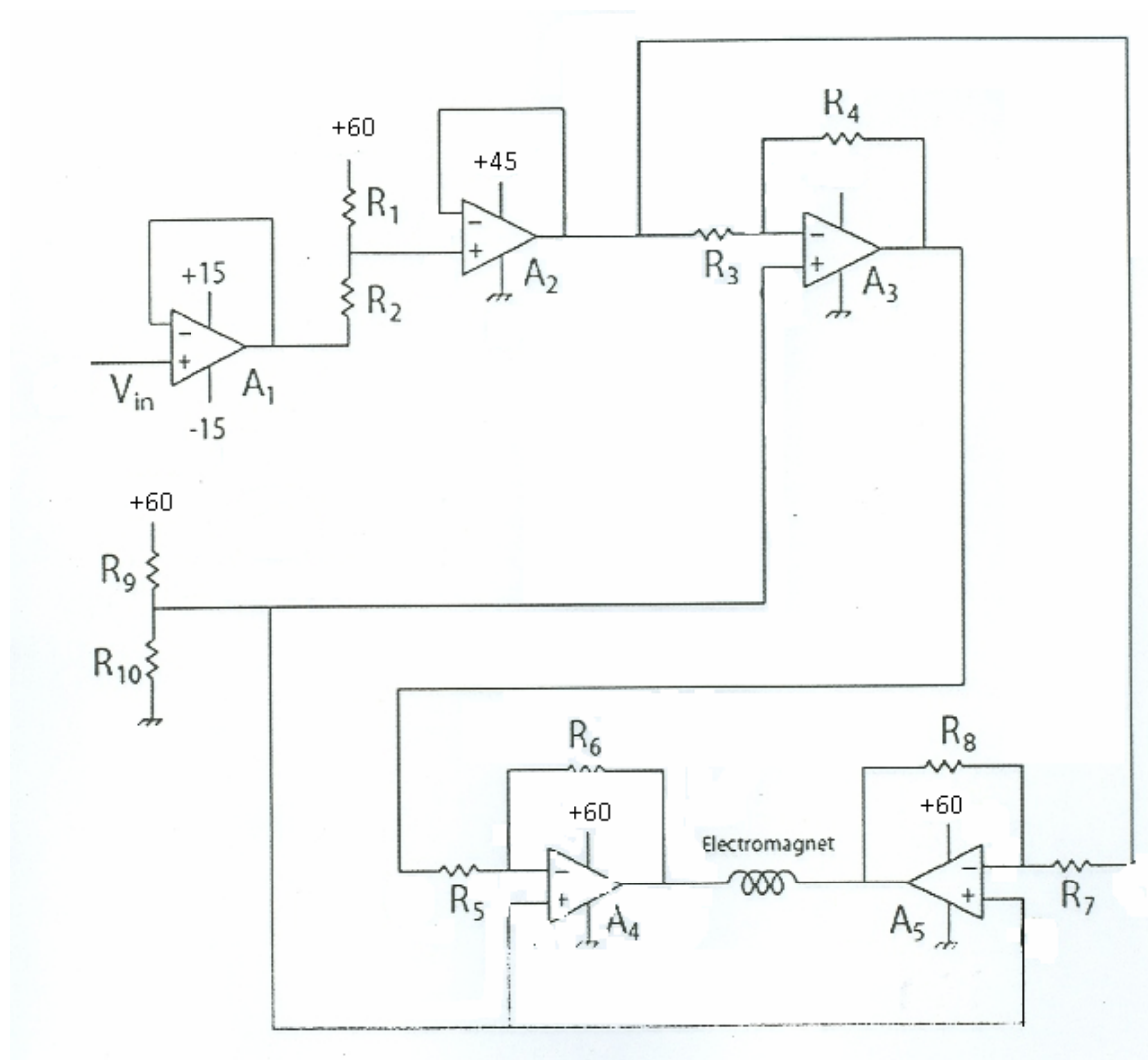
Figure 3-9 Circuit for driving the electromagnet

R1 = R2 = R3 = R4 = R5 = R7 = 10K ohms, R6 = R8 = 60K ohms and R9 = R10 = 1M ohms. A1, A2 and A3 are op-amps while A4 and A5 are the power-amps.
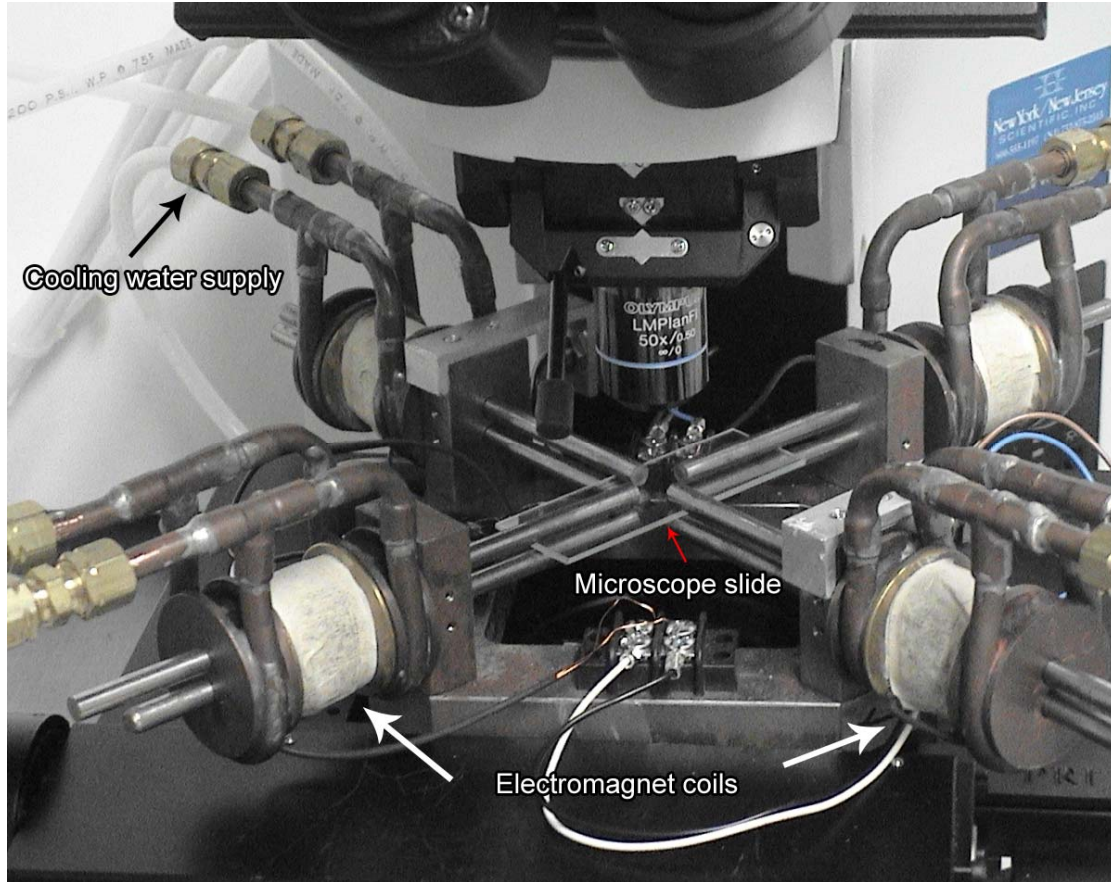
Figure 3-10. Experimental setup of the four magnet manipulator

3.5.1 Feedback Circuit

The feedback circuit is designed to control the magnetic fields at the pole faces, thus producing a magnetic field in the sample region whose value is not influenced by the nonlinear and hysteretic properties of iron, from which the poles and the base of the electromagnets is constructed. The hall sensors attached to each of the bottom poles of the magnets measure the magnetic field and send the voltage to the DAQ input card which in turn passes the signal to the Labview program. The program evaluates the

current needed to maintain the required magnetic field using a PID (proportional–integral–derivative) controller by comparing the actual output at the hall sensor with the desired output provided through the Labview interface. The amplifier circuit along with the power supply then provides the current to the electromagnet coil in the feedback loop. This process continues until the required magnetic field is obtained at the tips of the pole pieces. The response time of the system which is the time taken for the system to achieve (1/e)*dB of the desired value, where dB is the initial difference between the actual field and the desired field, was measured to be equal to 2.3±0.5 seconds. The short response time allows us to produce real time control of the field. Four such identical feedback circuits control the field produced at the individual poles in an independent manner. Figure 3-11 shows a schematic flowchart of the feedback circuit.

3.5.2   Field Mapping

The outer diameter of the wells used to hold the hydrogels is 8.4 mm and, in order to have accessibility of the sample, the pole to pole distance was set at 10 mm. A pre-programmed analog hall sensor (Sensor Solutions Corp, Steamboat Springs, CO) attached to a micro-positioning stage was used to probe the space between the four pole pieces in two perpendicular directions. Although the distance between the opposing poles is adjusted to be 10 mm, due to the thickness of the hall sensor, the space over which the field could be mapped was reduced to a 5 mm x 5 mm square area. The feedback circuit shown in Figure 3-11 was utilized to maintain the pole pieces at a constant field. Poles 3 and 1 were aligned along the x-axis and poles 2 and 4 were aligned along the y-axis (Figure 3-8).
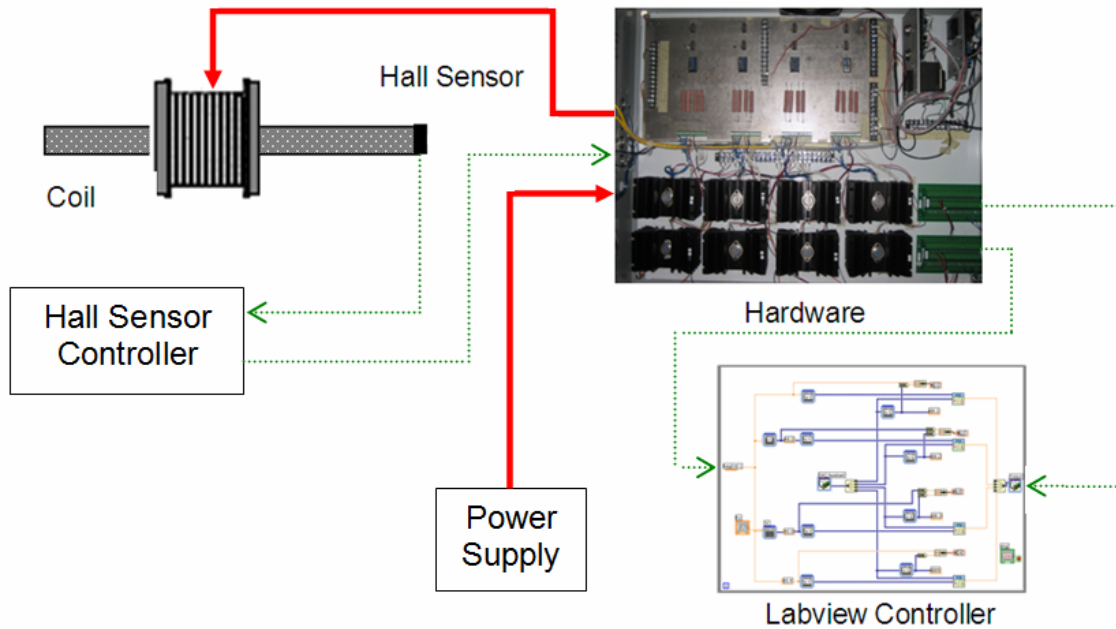
Figure 3-11. Flowchart of the feedback control system

Hall sensor provides a measurement of the field in Gauss which is compared with the required value. If the required value is different from the Hall sensor measurement, the Labview software computes the PID feedback to adjust the field at the tip of the pole.

When a force acts on a needle shaped object, the object displaces and rotates based on the magnitude and direction of the applied force. The motion of the object can be represented by the sum of the translation and rotation as shown in Figure 3-12. In this dissertation, the force and the torque are decoupled by applying appropriate individual force and torque fields on the microneedles. To obtain a force field, a strong field was generated at the attracting pole (Pole 3) and smaller common valued fields were applied at the remaining three poles. The ratio of the larger field to the common lower field is denoted by R. It was experimentally determined[2] that when four magnets are placed perpendicularly to each other, R has an optimal value for generating the maximum field

gradient. The value of R depends on the distance between the poles and the material of the poles. It was observed that increasing the gradient by increasing R, even by a few percent, results in forcing the field configuration away from the flux balance and this requires much higher coil currents for a very limited gradient increase. Similarly, lower values of R also require higher coil currents to produce the same gradient. For the magnet setup used in the current study, the magnetic field at the center was measured as the value of R was increased incrementally from 1.5 to 3.5 in steps of 0.1, while keeping the magnetic fields at poles 1, 2 and 4 at 350 Gauss. Figure 3-13 shows the graph plotted between the field at the center and R, from which the optimum R value was found to be in the range of 2.5±0.3.

Using this optimum value of R, field maps for the space between the four magnets were generated for two cases:

1) **Gradient (or force) field:** Figure 3-14 shows the graphical representation of the field between the four poles for the gradient field configuration. B (X, 0, 0) which is the change of x-component of magnetic field along x-axis is represented by the curve 3-1 while B (0, Y, 0) is the change of the x-component of magnetic field along y-axis and is represented by the curve 2-4. As discussed earlier, x-axis is aligned in such a way that it matches with the line joining the poles 3 and 1 while y-axis matches with the line joining the poles 2 and 4. Although the poles are separated by a distance of 10 mm, since the hall sensor is 5mm in width, we were only able to map fields from -2.5 mm to +2.5 mm. The magnetic fields applied at the poles (1, 2, 3, 4) were (350, -350, 885.5, 350) Gauss respectively. It can be seen from the graph that the magnetic field decreases from pole 3 towards pole 1, thus producing a gradient, while it reaches a maximum at $X = 0$ along the

Y-axis. The magnetic field along the Y-axis at poles 2 and 4 is at the same value and thus one expects there to be no field gradient along the Y-axis at $X = 0$. Needles placed along the x-axis of such a field will displace towards pole 3 due to higher magnetic flux density. Figure 3-15 is a mapping of the magnetic field in the 5 x 5 mm calibrated space. The length and direction of the arrows represent the magnitude and orientation of the magnetic field at that particular location.

2) **Uniform (or torque) field**: Fairly uniform magnetic fields can be obtained with the four magnet setup by holding the value of magnetic field at two opposite poles (poles 3 and 1) at the same magnitude while keeping the other two poles at zero magnetic fields. Figure 3-16 shows the graphical representation of the uniform magnetic field. It can be observed that the magnetic field does not change appreciably in x- or y-directions near $X = 0$ and $Y = 0$. This represents a uniform magnetic field. Needles placed at an angle with such a field will rotate and align in the direction of the magnetic field. Field mapping of a 5 x 5 mm space between the four magnets is shown in Figure 3-17. It can be observed that the length of the arrows remains constant from left to right indicating the presence of uniform magnetic field. For calculating the mechanical properties of the hydrogels in which microneedles are embedded, the gradient and the uniform fields need to be converted to the respective force and torque acting on the microneedles. This is discussed in the next section.
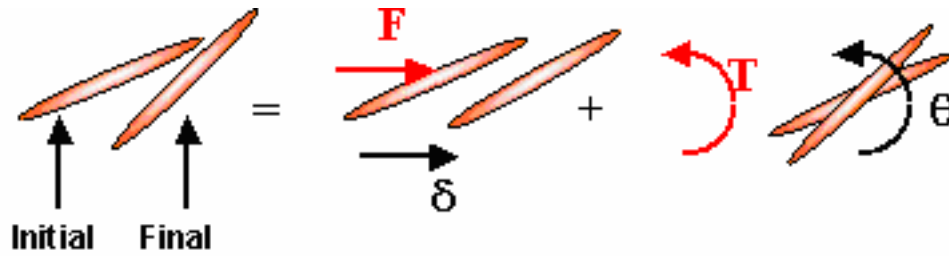
Figure 3-12. Decoupling of motion of needle-shaped objects

The translation is due to application of force only and the rotation is due to application of torque only
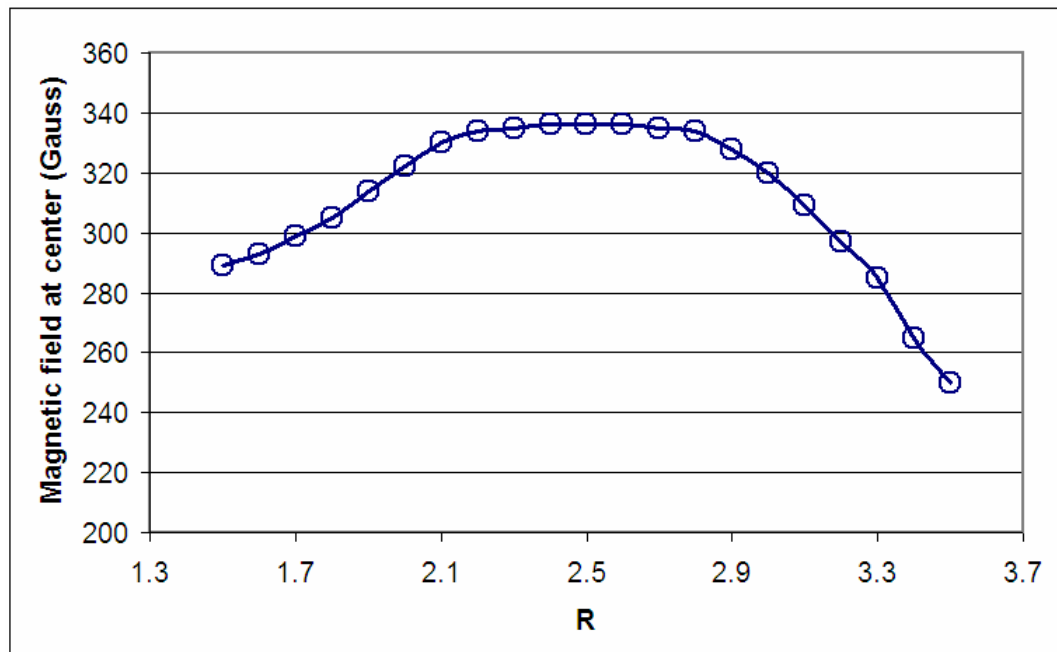
Figure 3-13. X-direction magnetic field at center of magnet v/s R

Poles 1, 2 and 4 were maintained at 350 Gauss while Pole 3 was maintained at (350 x R) Gauss.
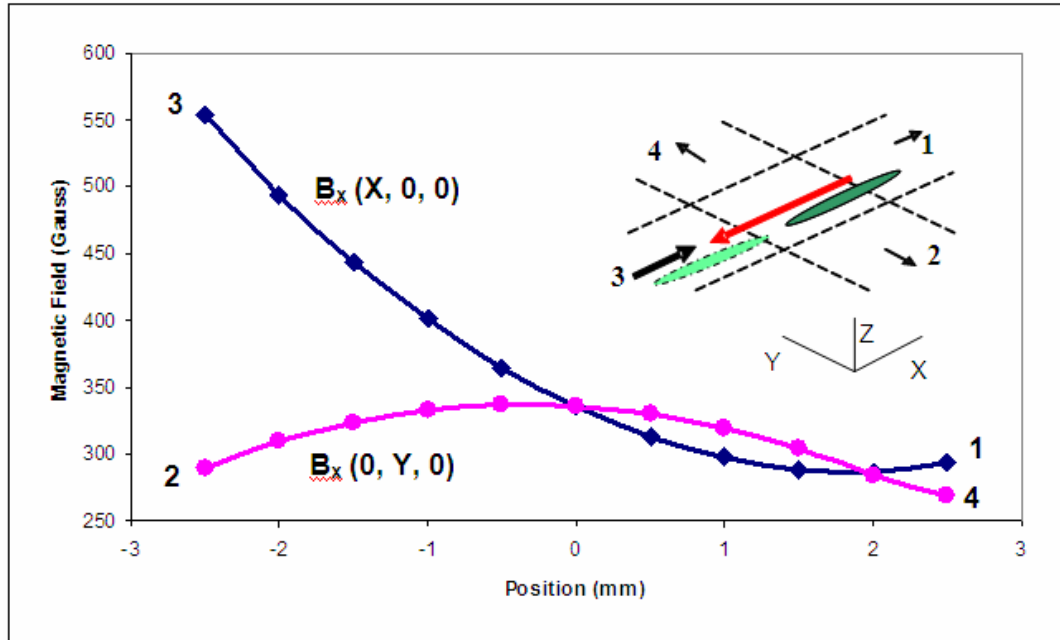
Figure 3-14. Gradient field generation with four-magnet setup

Pole 3 is set at larger magnetic flux density and needles will displace towards it.
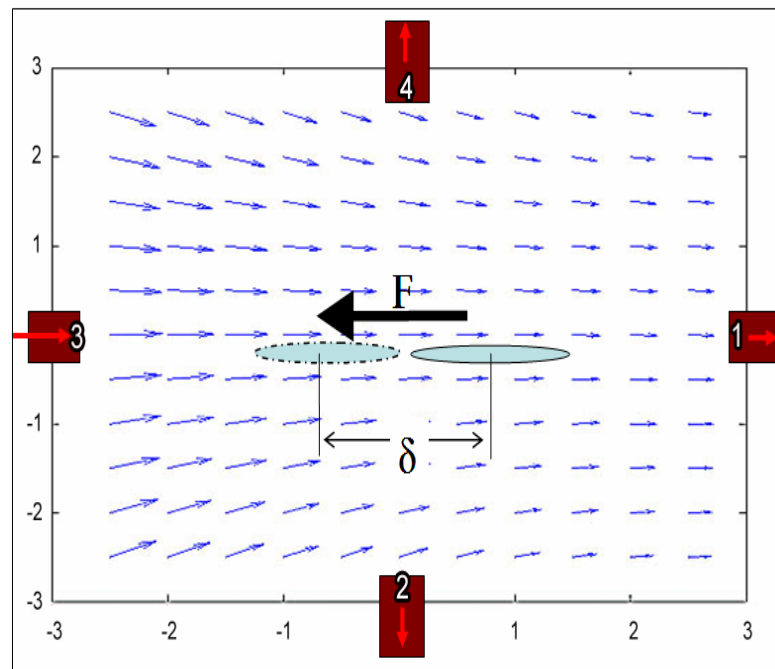
Figure 3-15. Gradient magnetic field map

Magnitudes of arrows are normalized values with respect to the maximum magnetic field.
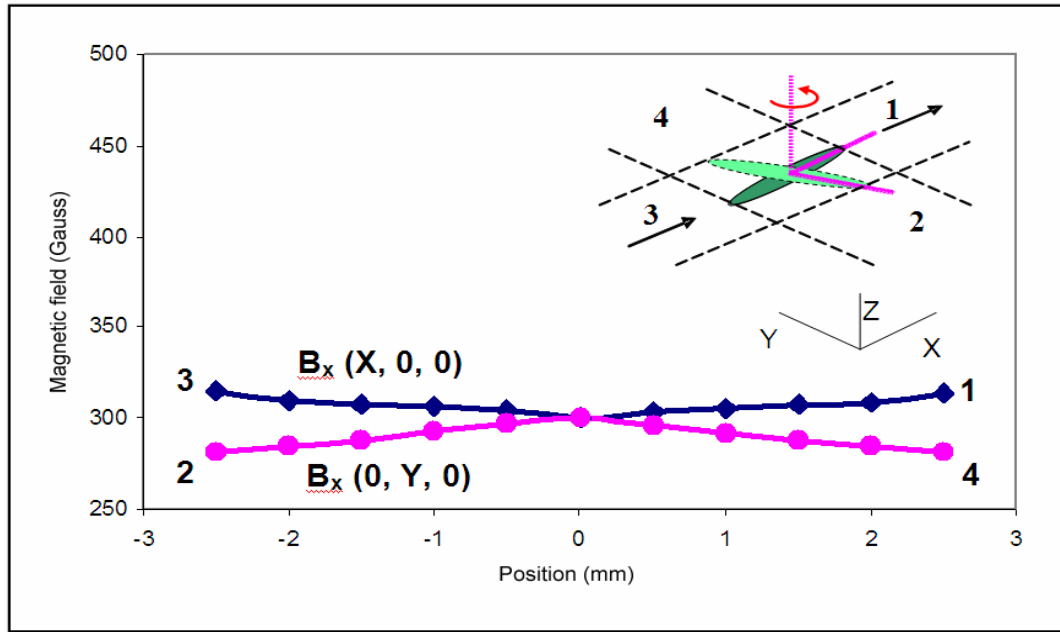
Figure 3-16. Uniform field generation with the four-magnet setup

Poles 1 and 3 are set at equal fields, while poles 2 and 4 are maintained at zero Gauss.
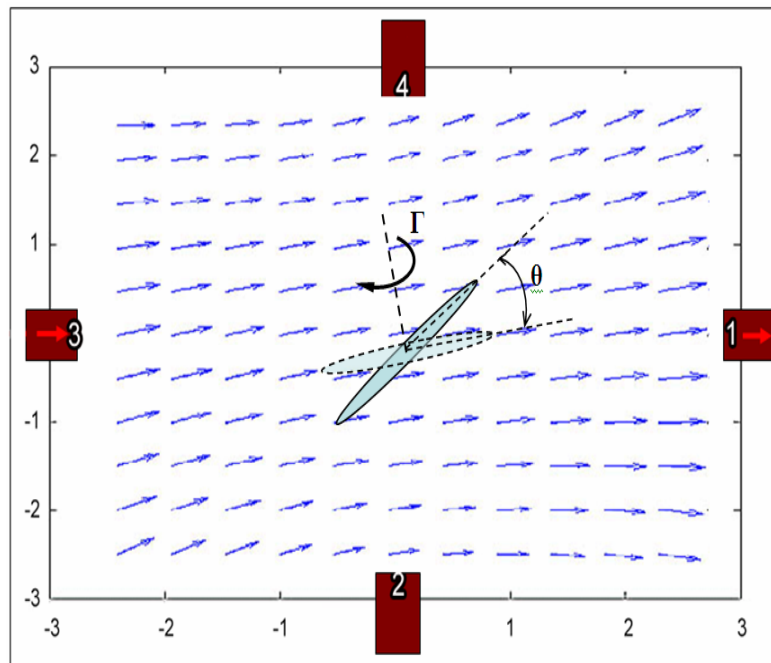
Figure 3-17. Uniform magnetic field map

Arrows have equal length and represent magnitude and direction of field at the location.

3.6   Converting Magnetic Fields into Force or Torque on Microneedles

When a magnetic object, such as nickel rod, is placed in a magnetic field, it experiences a force. The interaction energy (E_z)[47] between the applied magnetic field $\mathbf{B}_0$ and the magnetic object is given by

$$E_z = \int \mathbf{M} \cdot \mathbf{B}_0 dV \qquad\qquad \text{Eq. 5}$$

where $\mathbf{M}$ is the magnetization of the object and the integration is carried out over the volume of the object. For the case when the applied field $\mathbf{B}_0$ does not vary appreciably over the volume of the object this equation can be approximated as

$$E_z = \mathbf{m} \cdot \mathbf{B}_0 \qquad\qquad \text{Eq. 6}$$

where

$$\mathbf{m} = \int \mathbf{M} dV . \qquad\qquad \text{Eq. 7}$$

The force exerted on the object is the gradient of the magnetization times the field applied[10] and is given by

$$\mathbf{F} = grad(\mathbf{m} \cdot \mathbf{B}_0). \qquad\qquad \text{Eq. 8}$$

Torque is the cross product of the magnetization and the field and is given by

$$\mathbf{\Gamma} = \mathbf{m} \times \mathbf{B}_0 \qquad\qquad \text{Eq. 9}$$

as shown in Figure 3-18.

It is useful to consider two cases: 1) the object is a permanent magnet and 2) the object is a linearly magnetic material. For the case of an ideal permanent magnet, the magnetization $\mathbf{M}$ and, consequently, the magnetic moment $\mathbf{m}$, are independent of the applied magnetic field $\mathbf{B}_0$[1,18]. Hence, magnetic moment becomes a vector whose

magnitude is constant and which points along the direction of magnetization of the object. We denote this vector by $\mathbf{m}_p$

The expressions for the magnitude of the force and the torque then become

$$F = m_p \, grad\,(B_0)\cos\alpha \qquad\qquad \text{Eq. 10}$$

$$\Gamma = m_p B_0 \sin\alpha \qquad\qquad \text{Eq. 11}$$

where α is the angle between the vector $\mathbf{m}$ and the applied magnetic field $\mathbf{B}_0$.

However for the case of a soft linearly magnetic material, the magnetization of the body is a linear function of the applied magnetic field[14]. Further, if the relative permeability (μ) is substantially greater than 1 and the object is much longer than it is wide (as is the case for our magnetic needles), the direction of the magnetic moment vector, to a good approximation, lies along the length of the object. This shape anisotropy effect is due to the fact that the magnetic energy within the object is minimized when the magnetization points along the long axis of the object. The magnetic moment of the object can then be approximated as

$$m = \kappa(\mathbf{B}_0 \cdot \mathbf{n}) \qquad\qquad \text{Eq. 12}$$

where $\mathbf{n}$ is a unit vector along the object and κ is a constant of proportionality. One then finds that the magnitude of the torque and the force on the object are given by

$$F = 2\kappa B_0 (grad B_0)\cos^2\alpha \qquad\qquad \text{Eq. 13}$$

$$\Gamma = \kappa B_0^2 \sin\alpha \cos\alpha \qquad\qquad \text{Eq. 14}$$
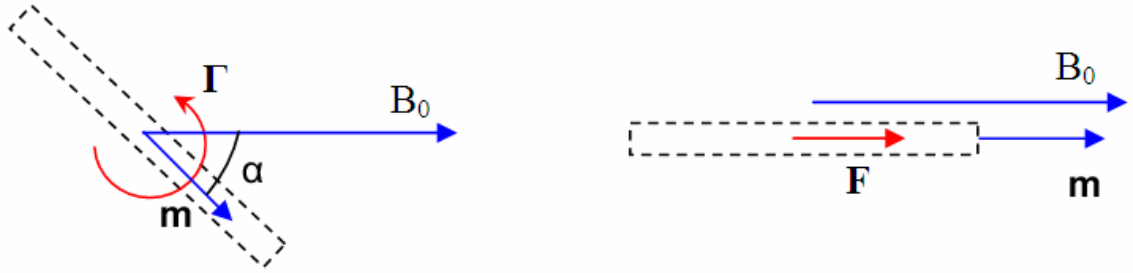
Figure 3-18. Force and torque on an object placed in a magnetic field

Thus the torque and force are proportional to the square of the applied magnetic field and also the angular dependence of the force is different from that of a permanently magnetized material. It can be observed that, by knowing the values of κ in the case of linear magnetic material and m_p in the case of permanent magnets, one can calculate the torque or the force being exerted on the needles. It should also be observed that when the needles are oriented along the magnetic field, the angle between the magnetization vector and the field is equal to zero. Thus *sin α* becomes equal to zero and the torque acting will also be zero. Thus the microneedles need to be placed at an angle to the magnetic field in order for them to rotate.

3.7   Measuring the Displacement and Rotation of Needles

The four-magnet setup is mounted on an Olympus BX51 microscope having a 50X objective lens with a working distance of 10 mm. The setup is turned on and a zero field is set inside the experimental space. A Gaussmeter (GM 200-A, Carlson Melton Inc, Sunnyvale, CA) is used to confirm that the field is 0 Gauss at every point in the space. Hydrogels with microneedles embedded in them, are prepared and placed within the

space between the four poles. The microscope stage is adjusted until a single microneedle is brought into focus. The magnetic field is then increased gradually to generate either a force field or a torque field. Images of the motion of the microneedles under the influence of this external magnetic field were taken using a Matrix Vision Bluefox USB camera with a 1600x1200 pixel sensor and a 12 mm lens. Using the initial image as a reference, the displacement or rotation of the needles was evaluated using ImageJ (U. S. National Institutes of Health, Bethesda, Maryland). Also the precise location of the needles in the field with respect to the poles is determined from the stage control software. This information coupled with the gradient of the field at the location provides us with the means to calculate the force or torque acting on the needles.

3.8   Behavior of Microneedles

Before we attempt to calculate the force and torque acting on the microneedles, it is essential to determine which of the two sets of equations described above, better model their magnetic behavior. In other words, we need to determine whether the needles behave as permanent magnets (Eq. 10 and Eq. 11) or as soft linear magnetic material (Eq. 13 and Eq. 14). A permanent magnetization can spontaneously occur when needle dimensions become comparable to the characteristic magnetic domain size of the magnetic material the needle is made of. Simple experiments were carried out to determine if magnetic particles at the micron level acquire a permanent magnetization when placed in a magnetic field. Needles were embedded in polyacrylamide hydrogels (details of which are discussed in Chapter 5) and the displacement of needles with respect to gradient of the field at the location of needles was measured. Results of this

experiment are plotted in Figure 3-19. It can be observed that the displacement of needles

is linearly proportional to the field gradient and increases with increase in the gradient. A

best fit of a linear curve yielded R^2 values close to 1 suggesting that the force is linearly

proportional to the gradient. In this manner, it was determined that the micron-sized

needles act as if they are permanently magnetized.
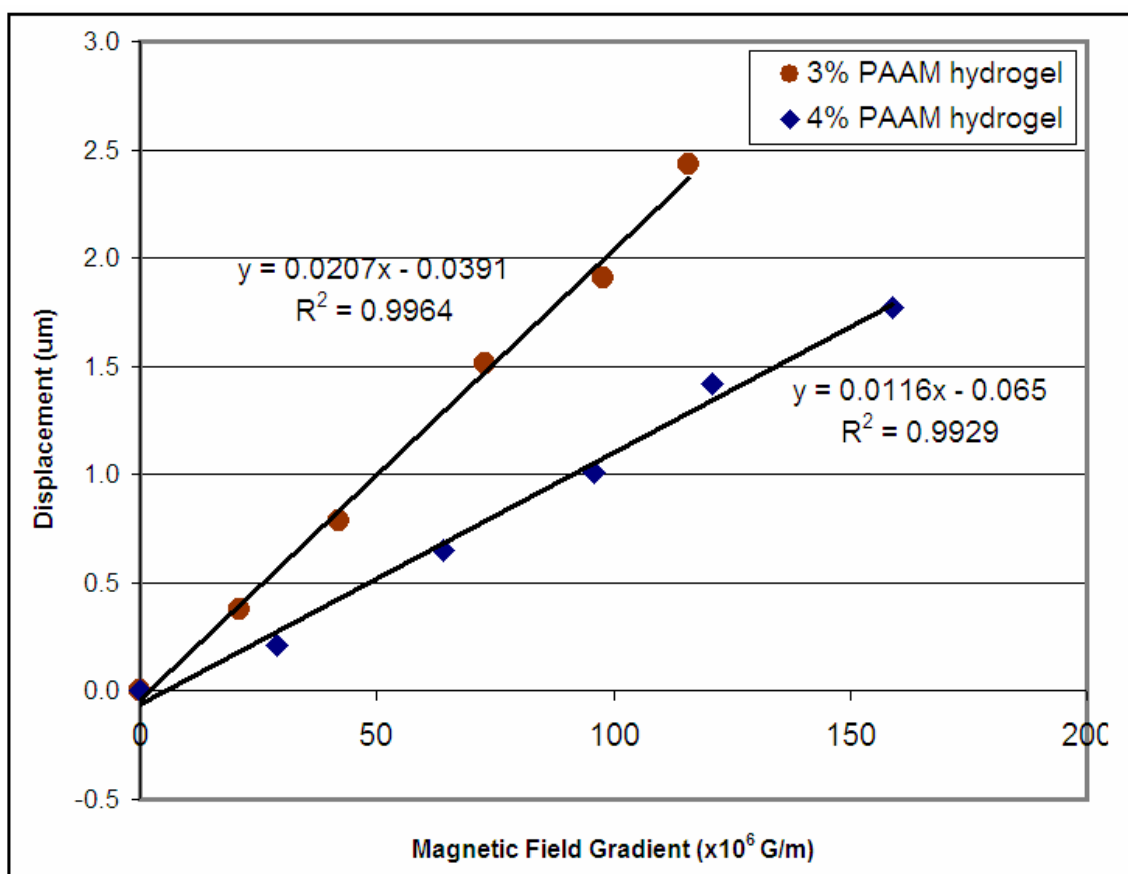
Figure 3-19. Behavior of microneedles in a magnetic field

Linear relationship between field gradient and displacement of needles for 3% and 4%
polyacrylamide hydrogels confirms the hypothesis that needles at micron level behave as
permanent magnets.

3.9 Summary

A microscope stage mounted electromagnet system capable of applying either force or torque on microneedles embedded in soft hydrogels has been presented. Some of the important features of the magnet setup are

1) Ability to apply force on microneedles embedded in hydrogels

2) Ability to apply torque on microneedles embedded in hydrogels

3) Ability to change the force or torque by varying the field strength at the poles. This feature along with computer control allows us to fully automate data collection.

4) Ability to change magnetic fields with minimal mechanical vibrations

5) Ability to be mounted on a microscope stage to measure microneedle displacements and observe cells at the same time

References

1. Abbott JJ, Ergeneman O, Kummer MP, Hirt AM, Nelson BJ. Modeling magnetic torque and force for controlled manipulation of soft-magnetic bodies. IEEE Transactions on Robotics. 2007;23(6):1247-51.

2. Amblard F, Yurke B, Pargellis A, Leibler S. A magnetic manipulator for studying local rheology and micromechanical properties of biological systems. Review of Scientific Instruments. 1996;67:818.

3. Ambrosio L, De Santis R, Nicolais L. Composite hydrogels for implants. Proceedings of the Institution of Mechanical Engineers, Part H: Journal of Engineering in Medicine. 1998;212(2):93-9.

4. Anseth KS, Bowman CN, Brannon-Peppas L. Mechanical properties of hydrogels and their experimental determination. Biomaterials. 1996;17(17):1647-57.

5. Battista S, Guarnieri D, Borselli C, et al. The effect of matrix composition of 3D constructs on embryonic stem cell differentiation. Biomaterials. 2005;26(31):6194-207.

6. Bausch AR, Ziemann F, Boulbitch AA, Jacobson K, Sackmann E. Local measurements of viscoelastic parameters of adherent cell surfaces by magnetic bead microrheometry. Biophysical journal. 1998;75(4):2038-49.

7. Beningo KA, Wang Y. Fc-receptor-mediated phagocytosis is regulated by mechanical properties of the target. Journal of cell science. 2002;115(4):849-56.

8. Chen CS, Tan J, Tien J. Mechanotransduction at cell-matrix and cell-cell contacts. 2004.

9. Curtis A, Riehle M. Tissue engineering: the biophysical background. Physics in medicine and biology. 2001;46(4):47-65.

10. de Vries AHB, Krenn BE, van Driel R, Kanger JS. Micro magnetic tweezers for nanomanipulation inside live cells. Biophysical journal. 2005;88(3):2137-44.

11. Discher DE, Janmey P, Wang Y. Tissue cells feel and respond to the stiffness of their substrate. Volume 310: American Association for the Advancement of Science, 2005:1139-43.

12. Engler A, Bacakova L, Newman C, Hategan A, Griffin M, Discher D. Substrate compliance versus ligand density in cell on gel responses. Biophysical journal. 2004;86(1):617-28.

13. Engler AJ, Sen S, Sweeney HL, Discher DE. Matrix elasticity directs stem cell lineage specification. Cell. 2006;126(4):677-89.

14. Ergeneman O, Dogangil G, Kummer MP, Abbott JJ, Nazeeruddin MK, Nelson BJ. A magnetically controlled wireless optical oxygen sensor for intraocular measurements. IEEE Sensors Journal. 2008;8(1-2):29-37.

15. Evans ND, Minelli C, Gentleman E, et al. Substrate stiffness affects early differentiation events in embryonic stem cells. European cells & materials. 2009;18:1.

16. Fabry B, Maksym GN, Hubmayr RD, Butler JP, Fredberg JJ. Implications of heterogeneous bead behavior on cell mechanical properties measured with

magnetic twisting cytometry. Journal of magnetism and magnetic materials. 1999;194(1):120.

17. Georges PC, Miller WJ, Meaney DF, Sawyer ES, Janmey PA. Matrices with compliance comparable to that of brain tissue select neuronal over glial growth in mixed cortical cultures. Biophysical journal. 2006;90(8):3012-8.

18. Gillies GT, Ritter RC, Broaddus WC, Grady MS, Howard Iii MA, McNeil RG. Magnetic manipulation instrumentation for medical physics research. Review of Scientific Instruments. 1994;65:533.

19. Gosse C, Croquette V. Magnetic tweezers: micromanipulation and force measurement at the molecular level. Biophysical journal. 2002;82(6):3314-29.

20. Grenier G, Rémy-Zolghadri M, Larouche D, et al. Tissue reorganization in response to mechanical load increases functionality. Tissue engineering. 2005;11(1-2):90-100.

21. Harmon ME, Kuckling D, Frank CW. Photo-cross-linkable PNIPAAm copolymers. 5: Mechanical properties of hydrogel layers. Langmuir. 2003;19(26):10660-5.

22. Harris AK, Wild P, Stopak D. Silicone rubber substrata: a new wrinkle in the study of cell locomotion. Science (New York, NY). 1980;208(4440):177.

23. Ingber DE. Mechanosensation through integrins: cells act locally but think globally. Volume 100: National Acad Sciences, 2003:1472-4.

24. Jiang FX, Yurke B, Firestein BL, Langrana NA. Neurite outgrowth on a DNA crosslinked hydrogel with tunable stiffnesses. Annals of Biomedical Engineering. 2008;36(9):1565-79.

25. Jiang FX, Georges PC, Li B, et al. Cell growth in response to mechanical stiffness is affected by neuron-astroglia interactions. The Open Neuroscience Journal. 2007;1(1):7-14.

26. Khatiwala CB, Peyton SR, Putnam AJ. Intrinsic mechanical properties of the extracellular matrix affect the behavior of pre-osteoblastic MC3T3-E1 cells. American Journal of Physiology- Cell Physiology. 2006;290(6):1640-50.

27. Laurent VM, Hénon S, Planus E, et al. Assessment of mechanical properties of adherent living cells by bead micromanipulation: comparison of magnetic twisting cytometry vs optical tweezers. Journal of biomechanical engineering. 2002;124:408.

28. Li L, Sharma N, Chippada U, et al. Functional modulation of ES-derived hepatocyte lineage cells via substrate compliance alteration. Annals of Biomedical Engineering. 2008;36(5):865-76.

29. Li WJ, Cooper JA, Mauck RL, Tuan RS. Fabrication and characterization of six electrospun poly (-hydroxy ester)-based fibrous scaffolds for tissue engineering applications. Acta Biomaterialia. 2006;2(4):377-85.

30. Lin DC, Langrana NA, Yurke B. Force-displacement relationships for spherical inclusions in finite elastic media. Journal of Applied Physics. 2005;97:043510.

31. Lin DC, Yurke B, Langrana NA. Mechanical properties of a reversible, DNA-crosslinked polyacrylamide hydrogel. Journal of biomechanical engineering. 2004;126:104.

32. Lin DC, Yurke B, Langrana NA. Use of Rigid Spherical Inclusions in Young's Moduli Determination: Application to DNA-Crosslinked Gels. Journal of biomechanical engineering. 2005;127:571.

33. Lo CM, Wang HB, Dembo M, Wang Y. Cell movement is guided by the rigidity of the substrate. Biophysical journal. 2000;79(1):144-52.

34. Lodish H, Berk A, Matsudaira P, et al. Molecular Cell Biology. 2004. New York, NY: WH Freeman and Company.

35. Lopes CMA, Felisberti MI. Mechanical behaviour and biocompatibility of poly (1-vinyl-2-pyrrolidinone)–gelatin IPN hydrogels. Biomaterials. 2003;24(7):1279-84.

36. Micic M, Zheng Y, Moy V, Zhang XH, Andreopoulos FM, Leblanc RM. Comparative studies of surface topography and mechanical properties of a new, photo-switchable PEG-based hydrogel. Colloids and Surfaces B: Biointerfaces. 2003;27(2-3):147-58.

37. Nedelec B, Ghahary A, Scott PG, Tredget EE. Control of wound contraction. Basic and clinical features. Hand clinics. 2000;16(2):289.

38. Nielsen LE, Landel RF. Mechanical properties of polymers and composites: Marcel Dekker Inc; 1994.

39. Panorchan P, Lee JSH, Kole TP, Tseng Y, Wirtz D. Microrheology and ROCK signaling of human endothelial cells embedded in a 3D matrix. Biophysical journal. 2006;91(9):3499-507.

40. Parekh A, Velegol D. Collagen gel anisotropy measured by 2-D laser trap microrheometry. Annals of Biomedical Engineering. 2007;35(7):1231-46.

41. Patel S, Thakar RG, Wong J, McLeod SD, Li S. Control of cell adhesion on poly (methyl methacrylate). Biomaterials. 2006;27(14):2890-7.

42. Pederson T, Aebi U. Nuclear actin extends, with no contraction in sight. Volume 16: Am Soc Cell Biol, 2005:5055-60.

43. Pelham RJ, Wang Y. Cell locomotion and focal adhesions are regulated by substrate flexibility. Volume 94: National Acad Sciences, 1997:13661-5.

44. Peyton SR, Putnam AJ. Extracellular matrix rigidity governs smooth muscle cell motility in a biphasic fashion. Journal of cellular physiology. 2005;204(1).

45. Radmacher M, Fritz M, Hansma PK. Imaging soft samples with the atomic force microscope: gelatin in water and propanol. Biophysical journal. 1995;69(1):264-70.

46. Radmacher M, Tillamnn RW, Fritz M, Gaub HE. From molecules to cells: imaging soft samples with the atomic force microscope. Science. 1992;257(5078):1900.

47. Skomski R, Coey JMD. Permanent magnetism: Institute of Physics Publishing Bristol and Philadelphia; 1999.

48. Sperling LH. Introduction to physical polymer science: Wiley-Interscience; 2006.

49. Stammen JA, Williams S, Ku DN, Guldberg RE. Mechanical properties of a novel PVA hydrogel in shear and unconfined compression. Biomaterials. 2001;22(8):799-806.

50. Swarbrick J, Boylan JC. Encyclopedia of pharmaceutical technology: Informa Health Care; 2002.

51. Thomson RC, Yaszemski MJ, Powers JM, Mikos AG. Hydroxyapatite fiber reinforced poly (-hydroxy ester) foams for bone regeneration. Biomaterials. 1998;19(21):1935-43.

52. Wang N, Butler JP, Ingber DE. Mechanotransduction across the cell surface and through the cytoskeleton. Science. 1993;260(5111):1124.

53. Wang YL, Pelham RJ. Preparation of a flexible, porous polyacrylamide substrate for mechanical studies of cultured cells. Methods in enzymology. 1998;298:489-96.

54. Wong JY, Velasco A, Rajagopalan P, Pham Q. Directed Movement of Vascular Smooth Muscle Cells on Gradient-Compliant Hydrogels. J Cell Sci. 1999;112:1967.

55. Yamada S, Wirtz D, Kuo SC. Mechanics of living cells measured by laser tracking microrheology. Biophysical journal. 2000;78(4):1736-47.

56. Yamaguchi N, Le Zhang BSC, Palla CS, Furst EM, Kiick KL. Growth factor mediated assembly of cell receptor-responsive hydrogels. Journal of the American Chemical Society. 2007;129(11):3040.

57. Yanai M, Butler JP, Suzuki T, et al. Intracellular elasticity and viscosity in the body, leading, and trailing regions of locomoting neutrophils. American Journal of Physiology- Cell Physiology. 1999;277(3):432-40.

58. Yeung T, Georges PC, Flanagan LA, et al. Effects of substrate stiffness on cell morphology, cytoskeletal structure, and adhesion. Cell Motility and the Cytoskeleton. 2005;60(1):24-34.

CHAPTER 4 Theory of Elasticity Formulation

4.1 Novelty and Significance

The elastic moduli of soft media were previously determined by many researchers using the theories of rubber elasticity and viscoelasticity. The medium was assumed to be a linear, elastic, isotropic, incompressible material and Poisson's ratio was assumed to be equal to one-half. Some of the methods employed were compression[10,13,31], macroscopic indentation[22,31], atomic force microscopy[24,25] and manipulation of embedded spherical beads. The manipulation of embedded spherical magnetic beads has been used by a number of researchers to obtain the local viscoelastic response of soft media[1,2,4,5,15-17,30,32]. Some have used linear viscoelastic theory[16] while others have used linear elasticity theory[19-21] to compute the equivalent Young's modulus of the soft media. However, a complete characterization of the elastic properties of the hydrogel would involve calculating two of the three unknown quantities; Young's modulus, shear modulus and Poisson's ratio of the material. In this study, analytical expressions for Young's modulus (E), shear modulus (G) and Poisson's ratio (v) are derived for a soft, homogenous, isotropic, linear elastic medium by using non-spherical inclusions, in the form of cylindrical rods, assuming no-slip boundary conditions.

The Poisson's ratio of a gel network system plays an important role in many phenomena, for example, the bending of polyelectrolyte gels in an electric field[26], gel surface pattern formation[27], network swelling kinetics[18,23] and gel volume phase transitions[11]. If measurements are performed on a time scale that is sufficiently long to

allow fluid flow in the medium, non-volume preserving distortions of the medium can be expected. In such cases the medium can exhibit Poisson's ratio which is substantially different from 0.5 as observed by some researchers[12]. Li et al.[18] have proposed a method for measuring the Poisson's ratio of polymer gels using different swelling behaviors of free and constrained gels. Poisson's ratio of polyacrylamide gels was found to be sensitive to the amount of polymerization initiator and varied between 0.3 and 0.36. In another study[6], a micropipette aspiration technique was used to measure the range of the Poisson's ratio values for polyacrylamide gels with concentrations in the range of *0.02% ≤ [Bis] ≤ 0.2%* and *3% ≤ [Acry] ≤ 10%*. A mean Poisson's ratio of 0.48 ± 0.012 was obtained for these hydrogels. Young's moduli and Poisson's ratios of hydrogels were also characterized at the micron scale using tensile tests at varying degrees of swelling[14]. The Poisson's ratio of the hydrogels was found to vary between 0.42 and 0.45 when the pH changed from 2.8 to 12. But most of these techniques were destructive in nature and cannot be used in the presence of cells.

Walpole[28,29] derived equations relating the force and the translation vectors or the couple and the rotation vectors for ellipsoidal inclusions in an elastic, isotropic and homogenous medium. Eshelby[7-9] has also carried out significant work in the field of inclusions in elastic medium. However, direct relations between force, displacement, torque, angle, elastic modulus, Poisson's ratio and shear modulus were not found in the literature.

Hydrogels usually exhibit tunable properties, meaning that the mechanical properties can be changed on the fly by increasing or decreasing the temperature, adding or removing crosslinker or by changing pH of the solution etc. For example, stiffness of

DNA crosslinked hydrogels can be increased by adding crosslinks and decreased by removing crosslinks[20]. Often for cell culture purposes, cells whose function depends on the stiffness of the substrate are attached to these hydrogels. Hence, there is need for a non-destructive technique to completely characterize the properties of the material.

4.2   Mathematical Formulation

Consider a cylindrical rod of length L and radius R in a homogenous, isotropic, linear elastic medium. No-slip boundary conditions are assumed and medium finite size effects are ignored, that is, the size of the rod embedded in the medium is taken to be very small compared to the distance between the rod and the gel surface.

In this study, two particular cases are considered

1) Translation of the rod – The rod is placed along the x-axis and a constant force is applied along its axis. This will cause the rod to displace along the x-axis as shown in Figure 4-1.

2) Rotation of the rod – The rod is placed along the x-axis and torque is applied about the z-axis which causes the rod to rotate as shown in Figure 4-2.
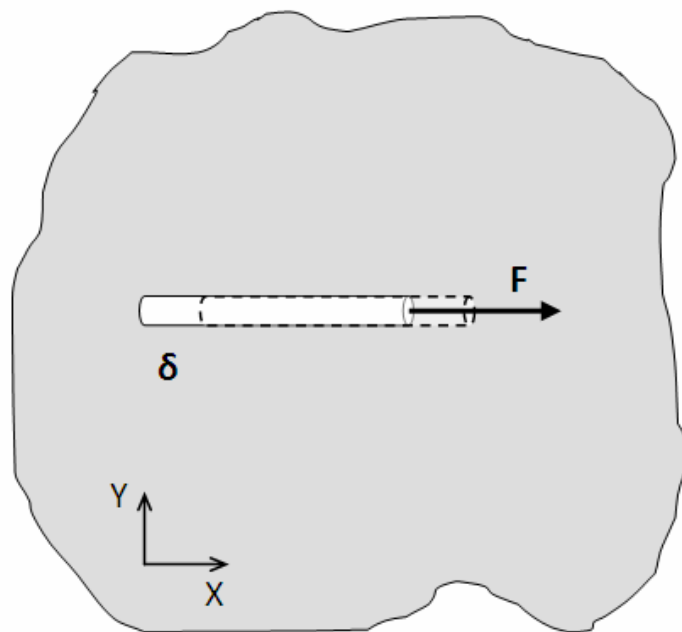
Figure 4-1. Translation of cylindrical rod in elastic medium
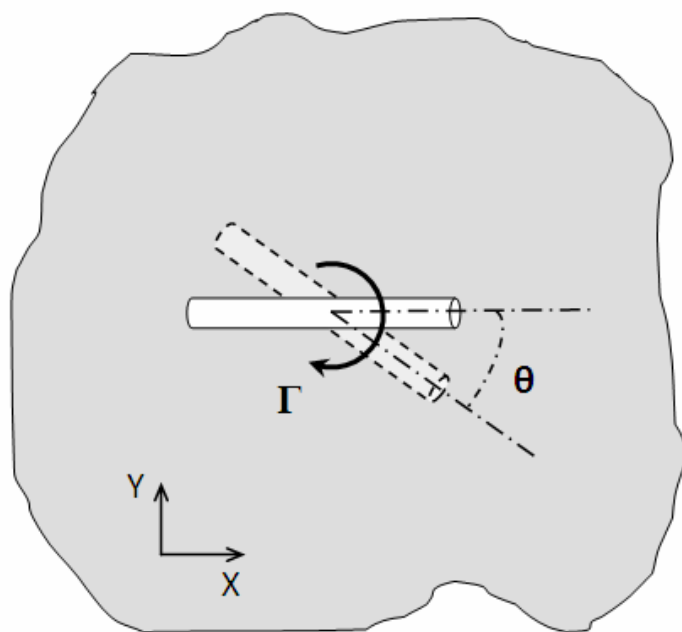
Figure 4-2. Rotation of cylindrical rod in elastic medium

4.2.1 Translation of a Cylindrical Rod

We start with the field equation for the displacement vector in a linear elastic medium and obtain the Galerkin solution[3] to the strain equations. The equilibrium equation in terms of the displacements is given by

$$\lambda \frac{\partial e}{\partial x} + 2\mu \left(\frac{\partial e_{xx}}{\partial x} \frac{\partial e_{xy}}{\partial y} + \frac{\partial e_{xz}}{\partial z} \right) + p_x = 0 \qquad \text{Eq. 15}$$

where λ and μ are Lame's constants given by

$$\lambda = \frac{Ev}{(1+v)(1-2v)} \qquad \text{Eq. 16}$$

$$\mu = \frac{E}{2(1+v)} \qquad \text{Eq. 17}$$

and E and v are the Young's modulus and Poisson's ratio respectively. In the absence of a body force ($p_x = 0$), substituting Eq. 16 and Eq. 17 into Eq. 15 yields the following field equation for the displacement vector of a linear elastic medium

$$\nabla(\nabla \cdot \mathbf{u}) + (1-2v)\nabla^2 \mathbf{u} = 0 \qquad \text{Eq. 18}$$

which has a Galerkin solution of the form

$$2G\mathbf{u} = -4(1-v)\mathbf{q} + \nabla(\mathbf{r} \cdot \mathbf{q} + \phi) \qquad \text{Eq. 19}$$

where $\mathbf{q}$ and ϕ are harmonic and G is the shear modulus of the medium.

Since force is acting along the x-axis, displacement will also be along the x-axis and can be represented in cylindrical coordinates as

$$\mathbf{u} = u(r)\mathbf{e}_x . \qquad \text{Eq. 20}$$

Hence

$$\nabla \cdot \mathbf{u} = 0, \tag{Eq. 21}$$

$$(\nabla^2 \mathbf{u})_r = (\nabla^2 \mathbf{u})_\varphi = 0, \tag{Eq. 22}$$

and

$$(\nabla^2 \mathbf{u})_x = \nabla^2 u(r). \tag{Eq. 23}$$

Eq. 18 thus reduces to

$$\nabla^2 u(r) = 0 \tag{Eq. 24}$$

which further reduces to

$$\frac{\partial}{\partial r}\left(r \frac{\partial u(r)}{\partial r}\right) = 0. \tag{Eq. 25}$$

Integrating Eq. 25 yields

$$u(r) = A \ln(r) + B. \tag{Eq. 26}$$

At the surface of the rod $u(R)$ equals the displacement of the rod. When Eq. 26 is applied

as an approximate solution for the case of a rod of finite length, the rod length L serves as

a natural cut off to the logarithmic dependence of u on r, that would otherwise result in a

divergence, if the boundary condition $u(\infty)=0$ were imposed. This cut off can be imposed

via the boundary condition $u(L/2) = 0$ and the resulting solution will yield accurate

expressions for the force displacement relationship of the rod, provided the rod length is

much greater than the rod radius. Thus applying the boundary conditions $u(R) = \delta$ and

$u(L/2) = 0$ we obtain

$$A = \frac{\delta}{\ln\left(2R/L\right)} \tag{Eq. 27}$$

$$B = -A \ln(L/2) \tag{Eq. 28}$$

Substituting the values of A and B in Eq. 26 yields

$$u(r) = \delta \frac{\ln\left(2r/L\right)}{\ln\left(2R/L\right)}.$$

Eq. 29

Now consider the shear stress tensor component (τ_{xr}) given by

$$\tau_{xr} = \frac{E}{2(1+v)}\left(\frac{\partial u_r}{\partial x} + \frac{\partial u_x}{\partial r}\right).$$

Eq. 30

For the present case, we have

$$\tau_{xr} = \frac{E}{2(1+v)}\left(\frac{\partial u(r)}{\partial r}\right)$$

Eq. 31

Simplifying Eq. 31 we obtain

$$\tau_{xr} = \frac{E\delta}{2(1+v)}\frac{1}{r\ln(L/2R)}.$$

Eq. 32

The total force along a cylinder of length L and radius R is then obtained by integrating shear stress over the length of the rod. Thus,

$$F = \int_0^L dx \int_0^{2\pi} R\tau_{xr}(R)d\theta.$$

Eq. 33

Solving the integral gives rise to

$$F = \frac{2\pi E\delta L}{2(1+v)\ln(L/2R)}.$$

Eq. 34

Hence

$$E = \frac{2(1+v)\ln(L/2R)}{2\pi L}\frac{F}{\delta}.$$

Eq. 35

4.2.2 Rotation of a Cylindrical Rod

In order to obtain the relationship between the shear modulus and the torque-rotation data, we start with the 2-D Kelvin solution which is also called as the fundamental solution.

$$u_{ij} = \frac{F_{ij}}{8\pi G} \left\{ (3 - 4v) \ln r \delta_{ij} + r_{,i} r_{,j} \right\}.$$ Eq. 36

Consider the cylindrical rod to be oriented along the z-axis and let the force act along the x-axis. This will make the rod to rotate about the y-axis.

Hence $\mathbf{F} = -F_x \, \bar{\mathbf{e}}_x$.

Substituting this in Eq. 36 we obtain

$$u_i = -\frac{F_x}{8\pi G} \left\{ (3 - 4v) \ln r \delta_{ix} + r_{,i} r_{,j} \right\}.$$ Eq. 37

Since $r = \sqrt{(x^2 + y^2)}$

we obtain

$$r_{,x} = \frac{x}{\sqrt{(x^2 + y^2)}} \quad and \quad r_{,y} = \frac{y}{\sqrt{(x^2 + y^2)}} \quad .$$ Eq. 38

The displacement in the direction of the applied force is obtained from Eq. 37 as

$$u_x = \frac{F_x}{8\pi G(1 - v)} \left\{ (3 - 4v) \ln r \delta_{xx} + r_{,x} r_{,x} \right\}$$ Eq. 39

$$u_x = -\frac{F_x}{8\pi G(1 - v)} \left\{ (3 - 4v) \ln r + \frac{x^2}{x^2 + y^2} \right\}.$$ Eq. 40

This is the displacement of any point on a plane whose normal is along the axis of the rod. In order to obtain the average displacement of all the points in this plane at radius r, we average the displacement obtained in Eq. 40 as

$$\langle u_x \rangle = -\frac{1}{2\pi r}\int_0^{2\pi} u_x(r)\, r d\theta.$$

<div align="right">Eq. 41</div>

Expressing the displacement in cylindrical coordinates, Eq. 40 can be written as

$$u_x = \frac{F_x}{8\pi G(1-v)}\left\{(3-4v)\ln r + \cos^2\theta\right\}.$$

<div align="right">Eq. 42</div>

Substituting Eq. 42 in Eq. 41 and simplifying yields

$$\langle u_x \rangle = -\frac{1}{2\pi r}\frac{F_x}{8\pi G(1-v)}\int_0^{2\pi}\left\{(3-4v)\ln r + \cos^2\theta\right\}r d\theta.$$

<div align="right">Eq. 43</div>

Carrying out the integration gives rise to

$$\langle u_x(r) \rangle = -\frac{F_x}{8\pi G(1-v)}\left\{(3-4v)\ln r + \frac{1}{2}\right\}.$$

<div align="right">Eq. 44</div>

From Eq. 44, one obtains an expression for the force-displacement relationship of a cylinder of radius R, displaced perpendicular to its axis, inside another cylinder of radius R_1, whose walls are held fixed as

$$\langle u \rangle = \langle u_x(R) \rangle - \langle u_x(R_1) \rangle = \frac{(3-4v)F_x}{8\pi G(1-v)}\ln\left(\frac{R_1}{R}\right)$$

<div align="right">Eq. 45</div>

This result can then be applied to the case of a rod of length L, aligned with the z-axis, and rotated about the y-axis at its midpoint, in a medium for which displacement vanishes at $r = \infty$. As in the case of the rod translated parallel to the z-axis, the rod length L provides a natural cut off of the divergence that would result if one set $R_1 = \infty$ in Eq. 45. Hence setting $R_1 = L/2$, the relation between the applied force and the displacement of the rod, at a point along the z-axis is given by

$$F_x(z) = \frac{8\pi G(1-v)}{(3-4v)\ln(L/2R)}\langle u_x(z)\rangle.$$

<div align="right">Eq. 46</div>

Eq. 46 will be accurate when L >> R.

The torque acting on the rod can now be obtained by using

$$\Gamma = \int_{-L/2}^{L/2} F_x z\, dz = \frac{8\pi G(1-v)}{(3-4v)\ln(L/2R)} \int_{-L/2}^{L/2} z\langle u_x(z)\rangle\, dz \,.$$

Eq. 47

Expressing the displacement $\langle u_x(z)\rangle$ in terms of the angle of rotation of the rod (θ) we obtain

$$\langle u_x(z)\rangle = z\theta \,.$$

Eq. 48

Substituting Eq. 48 into Eq. 47 yields

$$\Gamma = \int_{-L/2}^{L/2} F_x z\, dz = \frac{8\pi G(1-v)}{(3-4v)\ln(L/2R)} \int_{-L/2}^{L/2} z^2 \theta\, dz \,.$$

Eq. 49

Simplifying Eq. 49 and carrying out the integration gives

$$\Gamma = \frac{2\pi G(1-v)}{3(3-4v)\ln(L/2R)} \theta L^3 \,.$$

Eq. 50

Hence,

$$G = \frac{3(3-4v)}{2\pi(1-v)} \frac{\Gamma}{\theta} \frac{\ln\left(L/2R\right)}{L^3} \,.$$

Eq. 51

In Eq. 35, F is the force applied on the rod and δ is the independently measured displacement. Similarly in Eq. 51, Γ is the torque applied on the rod while θ is the independently measured rotation angle of the rod. In addition to Eq. 35 and Eq. 51, for a linearly elastic and isotropic material E, G and v are related by

$$E = 2G(1+v) \,.$$

Eq. 52

Thus we have three equations with which the three unknowns G, E, and v can be determined.

4.3   Finite Element Analysis

Exact mathematical solutions can be obtained for relatively simple geometries and forces using linear theory of elasticity. However, experimental setups and everyday practical applications cannot always be approximated as simple geometrical shapes. In such cases, finite element analysis (FEA) methods are suitable for simulating these complex experimental conditions. In the previous section, various assumptions were made in deriving the closed form solutions for the rod embedded in elastic medium. Conditions such as infinite medium and length of rod being very large compared to diameter, do not need to be assumed in an FEA simulation. Also the FEA method can be used as a verification tool to assess the accuracy of the closed form solutions. The strengths and limitations of the FEA method in comparison to the theoretical solutions are presented in Table 4-1.

A commercially available FEA software package, ANSYS® Workbench™, was used to perform the analysis on a cylindrical rod of length 10 μm and diameter 1 μm embedded in a cylindrical matrix of radius 300 μm and 30 μm height. The rod was glued to the gel using contact elements, thus ensuring rigid bonding and no-slip conditions. An arbitrary value of 3000 Pa was assumed for the Young's modulus of the gel. The rod was modeled using the properties of nickel, namely Young's modulus of 210 GPa and Poisson's ratio of 0.3. The model details are shown in

Table **4-2**. The periphery and the bottom surface of the medium were rigidly restrained, while the top surface was modeled using symmetric boundary conditions. A mesh convergence study was performed to determine the optimum tetrahedral mesh density. A representative image of the model is as shown in Figure 4-3.

Table 4-1. Comparison of strengths and limitations of theory and FEA

Method	Strengths	Limitations
Linear elasticity theory	Can provide exact, close form mathematical solutions	Limited to simple shapes Cannot obtain closed form solution in all cases
FEA	Can solve complex geometric shapes, sizes, boundary conditions and material properties Do not have to make simplifying assumptions	Computation might cost time and money Convergence analysis required Computed solution could sometimes be wrong

Table 4-2. Material and geometric properties used in the analysis

Parameter	Value
Radius of rod (R)	0.5 μm
Length of rod (L)	10 μm
Elastic modulus of rod (E_r)	210 GPa
Poisson's ratio of rod (v_r)	0.3
Height of medium (H)	30 μm
Radius of medium (R_m)	300 μm
Elastic modulus of medium (E)	3000 Pa
Poisson's ratio of medium (v_m)	Varies between 0.36 and 0.499
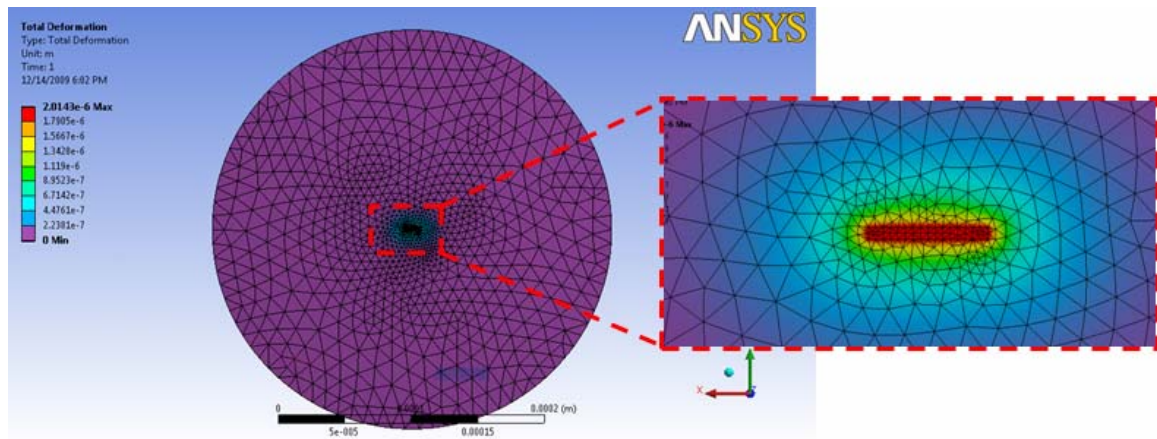
Figure 4-3. FEA model of cylindrical rod embedded in elastic medium.

A linear static analysis was then performed by applying an arbitrary load of 15 nN on the face of the cylindrical rod and varying the Poisson's ratio from 0.36 to 0.499 in steps of 0.01. The displacement of the rod in the medium was measured in each case and plotted in Figure 4-4. In order to compare the closed form equations with the finite element solution, it is convenient to write Eq. 35 in the form

$$\delta = \frac{2(1+v)\ln(L/2R)}{2\pi L} \frac{F}{E}.$$

Eq. 53

Using the same values for E, F, L and R as used in the finite element simulations (

Table **4-2**); the displacement δ is plotted against the Poisson's ratio v as shown in Figure 4-4. It is evident from the graph that the closed form solutions match well with the finite element solutions, although there is an increasing disparity between the displacements obtained from the two methods with increasing Poisson's ratio. From Eq. 53, it can be observed that the displacement is directly proportional to the term $(1 + v)$. As a result, the displacement increases with increasing Poisson's ratio. However in the finite element solution, as Poisson's ratio of the isotropic material approaches to 0.5, the errors in measurement increase due to the presence of a term in the linear elasticity field equations containing the quantity $(1 - 2v)$ which approaches zero as Poisson's ratio approaches 0.5. This results in a divide by zero error when Poisson's ratio equals one half.

In a similar manner, linear static analysis was performed by applying a torque of 15 nN-μm at the center of the cylindrical rod, in the form of two opposing forces of 1.5 nN each; perpendicular to the axis of the rod; at each end. The rotation angle of the rod under the influence of the applied torque is measured in each case as the Poisson's ratio is varied from 0.36 to 0.499. The results are plotted in Figure 4-5. Using Eq. 52, it is convenient to write Eq. 51 in the form

$$\theta = \frac{3(3-4v)(1+v)}{\pi(1-v)} \frac{\Gamma}{E} \frac{\ln\left(L/2R\right)}{L^3} .$$

Eq. 54

Using the same values of Γ, E, L and R as used in the finite element analysis, the angle of rotation θ is plotted against the Poisson's ratio as shown in Figure 4-5. The close match between the two methods gives us confidence in the closed form solutions derived.

The approach considered in this study is only appropriate within a limited range of deformation of the medium and is useful for determining the material properties in the linear elastic regime. It can be observed from Figure 4-4 and Figure 4-5 that in the range of motion of the needle considered in the study, the effect of Poisson's ratio on the displacement and the rotation angle is negligible. Also, no-slip boundary conditions were assumed and the finite size effects were ignored. So care should be taken to make sure that the length of the rods (L) is much smaller compared to the size of the medium. Otherwise the factor of R_m/L, where R_m is the defining dimension of the elastic medium, should be taken into consideration[19]. If slip boundary conditions apply, motion of the particles on the surface of the rod is restricted to the trajectories tangential to the rod's surface, Eq. 35 and Eq. 51 no longer hold. The treatment of these conditions is beyond the scope of this study.
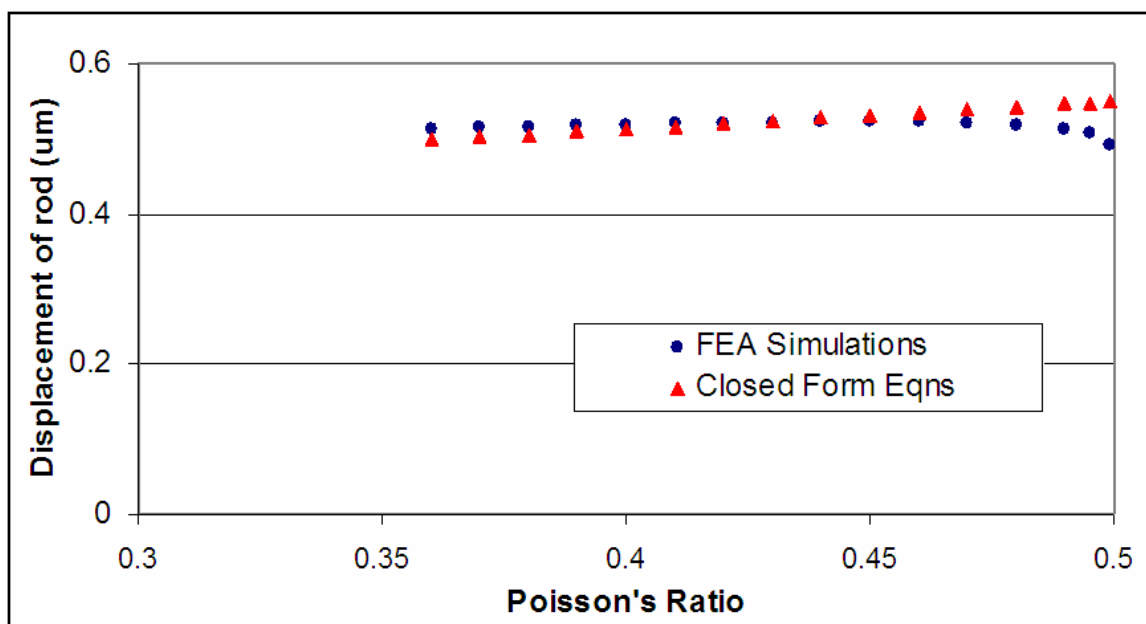
Figure 4-4. Displacement of rod using FEA and closed form equations
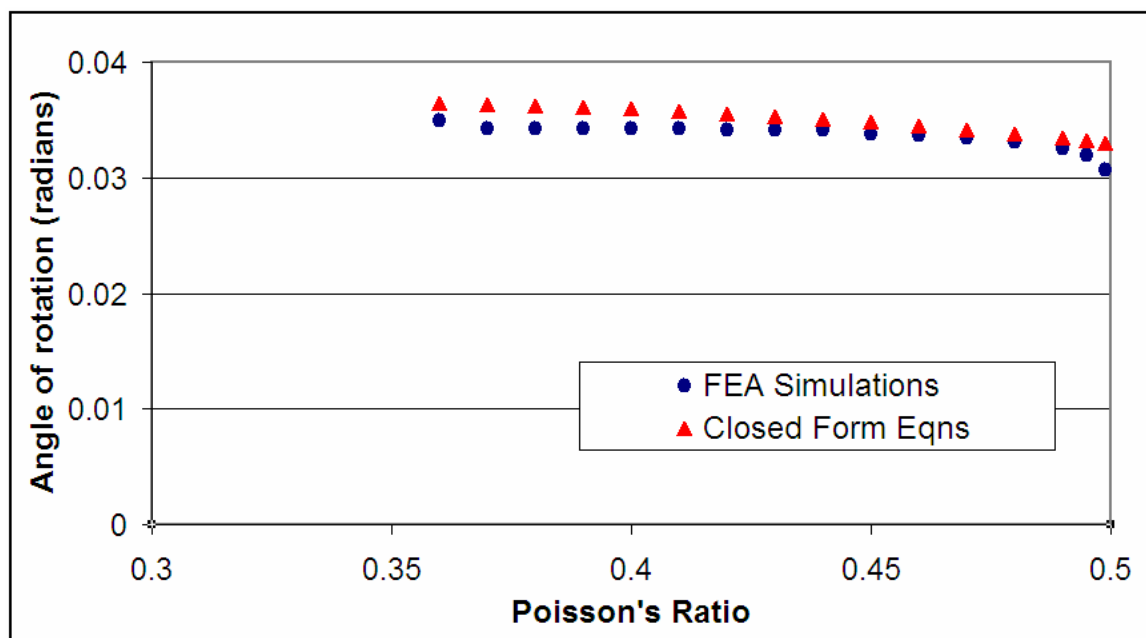
Figure 4-5. Angle of rotation of rod using FEA and closed form equations

4.4   Conclusions

In most of the studies involving measurement of stiffness, hydrogels are assumed to be incompressible and the Poisson's ratio is taken as 0.5. However, Poisson's ratio can differ from 0.5. Hence, a more complete characterization of the elastic properties of hydrogels requires that one experimentally obtain the value of at least two of the three quantities: Poisson's ratio, shear modulus, and elastic modulus. In this study, we obtained analytic expressions for force-displacement and torque-rotation of non-spherical rods placed in soft, homogenous, elastic and isotropic medium. These expressions can be used to obtain the elastic modulus, shear modulus and Poisson's ratio of soft hydrogels, in a non-destructive manner as described in Chapter 5 and Chapter 6. In addition to this, finite element analysis was utilized to validate the accuracy of the closed form equations obtained.

References

1. Amblard F, Maggs AC, Yurke B, Pargellis AN, Leibler S. Subdiffusion and anomalous local viscoelasticity in actin networks. Physical review letters. 1996;77(21):4470-3.
2. Amblard F, Yurke B, Pargellis A, Leibler S. A magnetic manipulator for studying local rheology and micromechanical properties of biological systems. Review of Scientific Instruments. 1996;67:818.
3. Barber JR. Elasticity: Kluwer Academic Pub; 2002.
4. Bausch AR, Möller W, Sackmann E. Measurement of local viscoelasticity and forces in living cells by magnetic tweezers. Biophysical Journal. 1999;76(1):573-9.
5. Bausch AR, Ziemann F, Boulbitch AA, Jacobson K, Sackmann E. Local measurements of viscoelastic parameters of adherent cell surfaces by magnetic bead microrheometry. Biophysical Journal. 1998;75(4):2038-49.
6. Boudou T, Ohayon J, Picart C, Tracqui P. An extended relationship for the characterization of Young's modulus and Poisson's ratio of tunable polyacrylamide gels. Biorheology. 2006;43(6):721-8.
7. Eshelby JD. The Determination of the Elastic Field of an Ellipsoidal Inclusion, and Related Problems. Proceedings of the Royal Society of London Series A, Mathematical and Physical Sciences (1934-1990). 1957;241(1226):376-96.
8. Eshelby JD. The Elastic Field Outside an Ellipsoidal Inclusion. Proceedings of the Royal Society of London Series A, Mathematical and Physical Sciences (1934-1990). 1959;252(1271):561-9.
9. Eshelby JD. Elastic inclusions and inhomogeneities. Progress in Solid Mechanics. 1961;2(3):87-140.
10. Gundogan N, Melekaslan D, Okay O. Rubber Elasticity of Poly (N-isopropylacrylamide) Gels at Various Charge Densities. Macromolecules. 2002;35(14):5616-22.
11. Hirotsu S. Elastic anomaly near the critical point of volume phase transition in polymer gels. Macromolecules. 1990;23(3):903-5.
12. Hirotsu S. Static and time-dependent properties of polymer gels around the volume phase transition. Phase Transitions. 1994;47(3):183-240.
13. Horkay F, Zrinyi M. Studies on the mechanical and swelling behavior of polymer networks based on the scaling concept. 4. Extension of the scaling approach to gels swollen to equilibrium in a diluent of arbitrary activity. Macromolecules. 1982;15(5):1306-10.
14. Johnson B, Bauer JM, Niedermaier DJ, Crone WC, Beebe DJ. Experimental techniques for mechanical characterization of hydrogels at the microscale. Experimental Mechanics. 2004;44(1):21-8.
15. Keller M, Schilling J, Sackmann E. Oscillatory magnetic bead rheometer for complex fluid microrheometry. Review of Scientific Instruments. 2001;72:3626.

16. Laurent VM, Hénon S, Planus E, et al. Assessment of mechanical properties of adherent living cells by bead micromanipulation: comparison of magnetic twisting cytometry vs optical tweezers. Journal of Biomechanical Engineering. 2002;124:408.

17. Lee J. Traction forces generated by locomoting keratocytes. The Journal of Cell Biology. 1994;127(6):1957-64.

18. Li Y, Hu Z, Li C. New Method for Measuring Poisson's Ratio in Polymer Gels. Journal of Applied Polymer Science. 1993;50(6):1107-11.

19. Lin DC, Langrana NA, Yurke B. Force-displacement relationships for spherical inclusions in finite elastic media. Journal of Applied Physics. 2005;97:043510.

20. Lin DC, Yurke B, Langrana N. Inducing reversible stiffness changes in DNA-crosslinked gels. Journal of Materials Research. 2005;20(6):1456-64.

21. Lin DC, Yurke B, Langrana NA. Mechanical Properties of a Reversible, DNA-Crosslinked Polyacrylamide Hydrogel. Journal of Biomechanical Engineering. 2004;126:104.

22. Pelham RJ, Wang Y. Cell locomotion and focal adhesions are regulated by substrate flexibility. Volume 94: National Acad Sciences, 1997:13661-5.

23. Peters A, Candau SJ. Kinetics of swelling of polyacrylamide gels. Macromolecules. 1986;19(7):1952-5.

24. Radmacher M, Fritz M, Hansma PK. Imaging soft samples with the atomic force microscope: gelatin in water and propanol. Biophysical Journal. 1995;69(1):264-70.

25. Radmacher M, Tillamnn RW, Fritz M, Gaub HE. From molecules to cells: imaging soft samples with the atomic force microscope. Science. 1992;257(5078):1900-5.

26. Shiga T, Hirose Y, Okada A, Kurauchi T. Bending of ionic polymer gel caused by swelling under sinusoidally varying electric fields. Journal of Applied Polymer Science. 1993;47(1):113-9.

27. Tanaka T, Sun ST, Hirokawa Y, et al. Mechanical instability of gels at the phase transition. Nature. 1987;325(6107):796-8.

28. Walpole LJ. A Rotated Rigid Ellipsoidal Inclusion in An Elastic Medium. The Royal Society, 1991:179-207.

29. Walpole LJ. A Translated Rigid Ellipsoidal Inclusion in an Elastic Medium. The Royal Society, 1991:571-85.

30. Wilhelm C, Elias F, Browaeys J, Ponton A, Bacri JC. Local rheological probes for complex fluids: Application to Laponite suspensions. Physical Review E. 2002;66(2):21502.

31. Wong JY, Velasco A, Rajagopalan P, Pham Q. Directed Movement of Vascular Smooth Muscle Cells on Gradient-Compliant Hydrogels. J Cell Sci. 1999;112:1967.

32. Ziemann F, Rädler J, Sackmann E. Local measurements of viscoelastic moduli of entangled actin networks using an oscillating magnetic bead micro-rheometer. Biophysical Journal. 1994;66(6):2210-6.

CHAPTER 5   Mechanical Properties of Bis-Crosslinked Hydrogels

5.1   Acrylamide and Polyacrylamide

Acrylamide is a synthetic monomer with a wide scope of industrial applications, mainly as a precursor in the production of several polymers such as polyacrylamide. Acrylamide is a highly water soluble vinyl monomer which is colorless and odorless, with a melting point of 84.5 °C. It is soluble in water, acetone and ethanol and is biodegradable[31]. Acrylamides are primarily carbon compounds with the basic chemical formula $R=CONH_2$ as shown in Figure 5-1. Acrylamide forms naturally in a wide variety of foods when they are cooked by the reaction of reducing sugars (such as glucose) with free asparagine, an amino acid present in many foods, during the browning reaction. Because of the potential of exposure to acrylamide, its effect in cells, tissues, animals and humans have been extensively studied[1,7,9,15,20,24,30,34]. Intensive research in this field is ongoing and significant progress has been already made.

Polyacrylamide (poly(2-propeneamide) or poly(1-carbamoylehylene)) is a polymer ($-CH_2CHCONH_2-$) formed from acrylamide subunits and can be readily crosslinked. The formation of polyacrylamide involves addition of ammonium persulphate (APS) and tetramethylenediamine (TEMED) to acrylamide. Ammonium persulphate forms free radicals when dissolved in water as shown in Figure 5-2. These free radicals react with acrylamide in the solution in a free radical addition reaction to form polyacrylamide. TEMED acts as a catalyst (electron carrier) and increases the reaction rate. Figure 5-3 shows the polymerization of polyacrylamide. However, in the

presence of a crosslinker such as *N,N'*-methylene-bis(acrylamide), the polymerization will result in the formation of bis-polyacrylamide crosslinked gels (commonly referred to as **'bis-gels'**). Bis, as shown in Figure 5-4, has reactive ends that are identical to the reactive end of the acrylamide monomer. Due to this similarity, the crosslinker can be incorporated into a growing polymer chain by free radical polymerization. Figure 5-5 shows the co-polymerization of bis and acrylamide.

5.2   Applications of Polyacrylamide

Polyacrylamide gels are widely used as separation matrices in the electrophoresis of biomolecules such as proteins or DNA fragments. The polyacrylamide gel acts as a porous supporting medium through which the charged molecules migrate in the presence of an electric field. Polyacrylamide is ideal in this diagnostic role because of its chemical inertness as a result of which it does not react with the biomolecules. Recent advances in the field of biomaterials have given rise to many other applications of polyacrylamide. By adjusting the total acrylamide concentration, polyacrylamide gels with a wide range of pore size can be formed to suit the size fractionation of a variety of proteins[5,12,25,29]. Owing to its stability over wide *p*H intervals (*p*H 3-11), applicability to the entire molecular weight range, as well as simplicity and economy, polyacrylamide has found widespread applications ranging from microanalysis to micro-fractionation for proteins, nucleic acids and other biomolecules. Polyacrylamide gels have also been used as carriers for delivery of drugs and bioactive compounds[11,33], as synthetic smart materials that can respond to stimulus[8,27], as matrices in extra-corporeal toxin removal modalities[19] and as non-absorbable soft tissue fillers in reconstructive surgery and tissue augmentation[2,9,35].
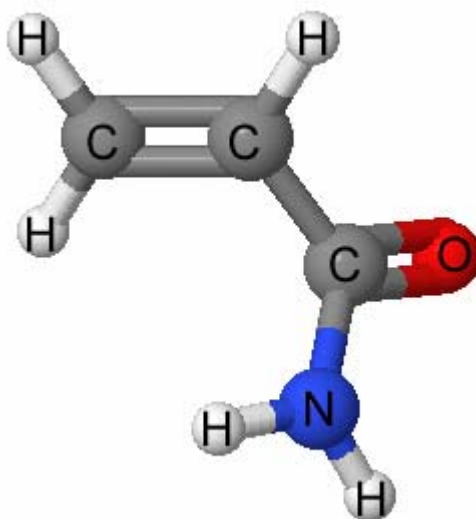
Figure 5-1. Chemical structure of acrylamide monomer
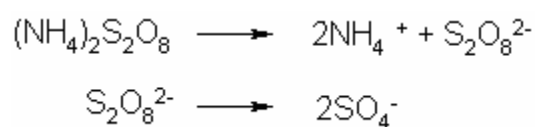
Figure 5-2. Free radicals created by dissolving APS in water
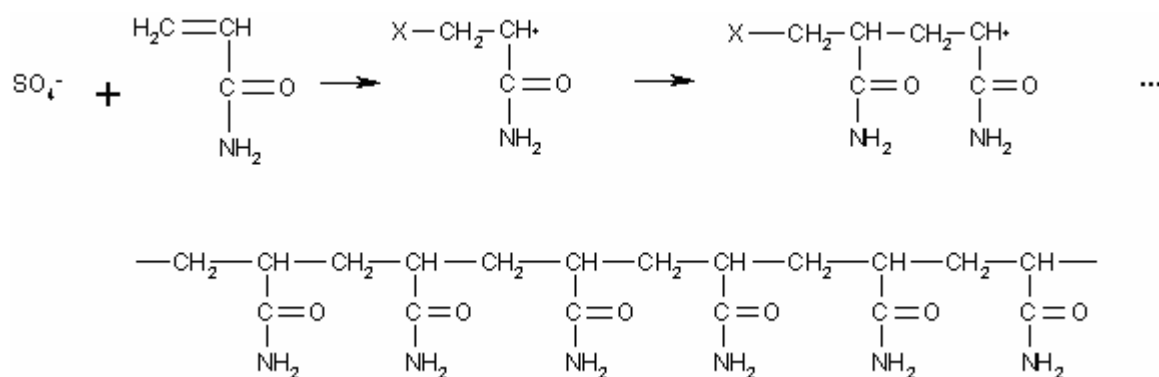
Figure 5-3. Free radical polymerization of acrylamide

$$H_2C\!=\!CH$$
$$|$$
$$C\!=\!O$$
$$|$$
$$NH$$
$$|$$
$$CH_2$$
$$|$$
$$NH$$
$$|$$
$$C\!=\!O$$
$$|$$
$$H_2C\!=\!CH$$
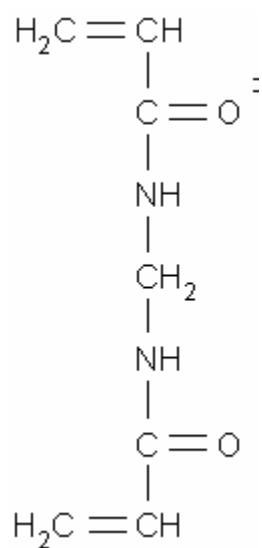
Figure 5-4. Chemical structure of bis crosslinker

acrylamide   N,N'-methylene-bis(acrylamide)   Representative element of crosslinked polyacrylamide
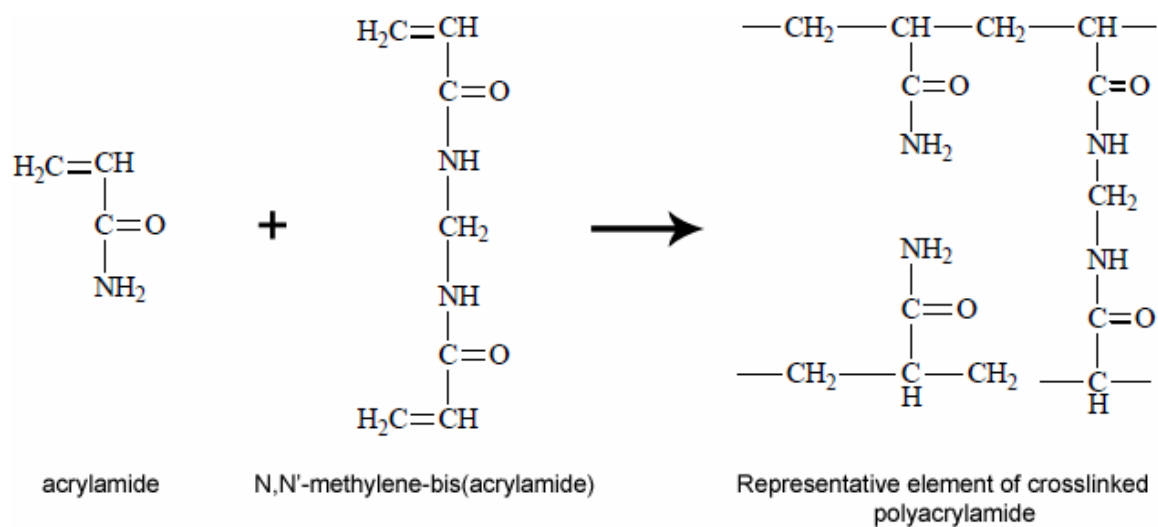
Figure 5-5. Co-polymerization of acrylamide chains with bis crosslinker

In addition, Wang and coworkers[37] have recently popularized bis-gels as substrates for cell culture. One of the main advantages of bis-gels is the vast range of stiffness that these gels can span over. The stiffness can be varied by modifying the monomer (%T) and crosslinker (%C) concentrations. Previous investigators have reported gels with stiffness ranging from as low as 21 Pa to 80,000 Pa. Over this wide range, the gels have been used as substrates for a variety of cell types such as rat kidney epithelial cells[26,36], neuronal cells[16,18], cortical cells[14], mouse spinal cord cells[13], hepatocytes[22,28], bovine vascular smooth muscle cells[38] and PC-12 neuronal like cells[21]. However these gels lack the ability to dynamically change their stiffness because of the covalent crosslinking. Thus cellular response is limited by the lack of an avenue to dynamically tune substrate mechanical properties. Dynamic mechanical stiffness can be achieved by introducing DNA as a crosslinker (instead of bis), the details of which are discussed in detail in Chapter 6. In this chapter, work in which the four magnet manipulator described earlier is utilized to characterize the mechanical properties of three different concentrations of bis-gels is described. The local Young's modulus, shear modulus and Poisson's ratio as a function of gel composition is determined and compared with global properties obtained using other techniques such as rheology and manipulation of beads.

5.3   Polyacrylamide Gel Preparation

Polyacrylamide gels with stiffness spanning over a wide range are generally prepared by varying the concentrations of acrylamide monomer and bis crosslinker. The two concentrations are defined by the values of %T (total acrylamide + bis concentration

in grams per 100 milliliters of gel) and %C (weight percent of bis in total acrylamide + bis monomer). Premixed monomer solutions are readily available in various mix ratios from chemical suppliers. For the present study, dilute polyacrylamide solutions were prepared by using a premixed 40% monomer solution of acrylamide and bis in a 29:1 mix ratio (Sigma-Aldrich, St Louis, MO). This corresponds to a %T value of 40 and %C value of 3.3. The premixed solution allows preparing polyacrylamide gels of different concentrations, by varying the amount of water and other components in the gel. The volume of acrylamide stock solution (V) required to prepare a particular concentration gel (%T) is then determined by using the formula:

$$V = (total\ gel\ volume)\frac{\%T}{40\%}$$
Eq. 55

Three different monomer concentrations of %T = 3, 4 and 5 were used to prepare the gels (referred to as '**3% bis-gels**', '**4% bis-gels**' and '**5% bis-gels**' hereafter). Polymerization is initiated by adding 2% total gel volume of 5% ammonium persulphate (APS) and 2% total gel volume of *N,N,N',N'*-tetramethylethylene (TEMED) at 1:5 dilution is used as a catalyst to speed up the gel formation. The total amount of deionized water to be added is determined by subtracting the combined amounts of acrylamide stock solution, APS and TEMED from the total gel volume. For the experiments involving the four magnet setup, deionized water with nickel needles dispersed in it, was used.

5.3.1 Gels for 'Rheometer Experiments'

In order to calculate the proportionality constant (m_p) that relates the magnetic field at the location of the needle to the force applied by the four magnet setup on the

needle (Eq. 10 and Eq. 11), a gel with known stiffness was required. For this purpose, a 3% bis-gel was prepared and its stiffness was independently measured using a Rheometrics SR-2000 parallel plate rheometer (TA Instruments, New Castle, DE). A 25 mm hole was punched in a 4 mm thick layer of poly-dimethyl siloxane (PDMS). 800 µL of the 3% bis-gel (60 µL acrylamide stock solution + 16 µL APS + 16 µL TEMED + 708 µL deionized water) was cast inside this PDMS well and the thin layer of gel was gently transferred using a spatula onto the bottom plate of the rheometer. The top plate was lowered to a height of 0.8 mm and the dynamic storage modulus (or shear modulus) was measured at 1% shear strain amplitude at frequencies ranging from 0.1 to 10 Hz.

5.3.2 Gels for 'Microneedle Experiments'

Since the space between the four poles of the magnet is limited to a 1 cm-square area, individual wells from a 96-well plate (Greiner Bio-One, Monroe, NC) (referred to as '**96 wells**' hereafter) were used to hold the gels. These wells have an inner diameter of 8 mm, and thus 50 µL gives rise to a 1 mm thick gel. Large samples (500 µL) of 3%, 4% and 5% bis-gels were prepared in 2.0 mL graduated, flat cap microcentrifuge tubes (Fisher Scientific) to maintain homogeneity across different samples. Acrylamide stock solution, deionized water with microneedles and APS were added initially, while TEMED was added just before starting the experiment. After adding TEMED the contents of the centrifuge tube were vigorously mixed using a vortexer. 50 µL of the sample was then quickly transferred into each of the wells used for the experiments. The gels were then allowed to completely polymerize at room temperature.

5.3.3 Gels for 'Bead Experiments'

In order to verify the Young's modulus data obtained from the microneedle experiments, magnetic bead experiments as described in Lin et al.[23] were performed on 3%, 4% and 5% bis-gels. In brief, 200 µL samples of the bis-gels, with an embedded 0.79 mm stainless steel bead, were prepared in 0.6 mL centrifuge tubes and placed in the test apparatus as shown in Figure 3-3. Magnetic force was applied using the calibrated electromagnet and the linear displacement of the bead was measured by time lapse images using a video camera. The global Young's modulus of the medium was calculated using Eq. 4.

5.4   Results

It was determined in Section 3.8 that nickel needles at the micron level behave like permanent magnetic materials, as a permanent magnetization spontaneously occurs when the needle dimensions become comparable to the characteristic magnetic domain size of the magnetic material. Thus we use Eq. 10 and Eq. 11 to determine the force and the torque acting on the microneedles. However, this would require calibrating the four magnet setup first, to convert magnet fields into forces and torques.

5.4.1   Calibration Constant

For the purpose of calculating the calibration constant (m_p), a large sample (1000 µL) of 3% bis-gel was prepared and divided into two portions. 800 µL of the gel was used for the rheometer experiments, while 50 µL each, of the remaining gel was

transferred to four 96 wells for use in the four magnet experiments. A gradient magnetic field was applied and the displacement of the needles was measured in each case. By knowing the gradient of magnetic field ($grad(B_0)$), the shear modulus (G) and the displacement (δ) of the needles, the proportionality constant m_p was calculated from Eq. 10, Eq. 35 and Eq. 52 as

$$m_p = \frac{2\pi L}{\ln(L/2R)} \frac{G\delta}{grad(B_0)\cos\alpha}$$

Eq. 56

where L and R are the respective length (*10 μm*) and radius (*0.5 μm*) of the microneedles, and α is the initial angle at which the needle is aligned with the magnetic field.

Figure 5-6 shows a representative set of data for the rheological testing of 3% bis-gels, as frequency was varied between 0 and 10 Hz. The shear (or storage) modulus increased gradually and then dropped off at higher frequencies. Examination of the gels revealed that they ruptured at higher frequencies, and this could be the reason for the decrease in modulus. Table 5-1 shows the data obtained from four experiments performed using rheometer on 3% bis-gels. The average shear modulus of these gels was determined to be equal to **354 ± 16 Pa**. When the same gel was tested in the four magnet setup, application of a gradient field of 5.82 G/μm displaced the microneedle by 2.43 μm. By using the information, obtained from four such experiments, in Eq. 56, the average value of the calibration constant (m_p) was calculated to be **2.0x10^{-16} N-m/G**. This value of m_p was used to calculate the force and torque in all the remaining microneedle experiments.
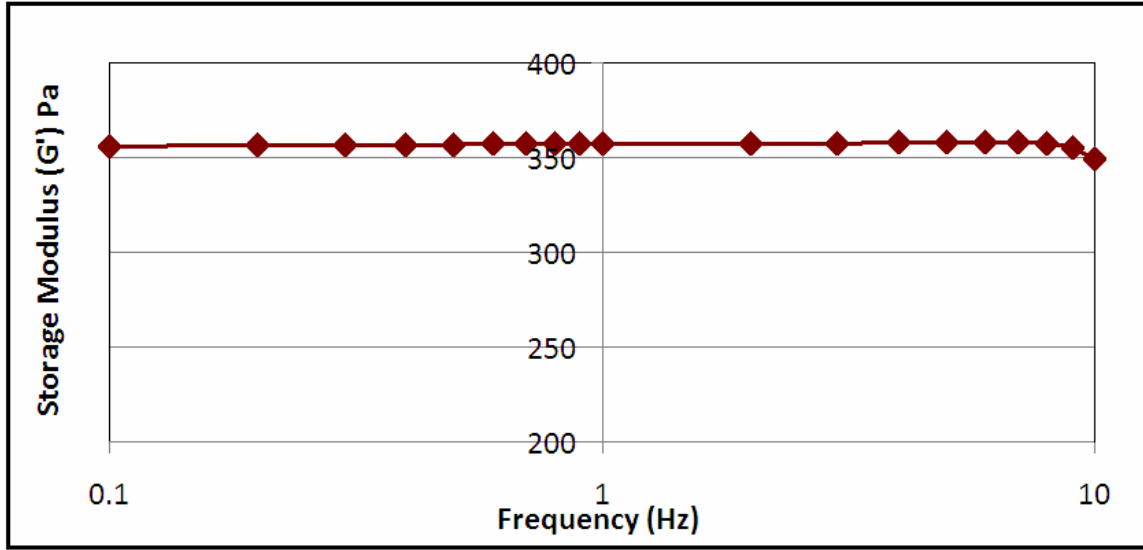
Figure 5-6. Shear modulus calculation using rheometer for 3% bis-gels

Table 5-1. Shear modulus of 3% bis-gels obtained from rheometer experiments

Sample	Shear Modulus (Pa)
1	375
2	337
3	348
4	356

5.4.2 Mechanical Properties of Bis-Gels

Four samples each of 3%, 4% and 5% bis-gels with microneedles embedded in them were prepared and tested in the four-magnet setup. In each sample, two needles at different locations were isolated and either a gradient magnetic field or a uniform magnetic field was applied. Figure 5-7 shows translation and rotation of the needles under the influence of these fields. In the gradient magnetic field, the needle displaced towards the left by a distance represented by δ. Similarly under the influence of the torque field, the needle rotated by an angle θ. The displacement and rotation angle data

under the influence of the corresponding force or torque is presented in Table 5-2. The samples are labeled from 1 to 4, while A and B represent two needles at different locations in the same sample. It was observed that the force acting on the needles varies according the location of the needle in the magnet setup. The needles closer to the attracting pole have a larger force compared to the needles farther away. It was also observed that as the crosslinker concentration increased from 3% to 5%, the displacements and rotation angles of the needles decreased. Young's modulus, shear modulus and Poisson's ratio values are shown in Table 5-3. The average Young's moduli for the 3%, 4% and 5% bis-gels was found to be equal to **890.66 ± 99.88 Pa**, **1414.23 ± 176.54 Pa** and **5668.26 ± 813.41 Pa** respectively. The average shear moduli for these gels were **309.47 ± 37.46 Pa**, **495.78 ± 65.32 Pa** and **1890.94 ± 282.19 Pa**. The Poisson's ratio for these gels varied between **0.38** and **0.49**.
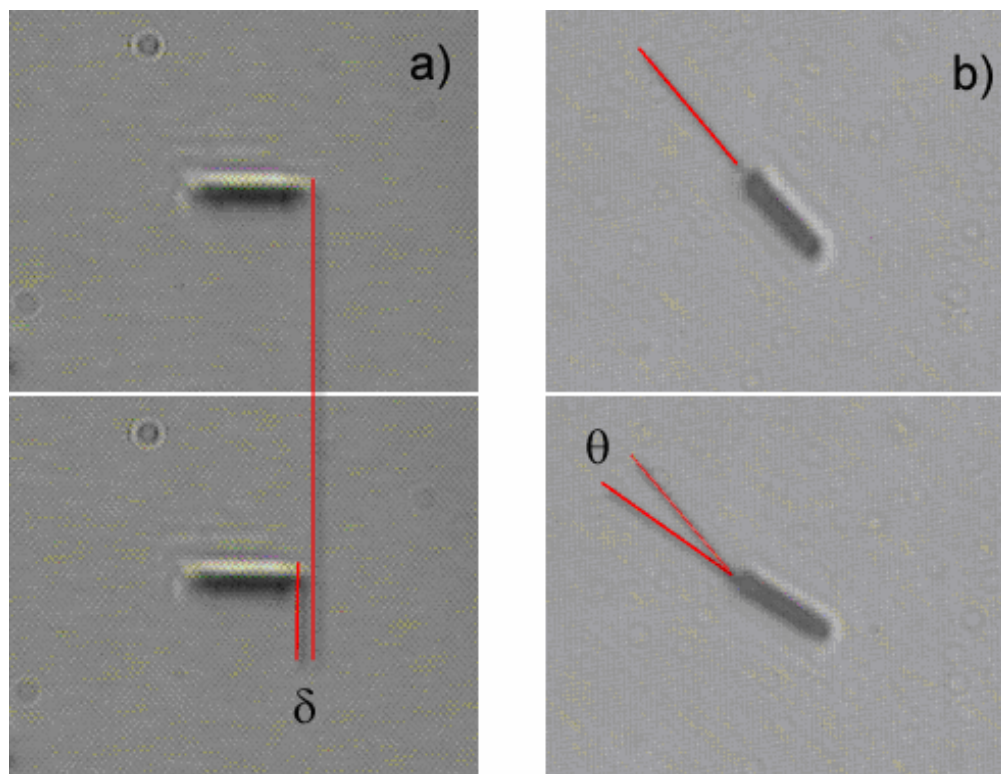
Figure 5-7. Representative images of needles taken using a 50X objective lens

a) Displacement of the needle under influence of a gradient magnetic field. b) Rotation of the needle under influence of uniform magnetic field

Table 5-2. Displacement and rotation angles of needles in bis-gels

Bis-gel conc.	#	Force (nN)	Displacement (µm)	Torque (nN-µm)	Rotation angle (deg)
3%	1A	23.3	2.43	26.1	10.3
	1B	22.9	2.67	26.2	11.2
	2A	20.1	3.21	30.1	17.1
	2B	30.3	3.40	26.2	12.1
	3A	23.3	2.80	25.5	11.1
	3B	14.0	1.60	23.1	10.8
	4A	21.1	2.67	27.1	12.6
	4B	26.7	2.89	25.9	10.6
4%	1A	31.7	2.15	25.8	7.0
	1B	22.8	1.76	22.4	6.6
	2A	26.7	1.77	19.7	4.7
	2B	15.4	1.32	29.5	9.7
	3A	16.6	1.41	21.2	6.3
	3B	16.2	1.43	24.0	8.4
	4A	26.8	1.72	23.2	5.9
	4B	21.4	1.42	27.1	7.5
5%	1A	24.7	0.39	53.8	3.3
	1B	24.3	0.39	54.5	3.2
	2A	40.9	0.80	57.9	4.1
	2B	44.6	0.91	54.6	3.4
	3A	36.4	0.73	44.5	1.1
	3B	26.4	0.51	47.7	3.3
	4A	26.7	0.63	49.0	4.2
	4B	33.7	0.78	54.1	4.7

Table 5-3. Young's modulus, shear modulus and Poisson's ratio of bis-gels

Bis-gel conc.	#	F/δ (x10^{-3}) (N/m)	Γ/θ (x10^{-13}) (N-m)	Shear Modulus (Pa)	Young's Modulus (Pa)	Poisson's Ratio
3%	1A	9.58	1.45	351.09	1013.77	0.44
	1B	8.57	1.34	314.05	919.38	0.46
	2A	6.27	1.01	229.91	680.88	0.48
	2B	8.92	1.24	327.07	900.90	0.38
	3A	8.30	1.32	304.34	896.49	0.47
	3B	8.77	1.23	321.30	888.52	0.38
	4A	7.89	1.23	289.25	846.59	0.46
	4B	9.24	1.40	338.73	978.72	0.44
4%	1A	14.75	2.11	540.44	1516.15	0.40
	1B	12.97	1.94	475.29	1365.87	0.44
	2A	15.10	2.40	553.37	1631.63	0.47
	2B	11.70	1.74	428.62	1227.26	0.43
	3A	11.74	1.93	430.15	1284.31	0.49
	3B	11.33	1.64	415.20	1170.50	0.41
	4A	15.57	2.25	570.62	1608.98	0.41
	4B	15.08	2.07	552.54	1509.17	0.37
5%	1A	63.25	9.34	2317.93	6610.94	0.43
	1B	62.27	9.77	2282.10	6693.62	0.47
	2A	51.11	8.09	1873.20	5514.26	0.47
	2B	48.98	9.21	1795.08	5568.23	0.55
	3A	49.88	23.20	1828.00	6198.53	0.70
	3B	51.70	8.27	1894.68	5602.04	0.48
	4A	42.42	6.69	1554.70	4569.63	0.47
	4B	43.16	6.60	1581.82	4588.83	0.45

As the percentage of crosslinker increased from 3% to 5%, the value of F/δ also increased. This means that for the same force the needle displaces by a smaller amount in the gel. Similarly, the value of Γ/θ also increased with increase in concentration, indicating that for the same amount of torque, the needle rotated by a smaller amount. The shear modulus and elastic modulus also increase with increasing concentration. Similar trend in the stiffness for bis-gels with increasing concentration was observed by numerous researchers[4,6,17,32,39].

5.5   Discussion of Bis-Gel Experiments

In order to check for any local creep and viscous relaxation effects, the needles were monitored after switching off the magnetic field. It was observed that due to small elastic deflections, the needles always returned to their starting positions following the completion of each measurement. Also the viscoelastic response was rapid compared to the 5-10 minutes time frame in which the measurements were performed. The linear force-delta curves obtained for each gel as shown in Figure 5-8, confirm that the viscoelastic components did not effect the measurements. The linearity of the load-displacement plots also justifies the application of linear elasticity theory in deriving the equations for the shear modulus and Young's modulus. Since the curve passes through $(0, 0)$, any point on the straight line can be taken to measure the stiffness (F/δ) of the gels. However, in this study the point with maximum displacement was considered in all the experiments, as the displacements and rotations are minute at lower magnetic fields and are comparable to the resolution of the camera (0.2 microns per pixel) when using a 50X objective lens.
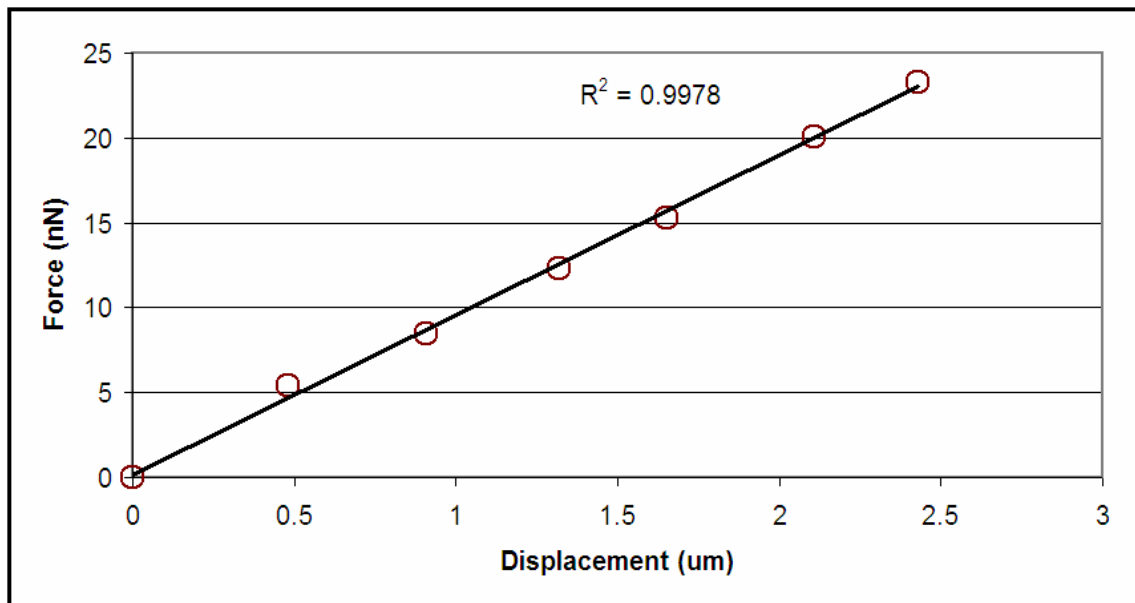
Figure 5-8. Force applied v/s displacement of needle

In order to compare the local properties obtained from the needle experiments with the bulk elastic properties, 3%, 4% and 5% bis-gels were cast as discs and tested in the rheometer as described previously. The bulk shear modulus obtained from the rheometer compared well with the local shear modulus obtained from needle experiments as shown in Figure 5-9. Statistical analysis was performed using Prism Software (La Jolla, CA). One-way ANOVA was performed on data with 3 or more conditions followed by Dunnett's Multiple Comparison Test comparing all conditions to the lowest percentage gel. It is obvious that the results match better for 3% bis-gels as the calibration was done using the same gels. However at higher stiffness, the difference between bulk modulus and local shear modulus increased. This inconsistency might be due to the very small displacements obtained in higher stiffness gels while using the four magnet setup. This

can be resolved by increasing the size of the magnets and the gradient field developed, which in turn increases the force acting on the needles.

In addition to the rheometer experiments, bead experiments as described before were also performed on the 3%, 4% and 5% bis-gels. The Young's modulus obtained by this method is referred to as the global elastic modulus of the gel. A comparison of the global elastic modulus with the local elastic modulus obtained from the needle experiments is done in Figure 5-10. The results match well, although the global elastic modulus, which assumes Poisson's ratio to be equal to one-half, was found to vary by 3-9% from the local elastic modulus. This disparity might be due to the inhomogeneities present in the hydrogels as seen from the increase in the error with increasing stiffness. In the studies performed on polyacrylamide by Cohen et al.[10] and Benguigui et al.[3], it was observed that at higher crosslinker densities, the inhomogeneities in a hydrogel are more prominent than those at lower crosslinker densities. The results obtained in the present study confirm this.

In order to assess the sensitivity of Poisson's ratio with respect to the gel stiffness, it is convenient to write Eq. 51 in the form

$$G = f(v)\frac{3\ln(L/2R)}{2\pi L^3}\frac{\Gamma}{\theta}$$
<div align="right">Eq. 57</div>

where

$$f(v) = \frac{3-4v}{1-v}.$$
<div align="right">Eq. 58</div>

Assuming Γ/θ to be a constant for a particular gel, the shear modulus would vary with Poisson's ratio as a factor of $f(v)$. This factor is plotted against the Poisson's ratio in Figure 5-11. It is observed that, as the Poisson's ratio is varied between 0.36 and 0.49,

f(v) changes by almost 20%. This is a large error in Poisson's ratio and will lead to an error of 20% in the determination of the shear modulus. This makes the accurate measurement of Poisson's ratio important in determining the local properties of soft media. However it should be observed that in the range of motion considered in the present study, Poisson's ratio may not have a significant effect on the displacement or the rotation angles.
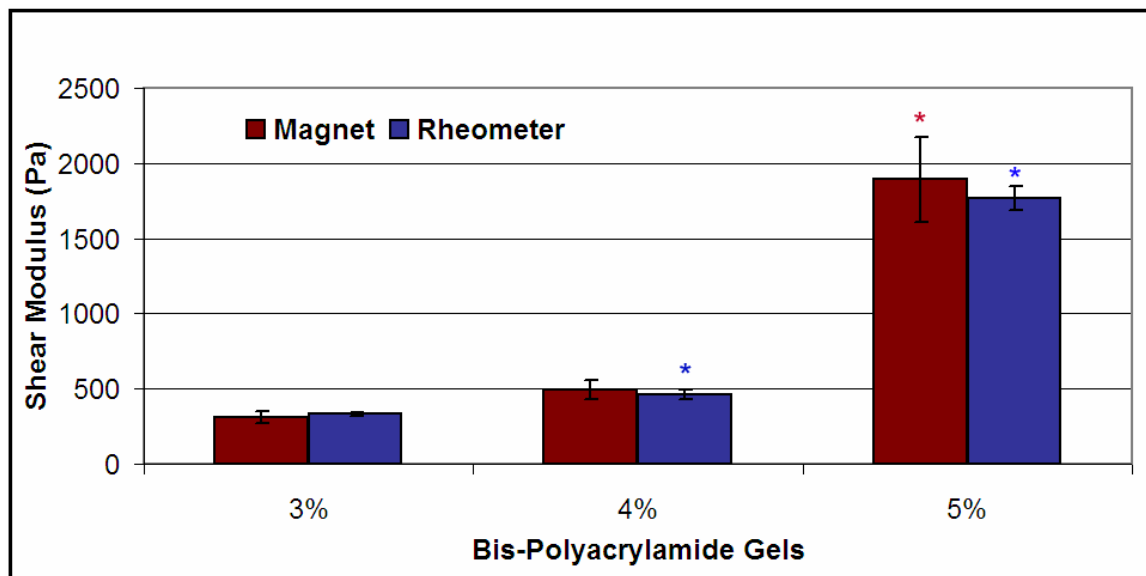
Figure 5-9. Shear modulus obtained by needle and rheometer experiments
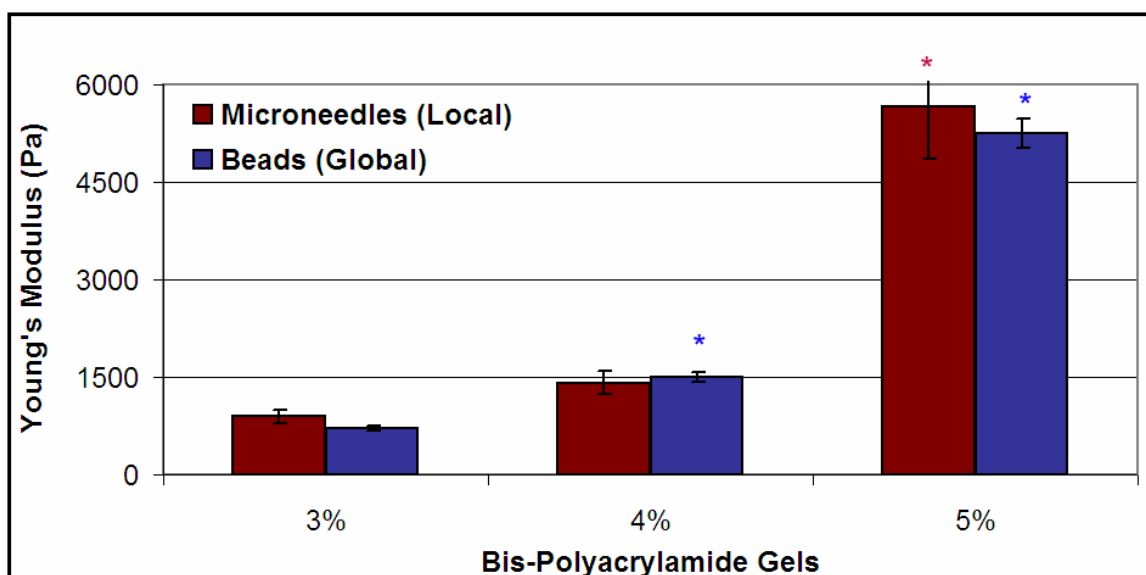
Figure 5-10. Young's modulus obtained by needle and bead experiments
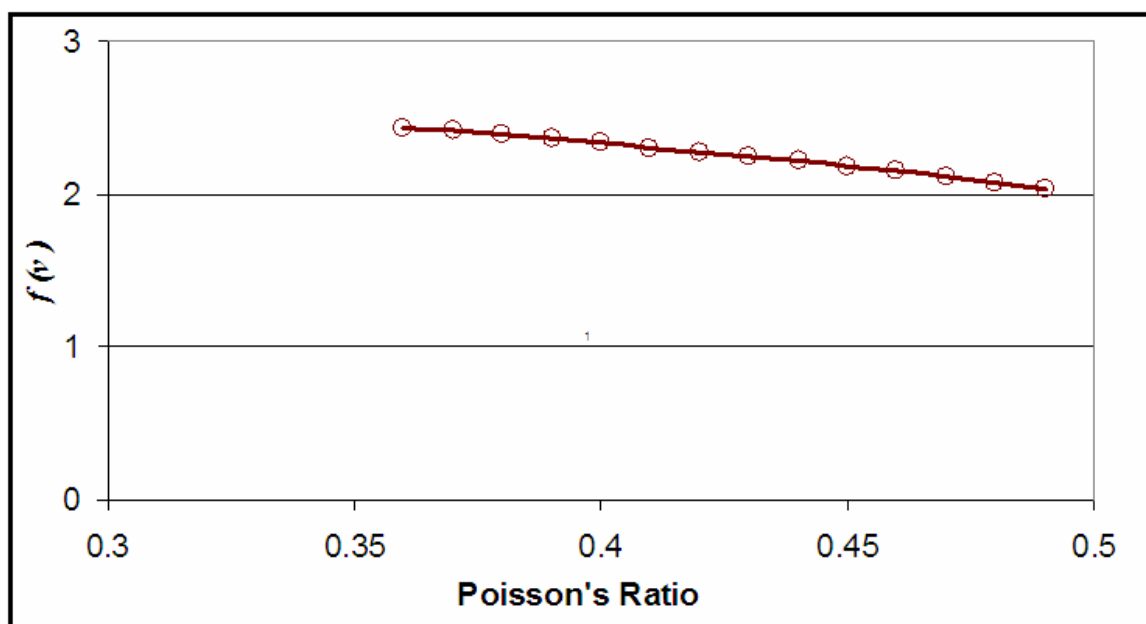
Figure 5-11. Effect of Poisson's ratio on the shear modulus of hydrogels

Shear modulus is directly proportional to *f(v)* and varies by almost 20% as Poisson's ratio is increased from 0.36 and 0.49.

It should be noted that the present method cannot completely characterize an anisotropic gel or material. In order to demonstrate that, one would have to be able to map out how the stiffness of the gel depends on the direction of the applied force and the direction of the applied torque for any arbitrary direction. Among other things, it would require that we be able to displace the inclusion along the z axis as well as the x and y axis which is beyond the scope of the present study. Also in the anisotropic case *G*, *E*, and *v* are no longer adequate to describe the mechanical properties of the material, these must, instead be replaced by tensor quantities.

It is also interesting to note from Table 5-2 and Table 5-3 that in the same sample, the properties obtained at different locations were dissimilar. For example, in sample 2 of the 3% bis-gel, the shear moduli were found to be 229.91 Pa and 327.01 Pa for the needles at locations A and B. Similarly the Young's moduli were found to be 680.88 Pa and 900.9 Pa respectively. This shows the heterogeneity of the gels and emphasizes the use of this method in calculating the local properties, rather than the global properties, of soft substrates. Also, it should be noted that the methodology used in the current study is independent of the medium, and thus the capabilities can be useful for the investigation of the local mechanical properties of various other soft materials at the micron scale.

5.6   Conclusions

Bis-crosslinked polyacrylamide gels are used by many researchers in tissue engineering as substrates for cell culture. The stiffness of these substrates plays an important role in the behavior of cells. Well established methods such as compression, indentation, manipulation of beads and AFM were used to characterize the stiffness of

these gels. However, these methods usually provide only the global elastic modulus and are either destructive or cannot be used in conjunction with cells. In this study we developed a non-intrusive, non-destructive apparatus and utilized it to determine the properties of inhomogeneous materials at the 10 μm scale. Measurements of the two independent quantities F/δ and Γ/θ were made to obtain the Young's modulus, shear modulus and Poisson's ratio of the soft substrates. It was also observed that Poisson's ratio could have about 3-9% effect on the measurement of the shear modulus of bis-gels. This gives us a better understanding of bis-gels and would enhance the study of the behavior of cells on these substrates.

References

1. Adler ID, Ingwersen I, Kliesch U, El Tarras A. Clastogenic effects of acrylamide in mouse bone marrow cells. Mutation research. 1988;206(3):379.
2. Bello G, Jackson IT, Keskin M, et al. The use of polyacrylamide gel in soft-tissue augmentation: an experimental assessment. Plastic and Reconstructive Surgery. 2007;119(4):1326.
3. Benguigui L, Boué F. Homogeneous and inhomogenous polyacrylamide gels as observed by small angle neutron scattering: A connection with elastic properties. The European Physical Journal B. 1999;11(3):439-44.
4. Beningo KA, Lo CM, Wang YL. Flexible Polyacrylamide Substrata for the Analysis of Mechanical Interactions at Cell—Substratum Adhesions. Methods in cell-matrix adhesion. 2002:325.
5. Bishop DH, Claybrook JR, Spiegelman S. Electrophoretic separation of viral nucleic acids on polyacrylamide gels. Journal of molecular biology. 1967;26(3):373.
6. Boudou T, Ohayon J, Picart C, Tracqui P. An extended relationship for the characterization of Young's modulus and Poisson's ratio of tunable polyacrylamide gels. Biorheology. 2006;43(6):721-8.
7. Bull RJ, Robinson M, Laurie RD, et al. Carcinogenic effects of acrylamide in Sencar and A/J mice. Cancer research. 1984;44(1):107.
8. Cao W, Cudney HH, Waser R. Smart materials and structures. Proceedings of the National Academy of Sciences of the United States of America. 1999;96(15):8330.
9. Christensen LH, Breiting VB, Aasted A, Jørgensen A, Kebuladze I. Long-term effects of polyacrylamide hydrogel on human breast tissue. Plastic and Reconstructive Surgery. 2003;111(6):1883.
10. Cohen Y, Ramon O, Kopelman IJ, Mizrahi S. Characterization of inhomogeneous polyacrylamide hydrogels. Journal of Polymer Science Part B Polymer Physics. 1992;30(9):1055-67.
11. Davis BK. Control of diabetes with polyacrylamide implants containing insulin. Cellular and Molecular Life Sciences (CMLS). 1972;28(3):348-.
12. Elson E, Jovin TM. Fractionation of oligodeoxynucleotides by polyacrylamide gel electrophoresis. Analytical biochemistry. 1969;27(2):193-204.
13. Flanagan LA, Yo-El Ju BM, Osterfield M, Janmey PA. Neurite branching on deformable substrates. Neuroreport. 2002;13(18):2411.
14. Georges PC, Miller WJ, Meaney DF, Sawyer ES, Janmey PA. Matrices with compliance comparable to that of brain tissue select neuronal over glial growth in mixed cortical cultures. Biophysical journal. 2006;90(8):3012-8.
15. He FS, Zhang SL, Wang HL, et al. Neurological and electroneuromyographic assessment of the adverse effects of acrylamide on occupationally exposed workers. Scandinavian journal of work, environment & health. 1989;15(2):125.

16.   Jiang FX, Yurke B, Firestein BL, Langrana NA. Neurite outgrowth on a DNA crosslinked hydrogel with tunable stiffnesses. Annals of Biomedical Engineering. 2008;36(9):1565-79.

17.   Jiang G, Huang AH, Cai Y, Tanase M, Sheetz MP. Rigidity sensing at the leading edge through V 3 Integrins and RPTP. Biophysical journal. 2006;90(5):1804-9.

18.   Jiang FX, Georges PC, Li B, et al. Cell growth in response to mechanical stiffness is affected by neuron-astroglia interactions. The Open Neuroscience Journal. 2007;1(1):7-14.

19.   Kaplan AA, Epstein M. Extracorporeal blood purification in the management of patients with hepatic failure. 1997:576.

20.   Kuperman AS. Effects of acrylamide on the central nervous system of the cat. Journal of Pharmacology and Experimental Therapeutics. 1958;123(3):180.

21.   Leach JB, Brown XQ, Jacot JG, Dimilla PA, Wong JY. Neurite outgrowth and branching of PC12 cells on very soft substrates sharply decreases below a threshold of substrate rigidity. Journal of Neural Engineering. 2007;4:26–34.

22.   Li L, Sharma N, Chippada U, et al. Functional modulation of ES-derived hepatocyte lineage cells via substrate compliance alteration. Annals of Biomedical Engineering. 2008;36(5):865-76.

23.   Lin DC, Yurke B, Langrana NA. Mechanical properties of a reversible, DNA-crosslinked polyacrylamide hydrogel. Journal of biomechanical engineering. 2004;126:104.

24.   LoPachin RM, Schwarcz AI, Gaughan CL, Mansukhani S, Das S. In vivo and in vitro effects of acrylamide on synaptosomal neurotransmitter uptake and release. NeuroToxicology. 2004;25(3):349-63.

25.   Maizel Jr JV. Polyacrylamide gel electrophoresis of viral proteins. Methods Virol. 1971;5:179-246.

26.   Pelham RJ, Wang Y. Cell locomotion and focal adhesions are regulated by substrate flexibility. Proceedings of the National Academy of Sciences of the United States of America. 1997;94(25):13661.

27.   Roy I, Gupta MN. Smart polymeric materials: emerging biochemical applications. Chemistry & biology. 2003;10(12):1161-71.

28.   Semler EJ, Ranucci CS, Moghe PV. Tissue assembly guided via substrate biophysics: applications to hepatocellular engineering. Advances in biochemical engineering, biotechnology. 2006;102:1-46.

29.   Shatkin AJ, Sipe JD, Loh P. Separation of ten reovirus genome segments by polyacrylamide gel electrophoresis. Journal of Virology. 1968;2(10):986.

30.   Shelby MD, Cain KT, Hughes LA, Braden PW, Generoso WM. Dominant lethal effects of acrylamide in male mice. Mutation research. 1986;173(1):35-40.

31.   Smith EA, Prues SL, Oehme FW. Environmental degradation of polyacrylamides. Ecotoxicology and Environmental Safety. 1997;37(1):76-91.

32.   Solon J, Levental I, Sengupta K, Georges PC, Janmey PA. Fibroblast adaptation and stiffness matching to soft elastic substrates. Biophysical journal. 2007;93(12):4453-61.

33.   Soppimath KS, Kulkarni AR, Aminabhavi TM. Chemically modified polyacrylamide-g-guar gum-based crosslinked anionic microgels as pH-sensitive

drug delivery systems: preparation and characterization. Journal of Controlled Release. 2001;75(3):331-45.

34.   Tyl RW, Friedman MA. Effects of acrylamide on rodent reproductive performance. Reproductive Toxicology. 2003;17(1):1-13.

35.   von Buelow S, von Heimburg D, Pallua N. Efficacy and safety of polyacrylamide hydrogel for facial soft-tissue augmentation. Plastic and Reconstructive Surgery. 2005;116(4):1137.

36.   Wang HB, Dembo M, Wang YL. Substrate flexibility regulates growth and apoptosis of normal but not transformed cells. American Journal of Physiology-Cell Physiology. 2000;279(5):C1345.

37.   Wang YL, Pelham RJ. Preparation of a flexible, porous polyacrylamide substrate for mechanical studies of cultured cells. Methods in enzymology. 1998;298:489-96.

38.   Wong JY, Velasco A, Rajagopalan P, Pham Q. Directed Movement of Vascular Smooth Muscle Cells on Gradient-Compliant Hydrogels†. Langmuir. 2003;19(5):1908-13.

39.   Yeung T, Georges PC, Flanagan LA, et al. Effects of substrate stiffness on cell morphology, cytoskeletal structure, and adhesion. Cell motility and the cytoskeleton. 2005;60(1):24-34.

CHAPTER 6   Mechanical Properties of DNA-Crosslinked Hydrogels

6.1   DNA (deoxyribonucleic acid)

DNA is a long biopolymer made from repeating units called nucleotides and carries the coded genetic instructions needed for the development and functioning of all living organisms[1]. Although each repeating unit is very small, DNA polymers can be very large molecules consisting of millions of nucleotides. Polymerization of DNA is limited to four such nucleotides; adenine (A), guanine (G), thymine (T) and cytosine (C); each of which consists of a nitrogen base, a 5 carbon sugar (2-deoxyribose) and one or more phosphate groups. Figure 6-1 shows the chemical structure of these nucleotides. In living organisms, DNA usually exists as a pair of molecules that are held together in a double stranded helical structure[26]. The sugars in DNA are joined together by phosphodiester bonds between the third and fifth carbon atoms of adjacent rings. These bonds are asymmetric and give a direction to the strands of DNA. The asymmetric ends are represented by 5' (5-prime) and 3' (3-prime) with the 5' end having a terminal phosphate group and the 3' end having a terminal hydroxyl group. The double helical phenomenon is mainly facilitated by the propensity to form complementary base pairs between A and T and between G and C. All of the bases of the DNA molecule are on the inside of the double helix, with the sugar phosphate backbone on the outside as shown in Figure 6-2. This arrangement places complementary bases in close proximity, thereby allowing hydrogen bonds to form between them[1,7,10]. Hydrogen bonds are formed when a hydrogen atom is shared between two electronegative atoms (e.g., nitrogen and nitrogen

or nitrogen or oxygen). Thymine and adenine form two hydrogen bonds while cytosine and guanine form three hydrogen bonds.
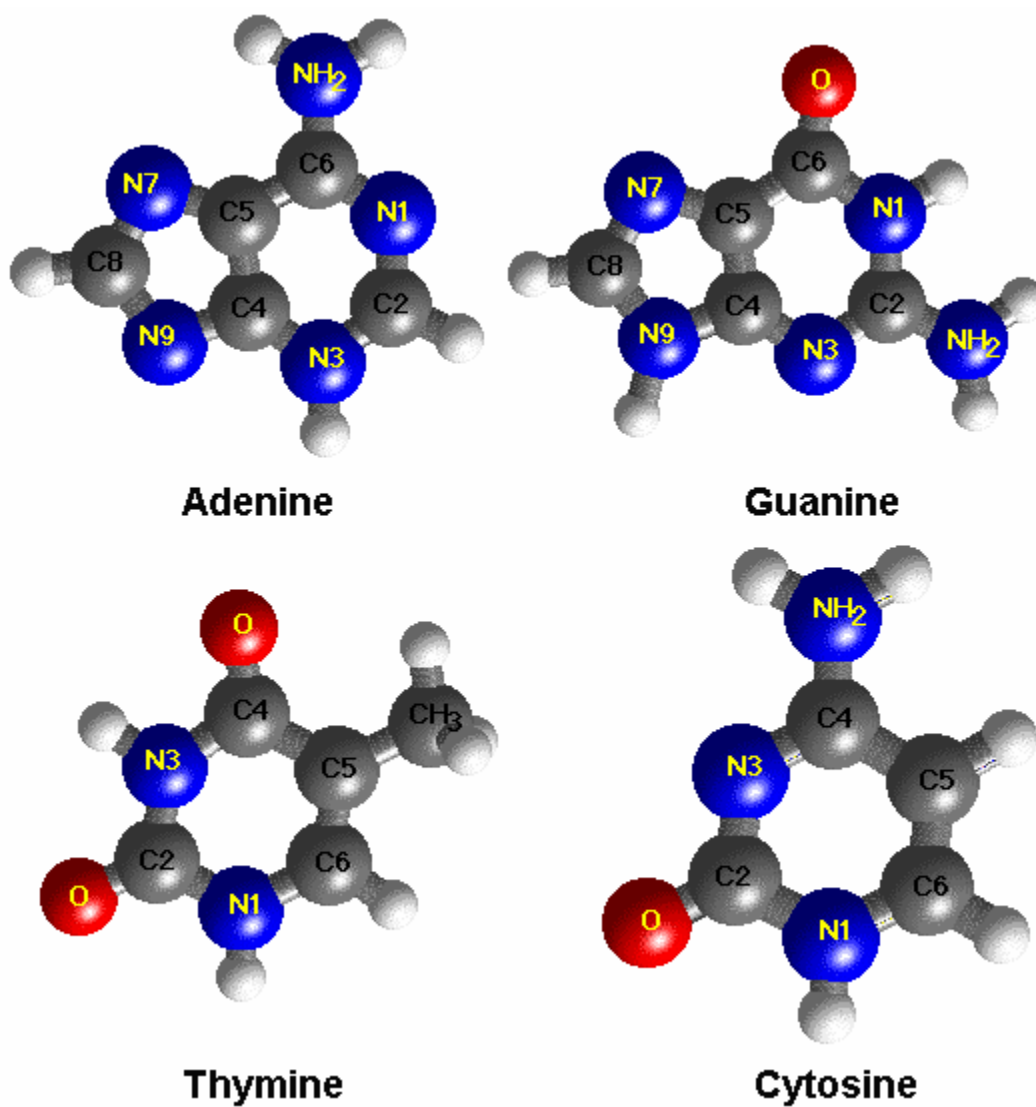
Figure 6-1. Chemical structures of nucleotides found in DNA
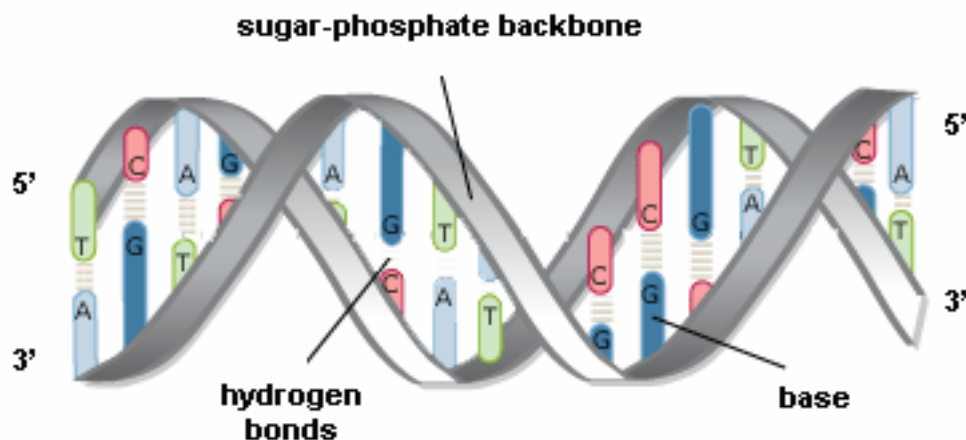
Figure 6-2. Double helical structure of DNA

Although DNA naturally occurs in cells as a carrier of biological information, recent advances have encouraged researchers to utilize individual strands of synthetic DNA as structural materials by incorporating random base sequences. Because certain sequences of DNA are mutually attractive (A – T and G – C), the synthetic strands can be programmed to achieve a minimum energy state, by decreasing the number of possible mismatched hybridizations in order to maximize efficiency of hybridization. Mismatch in hybridization can arise from undesired interactions between two strands or within the same strand, by the binding of complementary regions comprising of a small number of base pairs. This usually leads to the formation of secondary structures. In evaluating interactions, all possible pairs of strands must be considered: (1) the first strand and its compliment, (2) the second strand and its compliment, (3) the first strand and itself, (4) the second strand and itself, (5) the first and second strands and (6) the first strand and compliment of second strand. Seeman et al.[19,21] have pioneered the use of DNA as a structural material in nanotechnology by constructing a number of three dimensional geometric objects such as cubes[3], octahedron[28], knots[16], linked rings[15], two-dimensional

arrays[29] and molecular machines[20,23]. Several researchers have also designed and constructed DNA-based nanomachines driven by DNA motors and DNA nanoactuators. Others have created DNA-polymer conjugates for applications in gene therapy[2,8,27].

6.2 Hydrogels using DNA

Nagahara and Mastsuda[17] first demonstrated the use of short DNA strands to crosslink water-soluble polymer chains by reacting poly(*N,N*-dimethylacrylamide-co-*N*-acryloxyloxysuccinimide) with 5'-amino-modified 10-mer oligonucleotides consisting of adenine bases (oligoA) or thymine bases (oligoT). Two different crosslinked structures were produced as shown in Figure 6-3. Gelation of the polymers as well as thermo-reversibility of the crosslinking at elevated temperatures was demonstrated. In addition to the amino modifications, phosphoramidite, (trade name Acrydite) (Matrix Technologies, Hudson, NH) modifications have been designed for immobilizing synthesized, single-stranded DNA on solid supports for analysis. The reactive end of Acrydite-modified nucleotide is similar to that of acrylamide, and hence Acrydite-modified DNA molecules are commonly used in special gel electrophoresis applications such as capture assays, by copolymerizing the oligonucleotides with acrylamide monomer and bis crosslinker.
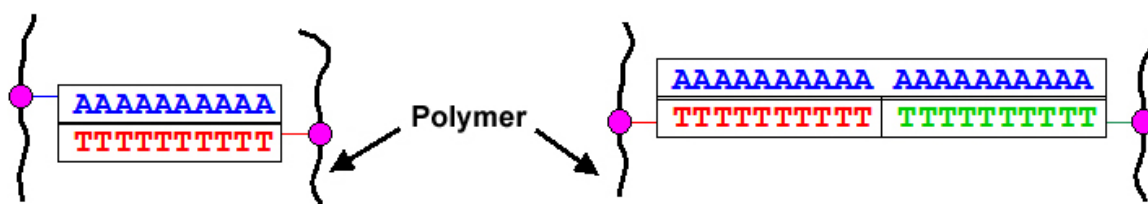
Figure 6-3. DNA-crosslinked structures of Nagahara and Matsuda

The oligonucleotides and their sequences are represented by rectangular boxes while the oligonucleotide-polymer connections are represented by dots.

Recently, Lin et al.[14] have devised a method in which two Acrydite-functionalized oligonucleotides were copolymerized with acrylamide, and a third DNA strand was added to crosslink the polyacrylamide chains, forming a DNA-crosslinked polyacrylamide hydrogel (referred to as "**DNA gels**" hereafter) as shown in Figure 6-4. The use of three-oligonucleotide system (SA1, SA2 and L2) imparts the polymer with greater capacity for altering its mechanical properties and provides many advantages over the traditional bis-crosslinked polyacrylamide hydrogels discussed in Chapter 5. Some of these advantages include:

- DNA hydrogels are thermo-reversible polymers with distinct melting points as the hydrogen bonds between complementary bases can be easily broken at higher temperatures.

- Additional crosslinker strands can be added to an existing DNA hydrogel and upon reheating, they hybridize with the existing side branches. Thus, stiffness of the gels can be altered on the fly.

- A "toehold" region can be incorporated into the crosslinker strand, and the crosslinker can be eliminated by the addition of a removal strand. This branch migration process occurs through a random walk process and permits the gel to be reversibly assembled and disassembled.
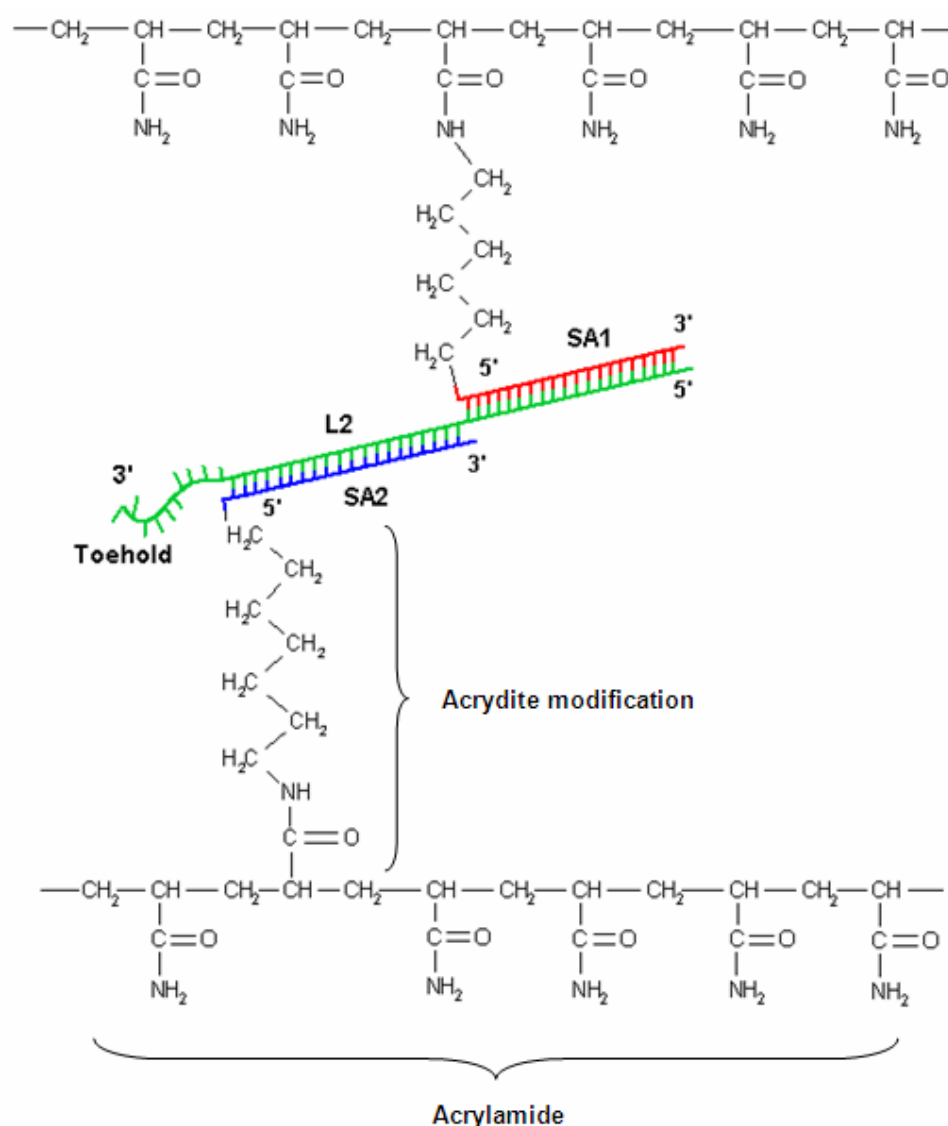
Figure 6-4. Two polymer chains crosslinked by a system of three DNA strands

The strands SA1 and SA2 are Acrydite-modified and L2 is the crosslinking strand (Lin et al.[14]).

6.3   Applications of DNA Hydrogels

Very recently, Jiang et al.[11,12] utilized such DNA hydrogels as substrates to examine the mechano-sensing of neural cells in the context of neuron-astroglia interactions. Owing to the dynamic nature of the local physiological environment of cells, bio-scaffolds with dynamic mechanical properties were desired. DNA hydrogels provide

one with the unique ability to modify mechanical properties of the scaffold via DNA delivery during cell culture without changing the environmental factors. Cell behavior was expected to be minimally influenced by the addition of DNA strands to the surrounding medium based on the difficulty with which DNA strands penetrate the cell wall of the Eukaryotic organisms. Also, should DNA enter the cell, it is expected to degrade without significantly altering the cell's biochemistry of behavior.

The freedom in the choice of base sequence allows for the construction of DNA-crosslinked hydrogels that can be degraded by particular restriction endonucleases or by particular messenger RNAs. This property combined with the reversible assembly and disassembly of the gel at temperatures below melting point of the crosslinks makes these gels attractive candidates for drug delivery applications. Such gels can also be engineered to possess tensegrity in which the polymer is under extension while the DNA crosslinks are under compression. These prestressed gels are biomimetic, in that they mimic fundamental features that are also displayed by living organisms, including cytoskeleton and nuclei of living cells[9]. Thus they can be particularly useful as model experimental systems to dissect the mechanical basis of cell shape stability. DNA gels can also actively respond (swell or contract) to the presence of particular strands of DNA which makes them suitable for use as prosthetic devices, particularly those involving soft tissues.

6.4   DNA Gel Nomenclature for the Present Study

We follow the nomenclature employed by Lin et al.[13], wherein the two side branches were referred to as SA1 and SA2 while the crosslinker was referred to as L2 (as shown in Figure 6-4). Three different composition DNA gels were employed in the current study: D-10, D-14 and D-20. The numbers represent the number of bases in each

of the side branches (or chains). D-10 gels have 10 nucleotides each in SA1 and SA2 side branches and 20 nucleotides in L2 crosslinker. D-14 gels have 14 nucleotides in SA1 and SA2 chains and 40 nucleotides in L2 crosslinker. Similarly D-20 gels have 20 nucleotides in SA1 and SA2 side chains and 40 nucleotides in L2 crosslinker. These gels are also sometimes referred to as 10/10/20, 14/14/40 and 20/20/40 gels respectively (based on the lengths of SA1/SA2/L2). A Microsoft Visual Basic code developed by Lin et al.[14] based on a genetic algorithm where a fitness value incorporating the maximum number of base pairs, maximum number of AT base pairs, maximum number of GC base pairs and maximum number of base pairs in a row was utilized to obtain the optimum sequences that result in minimum secondary interactions. The oligonucleotide base sequences for D-10, D-14 and D-20 gels obtained using the algorithm are shown in Table 6-1, Table 6-2 and Table 6-3 respectively.

The molar concentrations of SA1 and SA2 are always equal in all DNA gels. However, the ratio of molar concentrations of L2 and SA1/SA2 determines the concentration (or percent concentration) of the gel. For example if equimolar concentrations of SA1/SA2 and L2 are present in the gel network, the gel is referred to as 100% or fully crosslinked gel. Similarly when the molar concentration of L2 is only 50% or 60% of the molar concentration of SA1 or SA2, the gel is referred to as 50% crosslinked or 60% crosslinked respectively. In addition to composition of strands and concentration of crosslinker, molar concentration of SA1 and SA2 stock solutions can also be varied (for e.g., 3 milli-molar (mM) or 6 mM) to alter the stiffness of DNA gels.

Table 6-1. Oligonucleotide base sequences for D-10 (10/10/20) gels

Strand	Sequence (5' to 3')	Molecular Weight	T_m (°C)
SA1	Acrydite-GCA CCT TTG C	3226.2	34.9
SA2	Acrydite-GTC AGA ATG A	3323.3	23.6
L2	TCA TTC TGA CGC AAA GGT GC	6117.0	56.0

Table 6-2. Oligonucleotide base sequences for D-14 (14/14/40) gels

Strand	Sequence (5' to 3')	Molecular Weight	T_m (°C)
SA1	Acrydite-CGT GGC ATA GGA CT	4551.1	46.9
SA2	Acrydite-GTT TCC CAA TCA GA	4470.0	40.2
L2	TCT GAT TGG GAA ACA GTC CTA TGC CAC GGT TAC CTT CAT C	12222.0	65.9

Table 6-3. Oligonucleotide base sequences for D-20 (20/20/40) gels

Strand	Sequence (5' to 3')	Molecular Weight	T_m (°C)
SA1	Acrydite-ACG GAG GTG TAT GCA ATG TC	6444.3	55.0
SA2	Acrydite-CAT GCT TAG GGA CGA CTG GA	6429.3	56.6
L2	TCC AGT CGT CCC TAA GCA TGG ACA TTG CAT ACA CCT CCG T	12151.9	68.8

Thus by varying the length and structure of DNA crosslinks and the molar concentrations of the side branches and crosslinker, the mechanical properties of the DNA gels can be altered over a wide range. In the present study we utilize the magnet setups described previously to characterize the mechanical properties of DNA gels by varying the design parameters as shown in Table 6-4. The proposed designs do not span the complete design space, but serve to provide trends that can guide in design optimization. In addition, the techniques used in this study can also be utilized for characterizing reversible stiffness changes. However, experiments involving reversibility are not discussed in this study.

Table 6-4. Summary of design parameters and experiments for DNA gels

"**RT"** is short for room temperature

Design Parameters	Design 1	Design 2			Design 3	Design 4
		Setup 1	Setup 2	Setup 3		
SA1 base length	10	14	14	14	20	20
SA2 base length	10	14	14	14	20	20
L2 base length	20	40	40	40	40	40
Crosslinker concentration (%)	40-100	40-100	40-100	40, 50, 60	40-100	40-100
SA1/SA2 molar concentration	3 mM	3 mM	3 mM	3 mM	3 mM	6 mM
Temperature	RT	RT	37 °C	RT	RT	RT
Experimental setup used	Magnetic Bead	Magnetic Bead	Magnetic Bead	4-magnet setup	Magnetic Bead	Magnetic Bead

6.5   Materials and Methods

The molecular weight of a DNA crosslink comprising of one SA1 strand, one SA2 strand and one L2 strand for the DNA gels described above, ranges between 12000 and 25000 as calculated from Table 6-1, Table 6-2 and Table 6-3. However the molecular weights of acrylamide monomer and bis crosslinker (used in Chapter 5) are 71 and 126.15 respectively. Owing to this large disparity in molecular weights, the established definitions of monomer concentration (%T) and crosslinker concentration (%C) are not appropriate in the context of DNA gels. However a scheme was developed by Lin et al.[14] wherein the quantity of DNA crosslinks on a stoichometric basis is converted to an equivalent quantity of bis molecules, which was then used to determine %T and %C. A similar approach is utilized in this study to determine the amounts of SA1, SA2 and L2 required for preparing any concentration DNA gel.

6.5.1   DNA Gel Preparation

DNA base sequences, optimized to minimize secondary structure formation were obtained from Integrated DNA Technologies (Coralville, IA). SA1 and SA2 strands of either 10, 14 or 20 bases in length were modified at the 5' end with Acrydite to allow for copolymerization with acrylamide. Stock solutions of the SA1 and SA2 strands were prepared at either 3 mM or 6 mM concentration in TE buffer, based on the design space. Dry nitrogen was bubbled for two minutes through a solution consisting of 10% acrylamide solution (40% acrylamide in H_2O), 60% SA1 stock solution, 20% H_2O, and 10% 10x TBE buffer solution. 5% ammonium persulphate was added to initiate the

polymerization and TEMED was used as a catalyst. Nitrogen was again bubbled to complete the polymerization of the individual stock solutions as described in Lin et al.[14]. SA2 mixture was prepared in a similar fashion by using SA2 stock solution instead of SA1 stock solution. L2 crosslinker was prepared at 3 mM concentration in TE buffer. Gels were cast by mixing SA1, SA2 and L2 in the ratio 1:1:0.6. At this ratio there are equal stoichometric amounts of SA1, SA2 and L2 in the gel. This would give rise to a 100% crosslinked gel. The amount of L2 can be proportionally decreased to obtain lower crosslink concentration gels. It was previously determined using viscosity experiments[14] that gelation in DNA gels occurs between 30 – 40% crosslinking. Hence 40% crosslink concentration was used as a starting point for all the experiments.

6.5.2 Mechanical Testing

Mechanical testing for most of the samples was done using the bead experiments as discussed earlier. SA1, SA2 and L2 stock solutions in 1:1:0.6 ratios respectively were mixed in a centrifuge tube and mixed vigorously. In order to ensure proper crosslinking, a pipette tip was also used to mix the viscous solution. 52 µL of this solution was then pipetted into another centrifuge tube and the stainless steel magnetic bead was dropped into the solution. The DNA gels were then heated above their melting point and the bead was quickly positioned in the center of the tube, as the gel formed around it. The displacement of the beads upon application of a magnetic force was recorded using a video camera and the global elastic modulus of the gels was determined using Eq. 4.

Experiments on DNA gels were also performed using the four magnet setup. However these were limited to the lower crosslinker densities, as at higher stiffness, the

force applied by the magnet system in its current state, is not sufficient to displace the needles. Needles dispersed in deionized water were used to dilute the TE buffer used in preparing the SA1 and SA2 stock mixtures. Gels were then cast in wells of the 96-well plates and placed in the space between the poles of the four magnets. Displacements and rotations of the needles under the influence of an applied force or torque respectively were measured and the Young's modulus, shear modulus and Poisson's ratio of the DNA gels were calculated.

Referring to Table 6-4, in Designs 1, 2 and 3, the length of the side chains and the crosslinker were altered keeping the molar concentration of the side chains and the temperature constant. It is expected that there exists an optimum length of the crosslinker that will yield the largest change in the mechanical properties of the material.

In Designs 3 and 4, the lengths of SA1, SA2 and L2 were kept constant, while the molar concentration of the side chains was increased from 3 mM to 6 mM. It is expected that an increase in the concentration of side chains would raise the stiffness of hydrogels as this would provide more sites for the crosslinker to bind to.

Crosslinking in DNA gels is achieved through hydrogen bonds between the nucleotides on the side branches and the crosslinker. The strength of the bonds is dependant on the ambient temperature. At higher temperatures, the hydrogen bonds become unstable and dissociate. This phenomenon was observed in the viscoelasticity studies performed by Lin et al.[14] on DNA gels. Also, most of the cellular studies are performed at incubator temperatures (37 °C). The stability of the substrates at this temperature affects the behavior of cells. Thus, for Design 2, in Setups 1 and 2, all the

design parameters were kept constant except the temperature was increased from room temperature (RT) to 37 °C.

In Design 2 - Setup 3, the four magnet setup was utilized to characterize the Young's modulus, Poisson's ratio and shear modulus of the hydrogels. This also serves as a proof of concept that the four magnet setup is not limited to bis-gels alone, but can be employed for a much larger range of hydrogels.

6.6   Results

Graphs of Young's modulus versus crosslinker concentration for the D-10, D-14 and D-20 gels are shown in Figure 6-5. In increasing order, the crosslinker concentrations investigated were 40, 50, 60, 70, 80, 90 and 100%. 40% crosslinked gels were prepared in each case and after testing the sample, 10% crosslinker was added and the gel was reheated to incorporate the extra crosslinks, and the gel was tested again. This process was repeated for densities up to the stoichometric value (100% crosslinked). The stiffness in all the gels was found to increase with increasing crosslinker concentration.

When the concentration of the side chains was increased from 3 mM to 6 mM, the elastic modulus of the gels was found to increase by almost 2-fold at 100% crosslinking as shown in Figure 6-6. The stiffness of D-20 gels at 3 mM concentration and 100% crosslinking was found to be 12,535±2793 Pa while that for D-20 gels at 6 mM concentration and 100% crosslinking was found to 25,730±4751 Pa.

D-14 gels were placed in a temperature controlled chamber maintained at 37 °C and the stiffness of the gels was measured. The results obtained are compared in Figure 6-7 with the results from room temperature. It can be seen that, the stiffness of the gels at

100% crosslinking decreased by 3-fold from 6150.7±719.6 Pa to 1867.8±110.6 Pa when the temperature was increased.

The mechanical properties of D-14 gels at 40%, 50% and 60% crosslinker concentration were also calculated using the four magnet setup. Two needles at different locations in each sample were isolated and their displacement and rotation under the application of a known force or torque was measured. Table 6-5 shows the properties obtained for these gels. The shear modulus and elastic modulus of the gels increased as the concentration of the crosslinker was increased from 40% to 60%. For a 40% crosslinked gel, the shear modulus and elastic modulus were found to be 325.4 ± 39.3 Pa and 925.3 ± 102.8 Pa respectively. When 10% more crosslinker was added to these gels to bring the total crosslinker percentage to 50%, the shear modulus increased to 534.3 ± 69.7 Pa while the elastic modulus increased to 1551.7 ± 188.1 Pa. Upon adding another 10% of crosslinker, the shear modulus increased to 1071.4 ± 134.6 Pa and the Young's modulus increased to 2964.6 ± 346.1 Pa. The Poisson's ratio of these gels varied between 0.36 and 0.49.
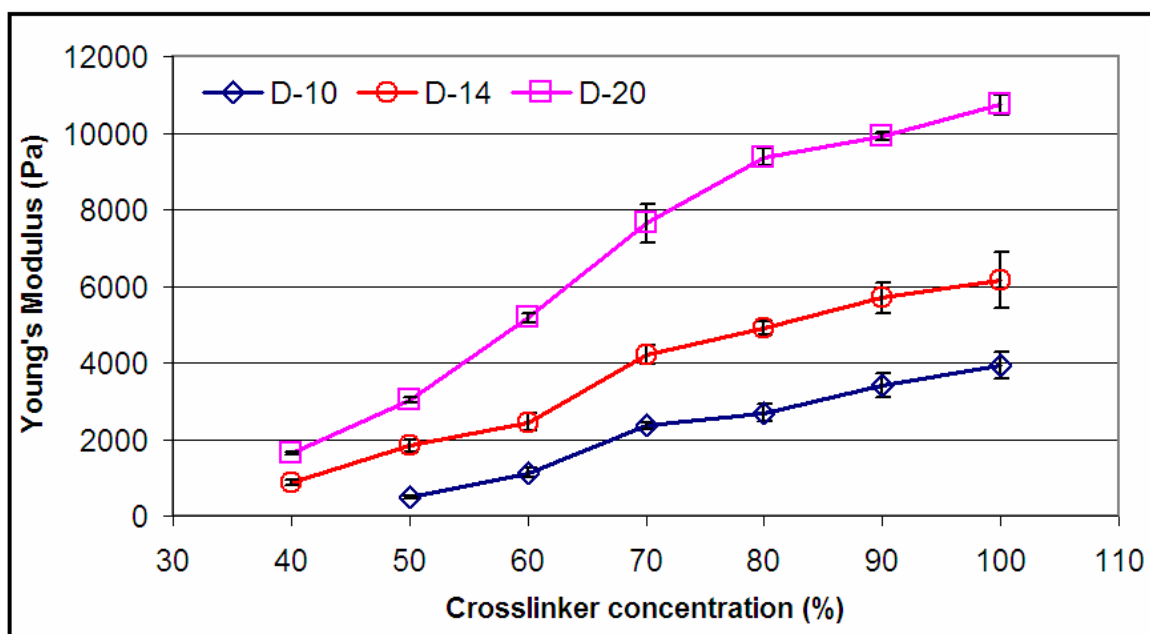
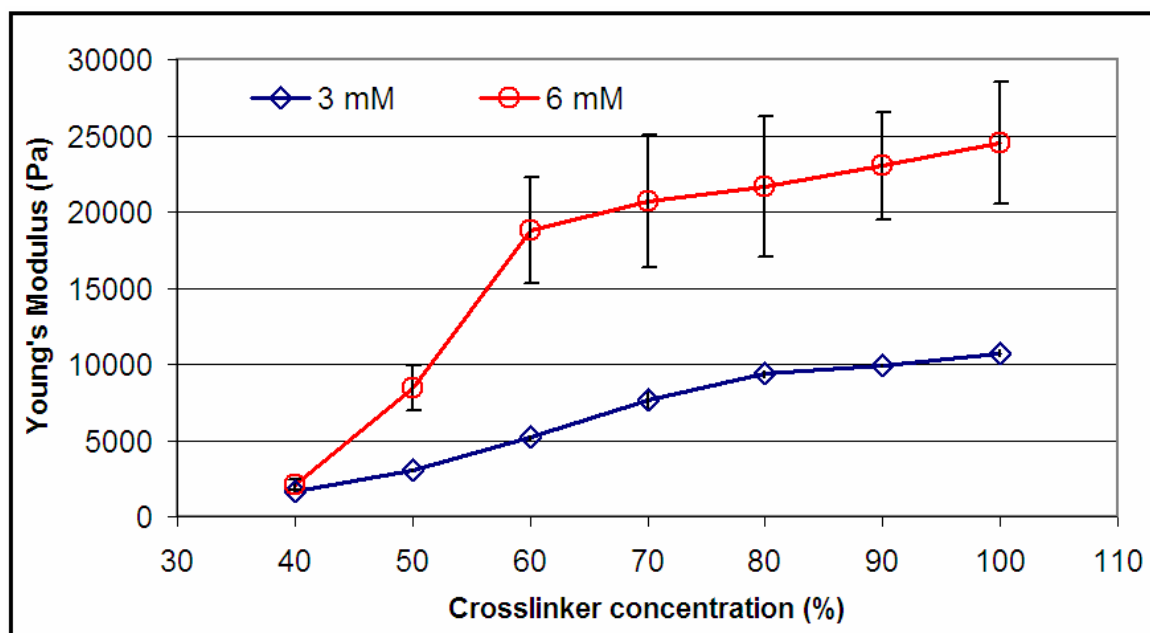**Figure 6-5.** Young's modulus of DNA gels at 3 mM concentration

Figure 6-6. Young's modulus of D-20 gels of 3 mM and 6 mM concentrations

Table 6-5. Young's modulus, shear modulus and Poisson's ratio of D-14 gels

| DNA gel conc.	#	F/δ (x10^{-3}) (N/m)	Γ/θ (x10-^{13}) (N-m)	Shear Modulus (Pa)	Young's Modulus (Pa)	Poisson's Ratio
40%	1A	6.98	1.12	255.91	757.94	0.48
	1B	8.33	1.34	305.11	904.21	0.48
	2A	8.17	1.13	299.46	821.83	0.37
	2B	9.23	1.26	338.12	921.10	0.36
	3A	8.89	1.33	325.96	935.82	0.44
	3B	10.50	1.52	384.95	1084.57	0.41
	4A	9.13	1.37	334.71	962.94	0.44
	4B	9.81	1.42	359.37	1014.28	0.41
50%	1A	15.70	2.37	575.48	1658.23	0.44
	1B	13.06	2.14	478.65	1427.48	0.49
	2A	13.72	2.11	502.88	1462.38	0.45
	2B	11.11	1.77	407.28	1202.23	0.48
	3A	16.55	2.47	606.64	1739.96	0.43
	3B	16.86	2.54	617.69	1778.28	0.44
	4A	14.73	2.43	539.70	1613.06	0.49
	4B	14.91	2.13	546.49	1532.02	0.40
60%	1A	32.07	4.61	1175.24	3303.18	0.41
	1B	26.42	3.82	968.28	2730.04	0.41
	2A	26.08	3.66	955.62	2647.97	0.39
	2B	23.18	3.30	849.29	2371.50	0.40
	3A	33.00	4.45	1209.18	3255.35	0.35
	3B	29.38	4.23	1076.74	3028.04	0.41
	4A	30.66	4.23	1123.50	3075.81	0.37
	4B	33.19	4.53	1216.34	3304.62	0.36
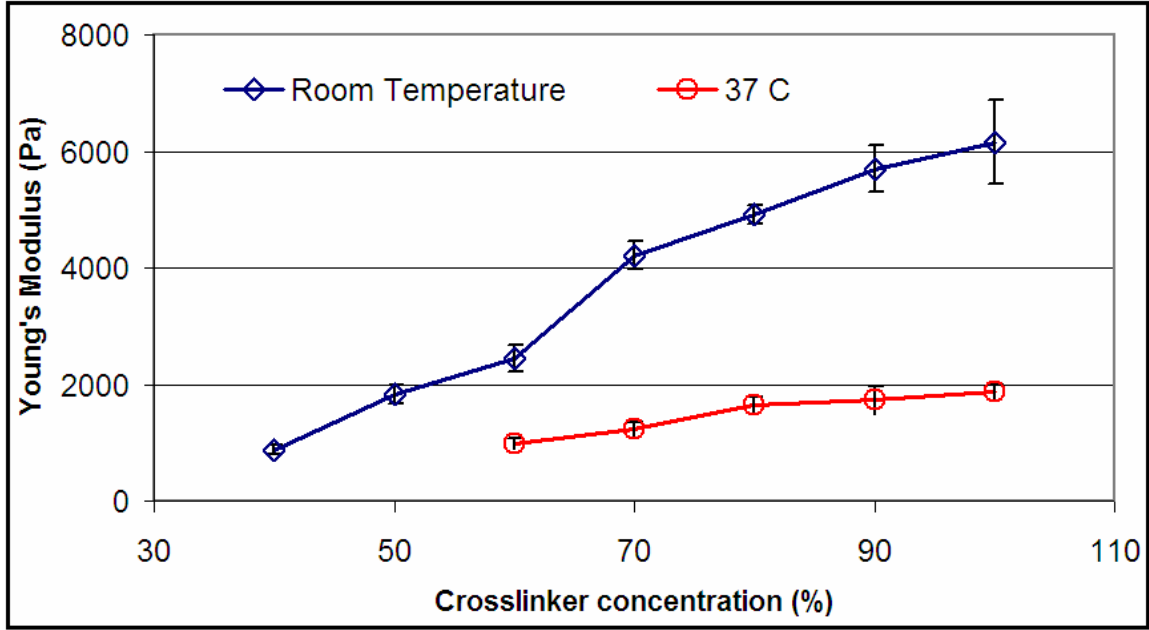
Figure 6-7. Young's modulus of D-14 gels at room temperature and 37 °C

6.7   Discussion of Mechanical Properties of DNA Gels

Polymer scaling laws, first developed by de Gennes[4], consist of proportionalities that mathematically relate many physical variables, molecular dimensions and thermodynamics of the polymer. The fundamental postulate of scaling law, given by Eq. 59, supposes that there exists a transition at some critical value x^* of a parameter x such that the variable S changes its form.

$$S \propto f\left(\frac{x - x^*}{x^*}\right).$$

Eq. 59

Two regimes of x in function f exist and are defined by

$$f\left(\frac{x - x^*}{x^*}\right) = 0 \;\; if \;\; \frac{x}{x^*} < 1,$$

Eq. 60

$$f\left(\frac{x - x^*}{x^*}\right) = \left(\frac{x - x^*}{x^*}\right)^m \;\; if \;\; \frac{x}{x^*} > 1,$$

Eq. 61

where m is known as the universal scaling exponent whose value depends on the specific polymer. For the DNA hydrogels described in this study, the parameter x is the crosslinking density (c) and x^* is the critical crosslinking density (c_g = *40% for DNA gels*) at which gelation occurs. The elastic modulus obeys a scaling law with concentration as given by the equation below[5,6,4,24].

$$E \propto \left(\frac{c - c_g}{c_g} \right)^t .$$ Eq. 62

where t is a scaling exponent. However it was experimentally determined[4,18,22] that for hydrogels that are well above their gelation threshold ($c \gg c_g$), the elastic modulus no longer scales with the crosslinker concentration. This trend was observed in most of the experiments performed in this study. Figure 6-8 shows a theoretical logarithmic plot of the elastic modulus as a function of crosslinker concentration. For values of c just above the gelation point, the curve is linear with a finite slope. However as c becomes much larger than c_g, the slope decreases until it becomes zero, at which point the modulus is independent of c. A similar graph was plotted for the elastic modulus of D-14 and D-20 gels as shown in Figure 6-9. A qualitative comparison between Figure 6-8 and Figure 6-9 shows that the DNA gels follow the same trend.
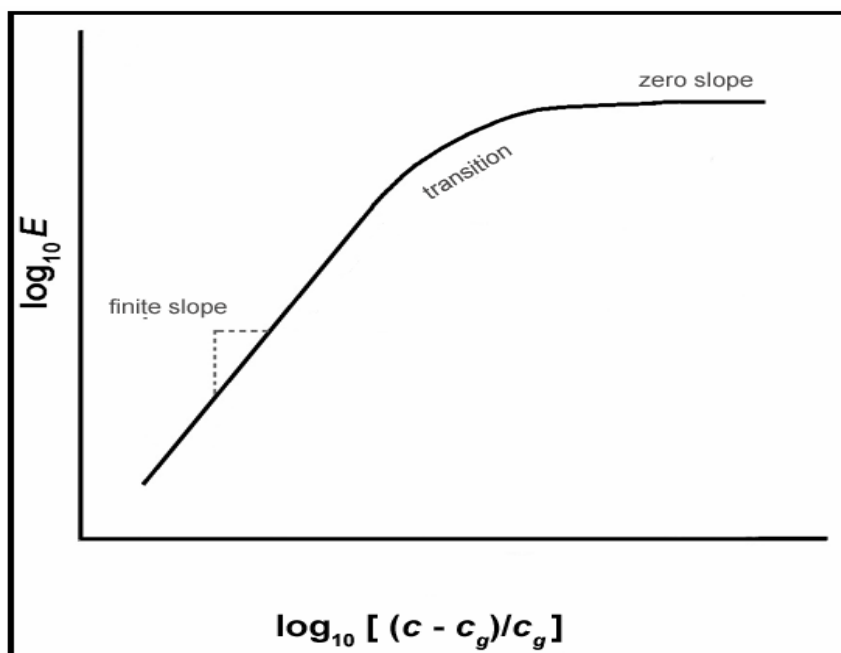
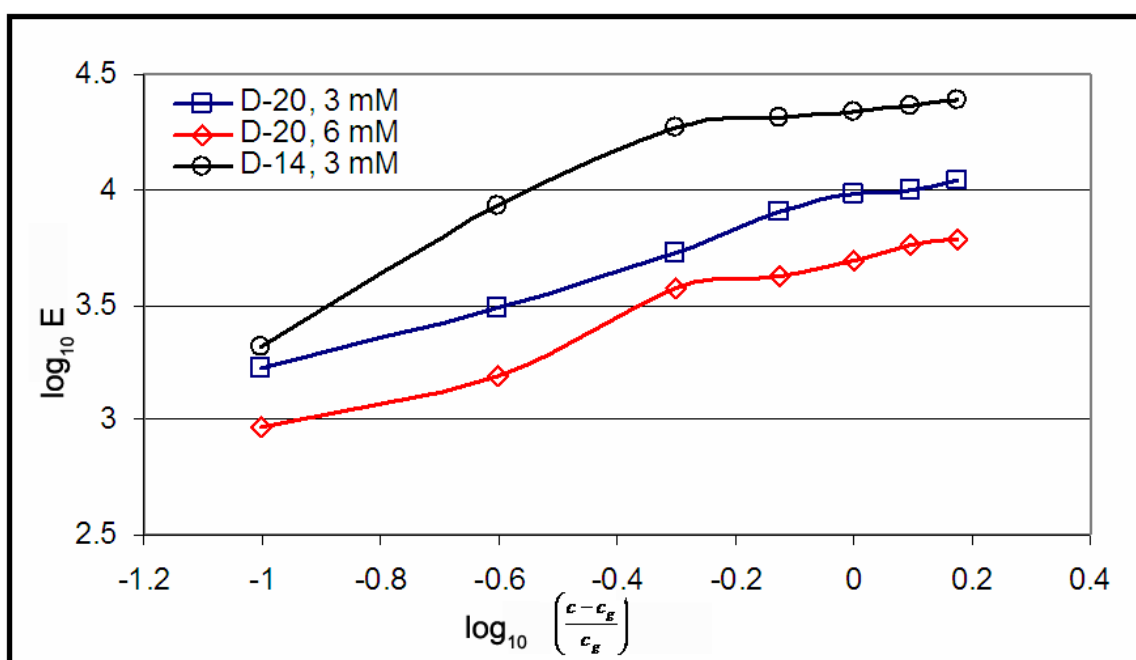**Figure 6-8.** Scaling of elastic modulus with crosslink concentration

Figure 6-9. Scaling of elastic modulus of D-20 and D-14 hydrogels with crosslinker

The stiffness of the gels at 100% crosslinking increased from 3.9 kilo-Pascal ("**kPa**" in short) for 10/10/20 gels to 10.7 kPa for 20/20/40 gels, when the length of the crosslinker was increased from 20 nucleotide bases to 40 nucleotide bases. In a previous study, our group has observed that for DNA gels with 20 nucleotide bases in SA1 and SA2 with a monomer content of 3.08×10^{-5} g/µL and a crosslink density of 8.34×10^{14} crosslinks/µL, the Young's modulus decreased from 10.9 kPa to 2 kPa when the number of bases in the crosslinker was increased from 40 to 80. When the crosslink is very short, little prestress will build up and there will be no significant change in the elastic modulus of the material. On the other hand, if the crosslink is very long, the double stranded DNA resulting from the hybridization of SA1/SA2 with L2 is likely to Euler buckle. This will also result in reduced build up of prestress. Thus, there exists an optimum crosslinker length at which we can obtain the maximum mechanical stiffness for the hydrogels. In our studies, we observed that for a 20/20/40 gel at 100% crosslinking, a maximum stiffness of 10 kPa was obtained. Thus a crosslinker length of 40 bases can be considered as an optimum length for future studies. The stiffness can be further increased by increasing the concentration of the side chains, as observed in Figure 6-6, wherein we obtained a maximum stiffness of 25 kPa at 6 mM concentration and 100% crosslinking. However, it should be noted that at higher SA1 and SA2 concentrations, the stock solutions of SA1 and SA2 become very viscous and transferring the solutions from one tube to another becomes very challenging.

For the D-10 gels of 40% crosslinking at room temperature and the D-14 gels of 40% and 50% crosslinking at 37 °C, data could not be obtained for measuring the stiffness, as the gels were very soft and the stainless steel beads sank to the bottom of the

tube owing to gravity. This is a drawback for the bead methodology and other techniques such as rheology or microneedles can be utilized to study the properties of such low stiffness gels.

A comparison between the local properties obtained using the four magnet setup and the global properties obtained using the magnet setup for 40%, 50% and 60% D-14 gels is made in Figure 6-10. The variation between the global elastic modulus, which assumes Poisson's ratio to be equal to one-half, and the local elastic modulus was found to increase with gel concentration. This inconsistency might be due to the very small displacements obtained during microneedle experiments in gels with stiffness greater than 3 kPa. These displacements fall in the range of the resolution of the camera employed for capturing the images. This can be resolved by increasing the size of the magnets and the gradient field developed, which in turn increases the force acting on the needles.
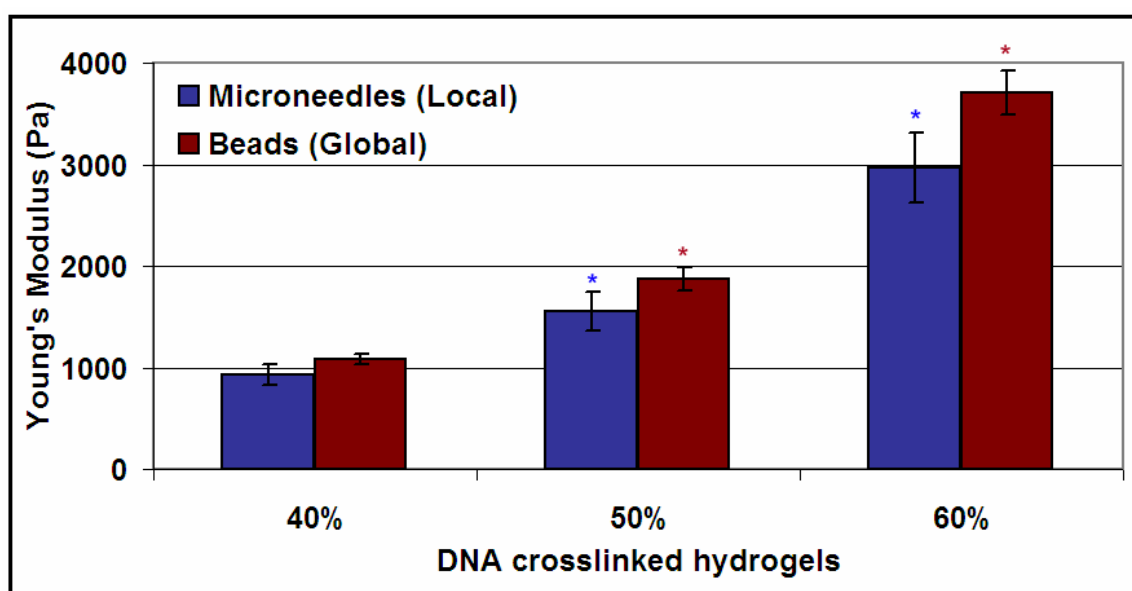

Figure 6-10. Local and global Young's modulus of D-14 gels

6.8   Conclusions

DNA-crosslinked polyacrylamide hydrogels provide many advantages over the traditional hydrogels such as bis-polyacrylamide, alginate and collagen gels. DNA gels are thermo-reversible and provide an avenue to alter the stiffness of the gels dynamically, without changing the environmental factors, by adding or removing crosslinks. DNA gels are biodegradable and can be reversibly assembled or disassembled at temperatures below the melting point of the crosslinks. This makes them attractive candidates for many applications such as drug delivery and prosthetic devices. In particular, their use as substrates for tissue engineering enables modifying the potential of modifying substrate stiffness in a controlled fashion which in turn enables investigating the cellular growth in response to the dynamic stiffness of the substrate.

A DNA gel design space involving parameters such as crosslinker concentration, base lengths of DNA strands, molar concentration of side chains and temperature was systematically developed and the linear elasticity paramters of the gels were evaluated. It was found that the stiffness of the gels can be modulated over a wide range by modifying the various design parameters. In particular, it was found that the elastic modulus increased with increase in crosslinker concentration and concentration of the side chains. However the stiffness of the gels decreased upon increasing the temperature to 37 °C, indicating that the hydrogen bonds formed between the nucleotides in the side chain and the crosslinker are not stable at higher temperatures. Local Young's modulus, shear modulus and Poisson's ratio of these gels were also evaluated using the four magnet setup and these values compared well with the global properties obtained using the bead experiments.

References

1.   Alberts B, Bray D, Lewis J, Raff M, Roberts K, Watson JD. Molecular biology of the cell. New York: Garland Science. 2002.
2.   Ali M, Lemoine NR, Ring CJ. The use of DNA viruses as vectors for gene therapy. Gene therapy. 1994;1(6):367.
3.   Chen J, Seeman NC. Synthesis from DNA of a molecule with the connectivity of a cube. 1991.
4.   de Gennes PG. Scaling concepts in polymer physics: Cornell Univ Pr; 1979.
5.   Flory PJ. Molecular Size Distribution in Three Dimensional Polymers. I. Gelation. Journal of the American Chemical Society. 1941;63:3083-100.
6.   Flory PJ. Principles of polymer chemistry: Cornell Univ Pr; 1953.
7.   Guerra CF, Bickelhaupt FM, Snijders JG, Baerends EJ. Hydrogen bonding in DNA base pairs: Reconciliation of theory and experiment. J Am Chem Soc. 2000;122(17):4117-28.
8.   Herweijer H, Wolff JA. Progress and prospects: naked DNA gene transfer and therapy. Gene therapy. 2003;10(6):453-8.
9.   Ingber DE. Tensegrity I. Cell structure and hierarchical systems biology. Journal of Cell Science. 2003;116(7):1157.
10.   Jeffrey GA. An introduction to hydrogen bonding: Oxford University Press, USA; 1997.
11.   Jiang FX, Yurke B, Firestein BL, Langrana NA. Neurite outgrowth on a DNA crosslinked hydrogel with tunable stiffnesses. Annals of Biomedical Engineering. 2008;36(9):1565-79.
12.   Jiang FX, Georges PC, Li B, et al. Cell growth in response to mechanical stiffness is affected by neuron-astroglia interactions. The Open Neuroscience Journal. 2007;1(1):7-14.
13.   Lin DC, Yurke B, Langrana NA. Inducing reversible stiffness changes in DNA-crosslinked gels. Journal of Materials Research. 2005;20(6):1456-64.
14.   Lin DC, Yurke B, Langrana NA. Mechanical properties of a reversible, DNA-crosslinked polyacrylamide hydrogel. Journal of biomechanical engineering. 2004;126:104.
15.   Mao C, Sun W, Seeman NC. Assembly of Borromean rings from DNA. Nature. 1997;386:137-8.
16.   Mueller JE, Du SM, Seeman NC. Design and synthesis of a knot from single-stranded DNA. Journal of the American Chemical Society. 1991;113(16):6306-8.
17.   Nagahara S, Matsuda T. Hydrogel formation via hybridization of oligonucleotides derivatized in water-soluble vinyl polymers. Polymer Gels and Networks. 1996;4(2):111-27.
18.   Peniche-Covas CAL, Dev SB, Gordon M, Judd M, Kajiwara K. The critically branched state in a covalent synthetic system and in the reversible gelation of gelatin. Faraday Discussions of the Chemical Society. 1974;57:165-80.

19. Seeman NC. DNA nanotechnology: novel DNA constructions. Annual Review of Biophysics and Biomolecular Structure. 1998;27(1):225-48.

20. Seeman NC. From genes to machines: DNA nanomechanical devices. Trends in biochemical sciences. 2005;30(3):119-25.

21. Seeman NC. Nucleic acid junctions and lattices. Journal of Theoretical Biology. 1982;99(2):237-47.

22. Senff H, Richtering W. Influence of cross-link density on rheological properties of temperature-sensitive microgel suspensions. Colloid & Polymer Science. 2000;278(9):830-40.

23. Sherman WB, Seeman NC. A precisely controlled DNA biped walking device. Nano Letters. 2004;4(7):1203-7.

24. Stockmayer WH. Theory of molecular size distributions and gel formulation in polymerization. Journal of Chemical Physics. 1943;11:45-55.

25. Trompette JL, Fabregue E, Cassanas G. Influence of the monomer properties on the rheological behavior of chemically crosslinked hydrogels. Journal of Polymer Science Part B Polymer Physics. 1997;35(15):2535-41.

26. Watson J, Crick F. Molecular structure of nucleic acids : A structure for deoxyribose nucleic acid. Nature. 1953;171:737-8.

27. Wolfert MA, Schacht EH, Toncheva V, Ulbrich K, Nazarova O, Seymour LW. Characterization of vectors for gene therapy formed by self-assembly of DNA with synthetic block co-polymers. Human gene therapy. 1996;7(17):2123-33.

28. Zhang Y, Seeman NC. Construction of a DNA-truncated octahedron. Journal of the American Chemical Society. 1994;116(5):1661-9.

29. Zheng J, Constantinou PE, Micheel C, Alivisatos AP, Kiehl RA, Seeman NC. Two-dimensional nanoparticle arrays show the organizational power of robust DNA motifs. Nano Lett. 2006;6(7):1502-4.

CHAPTER 7   Force Generating Potential of DNA Gels

7.1   Introduction

Spinal cord injury (**SCI**) affects approximately 450,000 people in the US, with over 10,000 new cases every year[22]. SCI often results in damage to axons in the white matter of the spinal cord which results in the interruption of neuronal communication[19]. This could lead to loss of function in legs, bowel and bladder, upper limbs and hands depending on the level of injury. Thus, the re-establishment of neural circuitry is a critical process in reversing the effects of SCI. Cajal's long held doctrine of neurobiology suggesting the improbability of spinal cord regeneration "*Once development was ended, the fonts of growth and regeneration of the axons and dendrites dried up irrevocably. In the adult centers, the nerve paths are something fixed, and immutable: everything may die, nothing may regenerate*" would then be fatalistic[6]. However, almost four decades ago, pioneering work by Altman & Das[1] suggested continuing neurogenesis throughout adulthood. Since the early 1990s, researchers have demonstrated that *new* neurons are indeed born in restricted regions of the adult mammalian central nervous system (**CNS**)[2,9,13,38]. This has brought forth a unique model system that facilitates the understanding of the basic mechanisms of neural development during spinal cord regeneration.

Numerous biological therapies such as glial cell and macrophage[24], stem cell[18,23,25,27,33], olfactory ensheathing cell[11,31], autoimmune T cell[15] and pharmacological therapy[29] are presently being pursued to enhance spinal cord regeneration. In addition,

two primary tissue engineering strategies have emerged as alternatives or compliments to the biological approaches. The first tissue engineering strategy is to introduce a biomaterial to serve as a bridge or a scaffold to support the growth of regenerating axons from proximal to the injury site to their distal target as shown in Figure 7-1. These scaffolds mimic the role played by autologous nerve grafts or autograft entubulation. However, for spinal cord regeneration, inhibitory factors mask the intrinsic ability for spinal cord axons to regenerate[12,16,20,39]. While the microenvironment following SCI is not inherently supportive of axonal regeneration, biomaterials can be improved by introducing chemical and structural modifications that mask inhibitory cues and present favorable ones. Researchers are attempting to identify the environmental cues that stimulate and direct growth cone migration during neurodevelopment and incorporate those cues into the biomaterial. Much progress has been made in using diffusible growth factors[37], supporting cells[3,37], and adhesion molecules[5,8,30,32,36] in improving the regenerative environment.

Figure 7-1. Biomaterial implant at injury site for neurite regeneration

Unlike the first strategy, which mimics the nervous system during axonogenesis, the second tissue engineering strategy attempts to duplicate the mechanisms of tissue growth during physical maturation. During this time, neural structures, such as the spinal

cord, are physically stretched, lengthen, and form neo-tissue to accommodate the stretch. Researchers have shown that axonal growth of spinal cord neurons can be achieved by stretching the underlying structures[20,39]. Bray first demonstrated this mechanism known as "towed growth" in chick sensory neuron cultures[4]. Heidemann and coworkers[16,20,39] found that a constant force of ~15-500 picoNewtons (pN) elicits a growth rate of ~1.5μm/hr. Under this condition, neurons were able to increase production of proteins to stabilize the neo-axoplasm. Below this threshold, axons did not grow, and above the threshold, presumably axons failed mechanically. Smith and Meaney[34] used these principles to physically stretch and grow groups of axons by allowing two sets of neurons cultured on adjacent coverslips to synapse, and then slowly pulling the neurons apart under controlled stretch, thereby lengthening the axons and forming a nerve-like structure. Recently, Fass and Odde[10] have shown that slow initial force ramps (~1.5-11pN/sec) were more likely to initiate neurites from chick embryo forebrain neurons than fast ramps (450 pN/sec). Together, these results demonstrate that axonal growth of spinal cord neurons can be achieved by stretching the neural structures and that a critical range of force exists to engage the towed growth mechanism.

In a previous study, Lin et al.[21] have demonstrated the ability to contract or swell DNA-crosslinked polyacrylamide gels by the addition of crosslinks or removal strands respectively. Jiang et al.[17] have recently utilized such DNA gels as tissue scaffolds to observe the cellular responses of spinal cord neurons to substrate compliances. It was found that spinal cord neurons extend more primary dendrites on stiffer gels. Gels possessing such reversible expansion and contraction functions have been explored by numerous researchers[7,14,26,28,35] and could be potentially used as actuators in applications

ranging from artificial muscles to pumps. The tendency of loosely crosslinked gels to contract as their crosslink density is increased can also be utilized as a force-generating mechanism. By dynamically modulating the stiffness of the hydrogel by adding crosslinks, we can force the tissue scaffold to shrink, thereby exerting traction on the emerging neurites and physically expanding the tissue.

In the present study, we attempt to characterize the force actuating potential of two DNA gels (D-14 and D-20 as described in Chapter 6). The amount of crosslinker strands is increased and the force generated when the gel shrinks is measured. It is hypothesized that the dynamics of the force can be controlled by the concentration and the rate of delivery of the crosslinks, and that this force can be matched to published criteria governing the physical growth of neural tissues.

7.2   Materials and Methods

Samples of 50% crosslinked D-14 and D-20 DNA gels were prepared in centrifuge tubes by mixing SA1, SA2 and L2 solutions as described in Section 6.5.1. Two methods were utilized to measure the force generated when these DNA gels contracted upon addition of crosslinks. In the first method, the deflection of a calibrated cantilever placed in the gel was measured as the gel contracted. Using simple beam deflection formulae the force applied by the hydrogel to cause that amount of deflection in the cantilever was calculated. In the second method, a thin slit was made in a PDMS layer and the DNA gel was glued on top of the slit. As the gel contracts, it pulls the PDMS layer together thus closing the gap in the slit. Knowing the stiffness of the PDMS layer

and the extension, the force needed to pull on the layer was calculated using linear elastic theory.

7.2.1 Cantilever Method

A special 20x5x5 mm chamber was designed and rapid-prototyped using a high resolution 3D Stereolithograph system, Viper™ SLA® (3D Systems, CA). A porous polymer block was rigidly glued to one end of the chamber and another porous block was placed in the center. 225 μL of the sample was pipetted into the space between the two porous blocks. The gel gets interlaced between the two porous polymers thus attaching rigidly after gelation. 1X TE buffer was then introduced into the chamber and the gel was allowed to swell for 24 hours. One end of a calibrated force transducer (in the form of a brass cantilever beam) was then attached to the free block and tethered to a rigid support on the other end. Figure 7-2 and Figure 7-3 show the schematic and the experimental setup for the force generation of DNA gels respectively. Neither the gel nor the porous blocks were allowed to come in contact with the floor of the chamber. This was achieved by placing a thin rubber strip (20x5x1 mm) on the floor of the chamber before polymerizing the DNA gel and was removed after swelling of the gel completed. This would ensure that there are no frictional losses. Additional crosslinks, well in excess of the number required to fully crosslink the gel, were then introduced into the chamber and the gel was allowed to contract for a 24 hour period. Time lapse images of the cantilever deflection as the gel contracted were taken using a USB camera (A1510 HDCE-10A) with a resolution of 1280x1024 pixels.
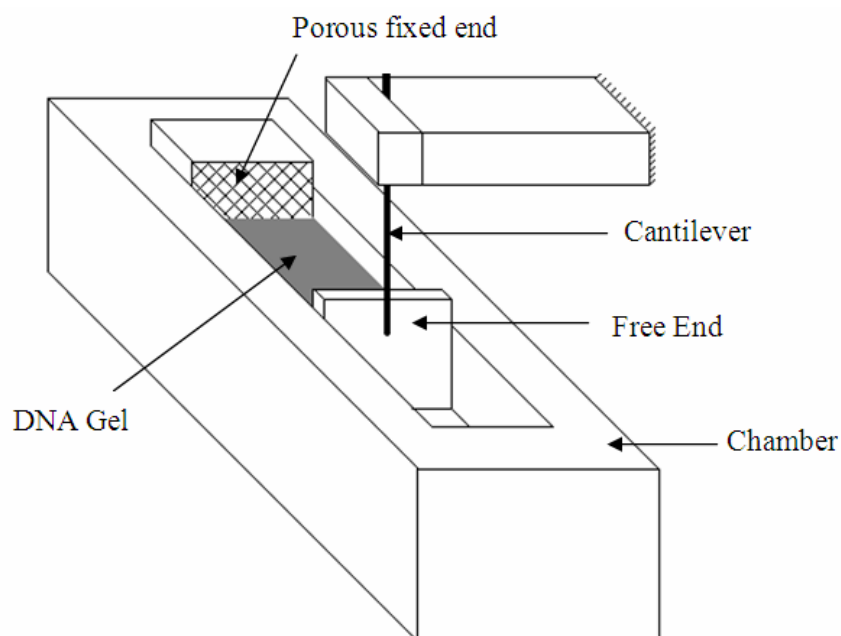
Figure 7-2. Setup for the force generation experiment

The DNA-crosslinked gel is formed in the chamber between the two supports. One end of the gel is fixed to the chamber and the other is tethered to a cantilever.
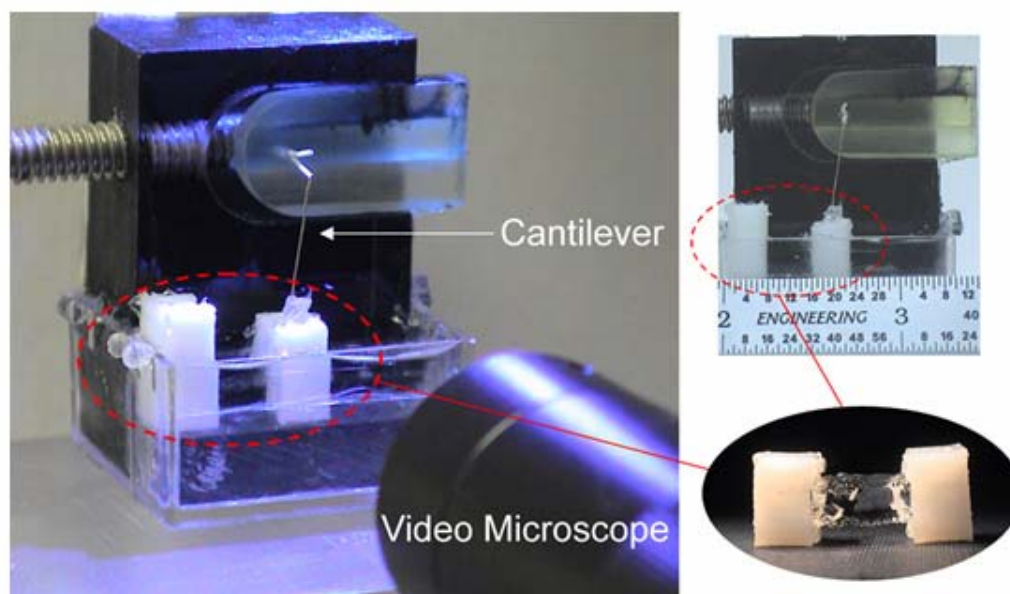

Figure 7-3. Experimental setup for force-generation using DNA crosslinked gels

Knowing the deflection of the beam, the force per unit length (q) acted upon by the DNA gel can be calculated using cantilever beam theory as

$$q = \frac{24\,E\,I\,\delta}{(3L^4 - 4a^3L + a^4)} \qquad \text{Eq. 63}$$

where E and I are the elastic modulus and bending rigidity of the cantilever and δ is the deflection of the cantilever measured using the time-lapse images. L is the total length of the cantilever and (L-a) is the length of the cantilever immersed in porous polymer block as shown in Figure 7-4.
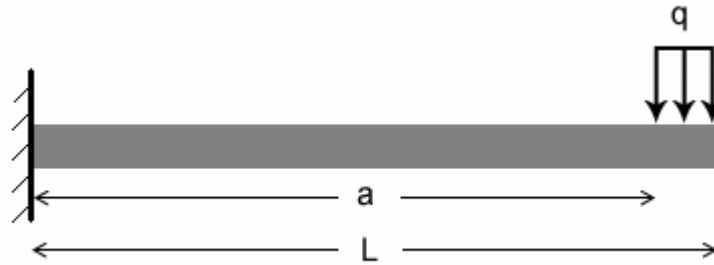

Figure 7-4. Total force per unit length (q) applied by DNA gel on cantilever

7.2.2   PDMS Stretch Method

A 2 mm thick layer of PDMS (SYLGARD 184, Dow Corning Corporation, Midland, MI) was prepared by mixing the silicone elastomer base and the curing agent in a 40:1 ratio in a 150x15 mm tissue culture plate. Two strips of 20x10 mm were cut out of the layer and each of them was placed on a pre-cleaned microslide (Gold Seal, Portsmouth, NH). The two slides were brought close together to leave a gap of about 100 µm between them as shown in Figure 7-5. Optical glue was applied to the top surface of

the PDMS, and DNA gel was poured on it and allowed to polymerize. As gelation occurs, the PDMS layers, the DNA gel and the optical glue bind together rigidly, in the presence of UV light. The entire setup was placed in 1X TE buffer and the DNA gel was allowed to swell for 24 hours. DNA crosslink strands, well in excess of the number required to fully crosslink the gel were then introduced and the gel is allowed to contract for another 24 hours. As the gel contracts, it brings the two PDMS layers together, and this motion was observed using a video microscope.
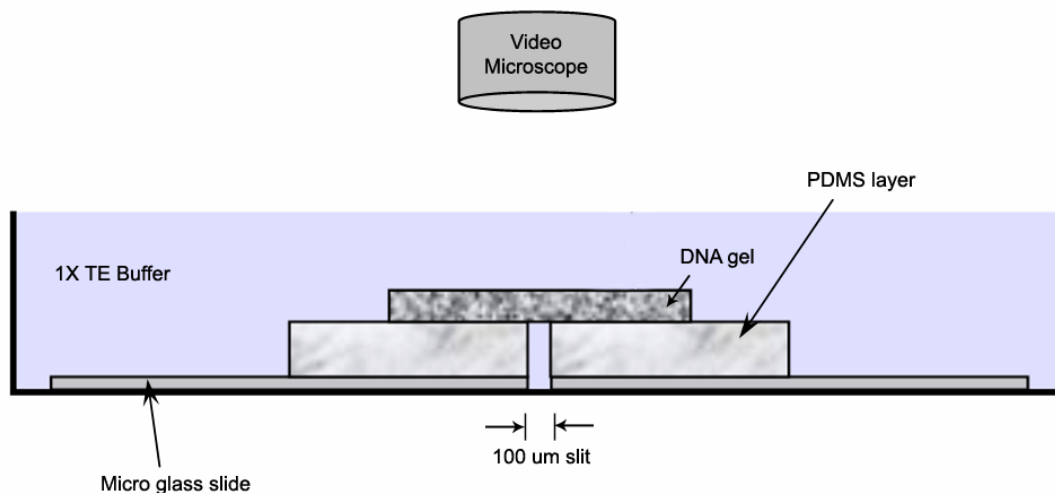

Figure 7-5. Setup for the PDMS stretch method

7.3   Results

The properties of the brass cantilever beam are as shown in Table 7-1. The cantilever was calibrated by fixing one end and applying small weights of 10 μg on the other end. Figure 7-6 shows the comparison between the experimental deflection

obtained and the theoretical values. The values obtained in experiments matched well with the predicted behavior using beam bending equations.

Table 7-1. Properties of the brass cantilever used in experiments

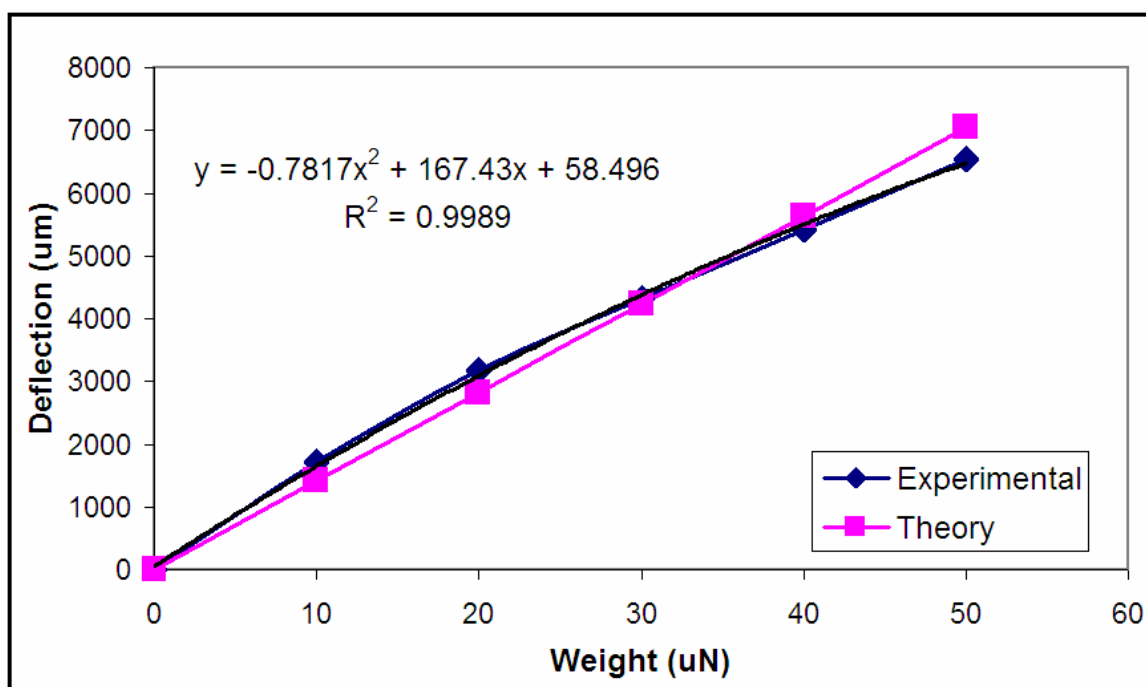| Property of Cantilever	Value
Modulus of elasticity (E)	3.01 GPa
Length of cantilever (L)	37 mm
Diameter of cantilever (d)	0.3 mm
Length of rod in gel (L-a)	5.2 mm

Figure 7-6. Calibration of cantilever of circular cross-section

Weights were applied to the free end and the deflection obtained was compared with theoretical values

Representative curves for two samples each of 50% crosslinked D-14 and D-20 gels are as shown in Figure 7-7 and Figure 7-8. The displacement of the cantilever with time, after adding excess crosslinks is measured and plotted with time. As the time progressed, the gel contraction increased linearly and after 16-18 hours, the contraction became negligible. This could mean that after 16-18 hours all the crosslinks got incorporated into the gel network and the gels were 100% crosslinked. It could also be possible that the rate of swelling and rate of shrinking become equal beyond 18 hours and thus no appreciable contraction was observed. It should be observed that, since the length of the gel is much larger than the width or height of the gel, we are only considering the uni-directional shrinking of the gel.

By knowing the deflection of the cantilever and the properties of the cantilever, the total force generated by the total volume of the hydrogel was calculated using Eq. 63 and shown in Figure 7-9. Graph shows the average values and the standard deviations of the force generated per unit volume of gel, for 3 samples of each gel. It was observed as the time progressed, the amount of force generated increased for both D-14 and D-20 hydrogels. Also it can be seen from the graph that D-20 hydrogels generated higher force compared to D-14 hydrogels. All the above experiments were performed at room temperature. However, in Chapter 6, we have showed that the elastic modulus of DNA hydrogels varies with temperature. Thus, in addition, we also quantified the force generated by D-20 hydrogels at incubator temperature (37 °C). The force generated by the hydrogel at higher temperature is compared with the force generated at room temperature in Figure 7-10. It was observed that the force generated at room temperature after 24 hours was more than 3 times higher than that generated at incubator temperature.
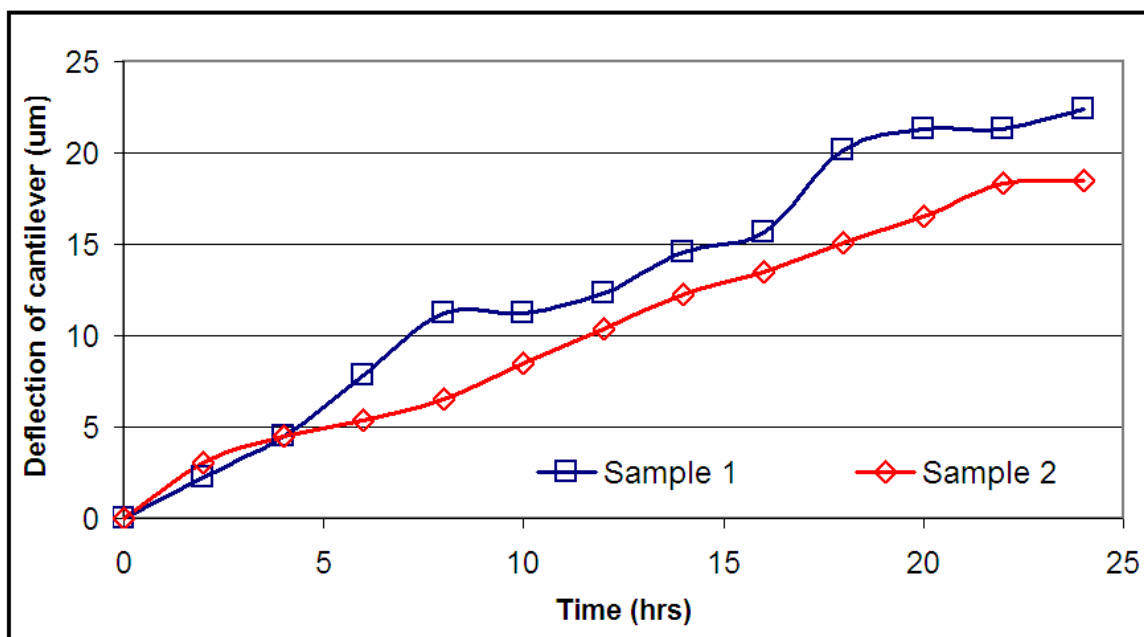
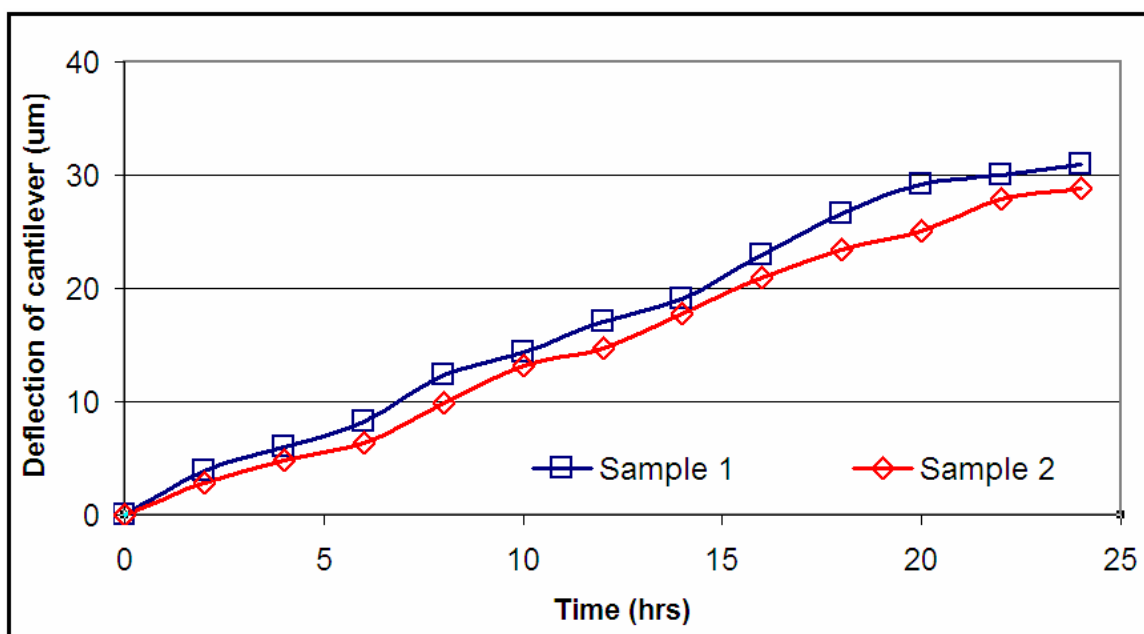**Figure 7-7.** Deflection of cantilever placed in D-14 gels

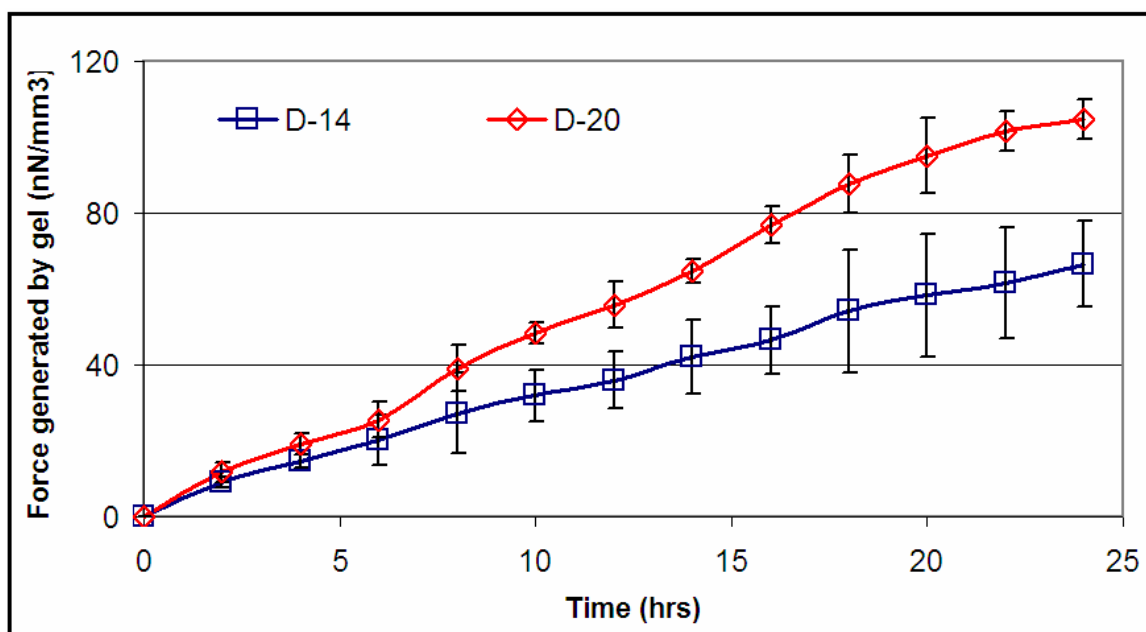**Figure 7-8.** Deflection of cantilever placed in D-20 gels

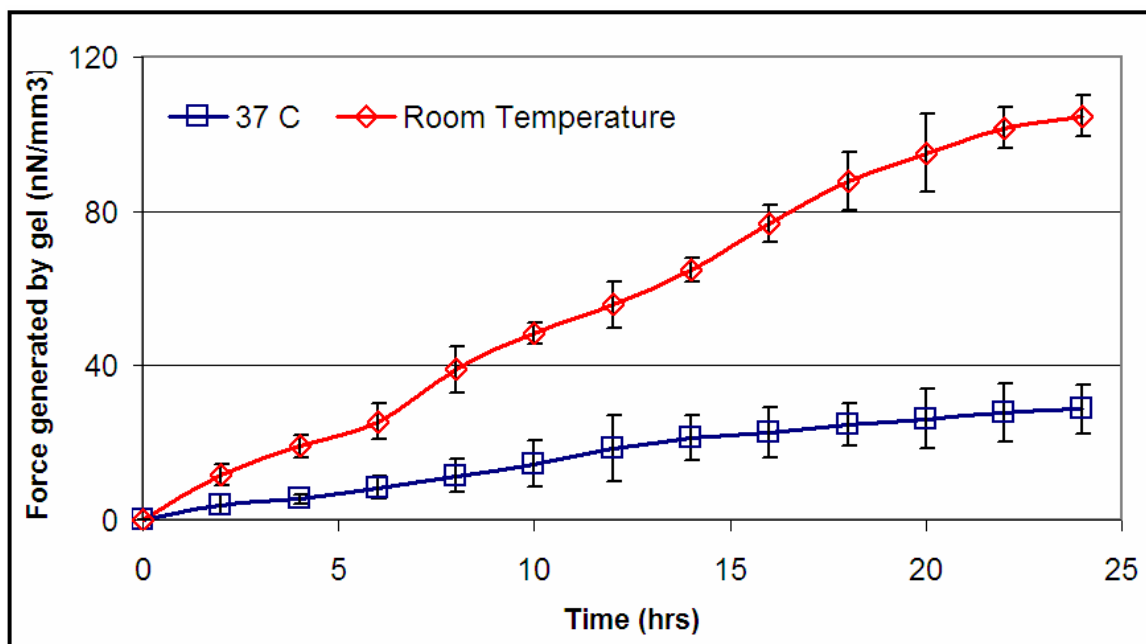**Figure 7-9.** Force generated by D-14 and D-20 hydrogels

Figure 7-10. Force generated at RT and incubator temperature for D-20 hydrogels

In addition to the cantilever method, we also utilized a PDMS block with a slit, and placed the DNA gel on top of the slit. As the gel contracted, it pulled on the top layer of the PDMS block thus expanding it. A schematic showing the expansion of the PDMS block is as shown in Figure 7-11. Since the bottom of the PDMS block is glued to the glass slide, we assumed that the bottom layer does not expand. Also assuming the PDMS block to be linearly elastic and perfect bonding between the DNA gel and the PDMS block, the shear stress is given by

$$\tau = \frac{F}{A}$$ Eq. 64

where F is the shear force applied by the DNA gel and A is the area of contact between the gel and the PDMS block. The shear strain is given by

$$\gamma = \frac{\delta}{h}$$ Eq. 65

where δ is the deflection as shown in Figure 7-11 and h is the thickness of the PDMS block.
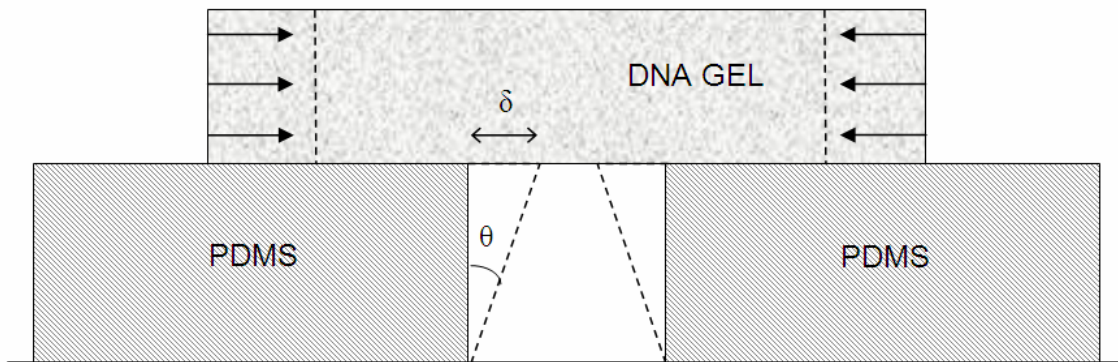

Figure 7-11. Shear force applied by DNA gel on top layer of PDMS block

The force applied by the hydrogel (F) was then calculated as

$$F = G \frac{A\delta}{h}$$

Eq. 66

where G is the shear modulus of the PDMS block. Using Eq. 66, the force was calculated

for 2 samples of D-20 hydrogels, and plotted in Figure 7-12. A similar trend as seen in

the cantilever experiments was observed using this method as well. The amount of

contraction became negligible after 15-18 hours and the force generated remained
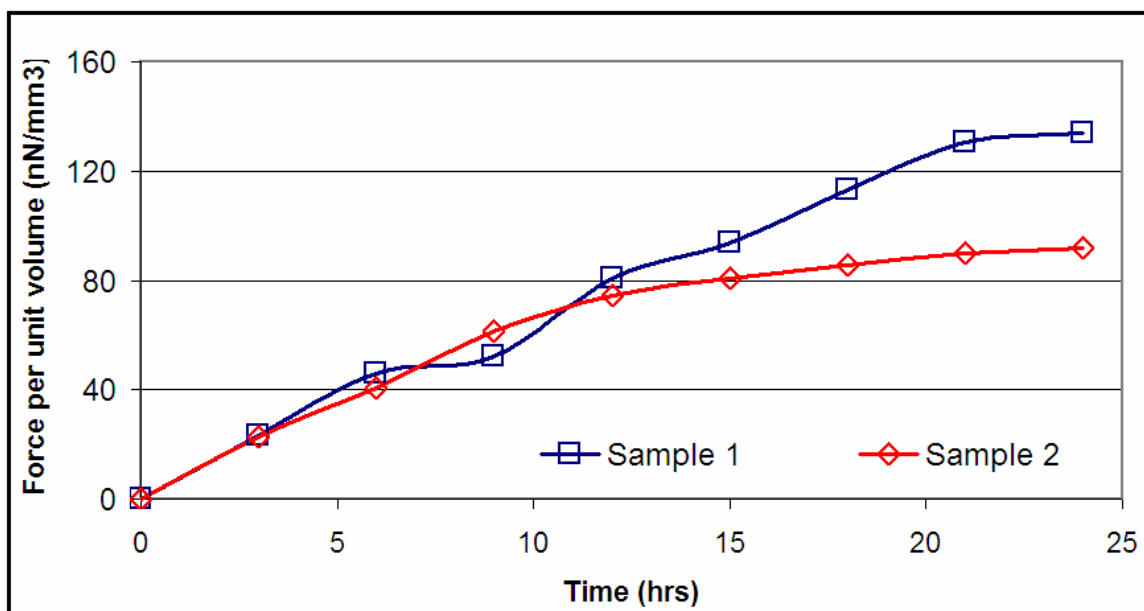
constant beyond this point.

Figure 7-12. Force generated by D-20 hydrogels using PDMS stretch method

7.4   Discussion of Force Generation Experiments

The close match between the experimental deflection and the theoretical values justifies the use of beam theory for measuring the force generated while using the cantilever experiments. It should be observed that the deflections obtained in the experiments were very minute compared to the length of the cantilever and at such small deflections the beam can be assumed to be in the linear elastic regime. Comparison of the D-14 and D-20 gels revealed that D-20 gels contracted more in comparison to the D-14 gels thus generating more force. The contraction of the gel upon addition of crosslinker is analogous to the linear thermal expansion of a metal rod upon heating. The change in the rod's length is given by

$$\Delta L = \alpha\, L\, \Delta T \qquad\qquad\qquad \text{Eq. 67}$$

where L is the original length, α is the linear expansion coefficient of the material and ΔT is the change in temperature. The force generated by the rod is then given by

$$F = E\, A\, \alpha\, \Delta T \qquad\qquad\qquad \text{Eq. 68}$$

Thus the force generated is dependant on the elastic modulus of the material. In a similar way the force generated by the hydrogel is also proportional to the elastic modulus of the gel. The Young's moduli of a D-20 and D-14 hydrogels were previously obtained (Chapter 6) to be equal to 10.5 kPa and 6.5 kPa respectively. A similar trend was observed for the contraction forces as well. The ratio of the elastic modulus to the contraction force for D-20 and D-14 gels is plotted in Figure 7-13. The proximity of the results shows that the contraction force is indeed dependant on the elastic modulus. It should also be observed that for D-20 hydrogels, as the crosslinker concentration

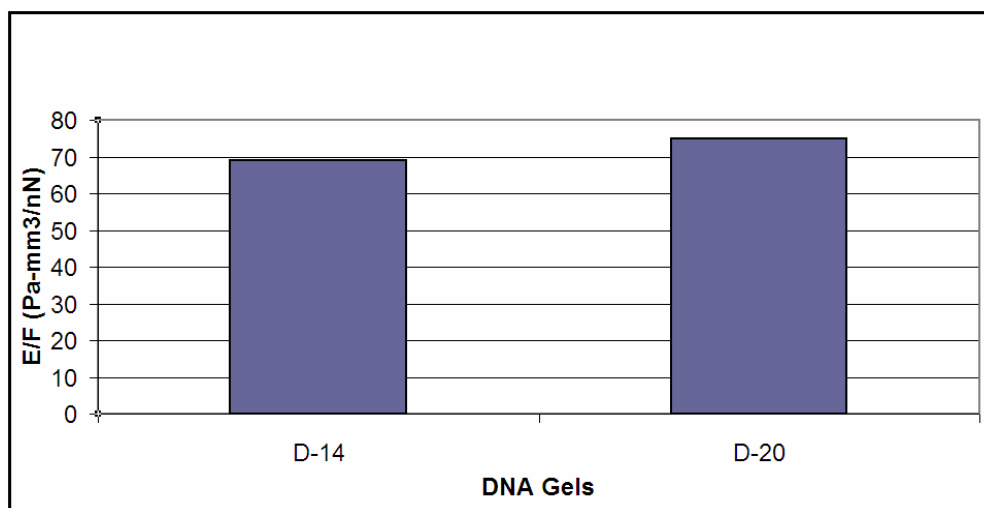increases the gels get much tightly packed as compared to the D-14 gels thus resulting in larger contraction.

Figure 7-13. Ratio of Young's modulus to contraction force for D-14 and D-20 gels

A comparison of the results obtained using the cantilever method and the PDMS stretch method for D-20 gels over a period of 24 hours is shown in Figure 7-14. It was observed that the amount of force generated is approximately same in both the experiments. This gives us confidence that the methods presented in this study can be successfully utilized for quantifying the force generated by soft substrates. Thus, the ability of the hydrogel to apply contract could be implemented *in vivo* to induce growth cone migration and apply mechanical tension to the spinal cord.

The dimensions of the swollen gel used in all the experiments were around 15x5x3 mm. Since the length of the gel is the defining dimension, only the contraction in that direction was used to measure the force generated. However it should be observed that the actual force generated is larger, if the total volume contraction is taken into

account. For example, the average force generated by a D-14 gel at room temperature after 24 hours of contraction was calculated to be equal to about 70 nN/mm^3. So the total force generated by the gel per unit length is approximately equal to 1050 pN/µm (70x5x3). This force is in the same order of magnitude as that observed by Heidemann and coworkers[16,20,39] for axonal growth of spinal cord neurons.

It should also be noted that the gels used are relatively thick and hence it is possible that the crosslinker strands added may not have sufficient time (which may be a couple of weeks) to diffuse throughout the gel during the course of the experiment. Instead, the extra crosslinking might occur primarily near the gel surface. As a result the force obtained in the above experiments might be much smaller than the actual force that one might obtain if the gel was uniformly crosslinked throughout its volume. To verify this hypothesis, experiments could be performed using dye labeled DNA strands, to observe how the crosslinker strands are distributed within the gel during the course of the experiment. If it is observed that the added DNA only forms crosslinks at the surface, the surface stresses could be calculated by calculating the deflection of the cantilever. This data can then be used to calculate how large the contraction would be if the gel was crosslinked uniformly throughout. In other words, if in fact the DNA is confined near the gel surface, the stresses and strains inferred above could be much smaller than the actual stresses and strains in the surface region.
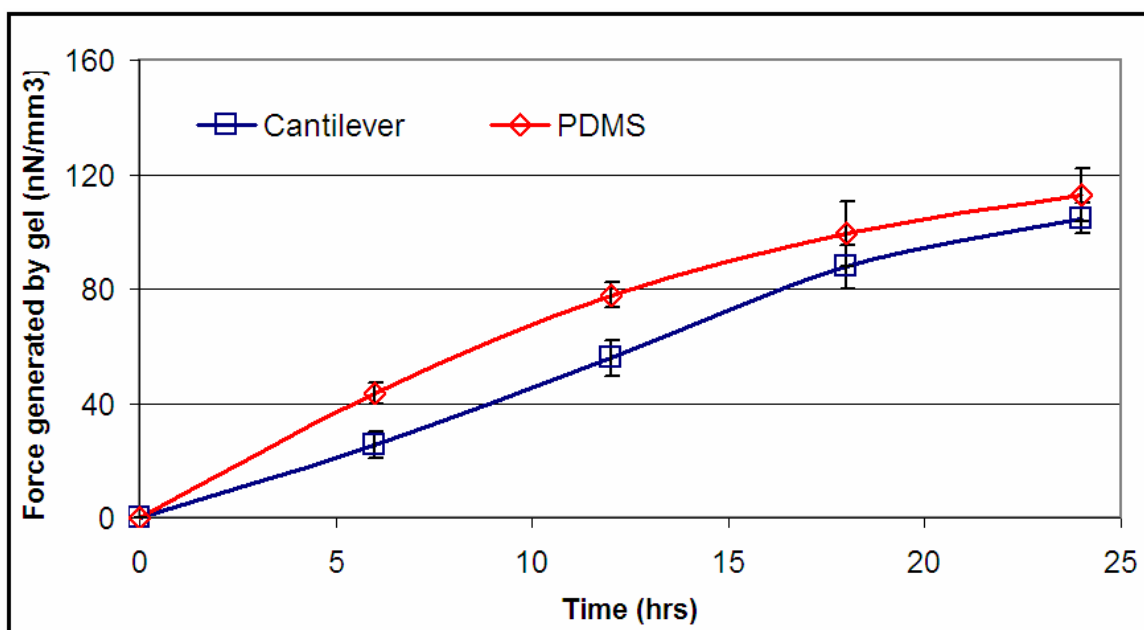
Figure 7-14. Force generated by D-20 gels using cantilever and PDMS stretch method

7.5   Conclusions

Addition of DNA crosslinks generates force and alters the mechanical properties of the DNA hydrogels, which has implications in cell mechanics. Two methods to characterize the force generating potential of DNA-crosslinked polyacrylamide hydrogels have been presented. The force generated by 15x5x3 mm blocks of D-14 and D-20 gels were calculated at room temperature and incubator temperature. It was found that the force generated was proportional to the elastic modulus of the gel. D-20 gels with higher modulus of elasticity produced larger forces as compared to D-14 gels. Also at higher temperatures as the stiffness of the gels decreases, the amount of force generated also reduced. A comparison of the force generated in both the methods showed that either method can be successfully used. The force was found to be in the range of values obtained in literature by previous researchers for axonal growth in spinal cord neurons.

References

1. Altman J, Das GD. Autoradiographic and histological evidence of postnatal hippocampal neurogenesis in rats. The Journal of comparative neurology. 1965;124(3):319-35.
2. Alvarez-Buylla A, Garcia-Verdugo JM. Neurogenesis in adult subventricular zone. Journal of Neuroscience. 2002;22(3):629.
3. Boruch AV, Conners JJ, Pipitone M, et al. Neurotrophic and migratory properties of an olfactory ensheathing cell line. Glia. 2001;33(3):225-9.
4. Bray D. Axonal growth in response to experimentally applied mechanical tension. Developmental biology. 1984;102(2):379.
5. Burden-Gulley SM, Pendergast M, Lemmon V. The role of cell adhesion molecule L1 in axonal extension, growth cone motility, and signal transduction. Cell and tissue research. 1997;290(2):415-22.
6. Cajal SR. Degeneration and regeneration of the nervous system. New York: Hafner; 1928.
7. De Gennes PG, Okumura K, Shahinpoor M, Kim KJ. Mechanoelectric effects in ionic gels. Europhysics Letters. 2000;50(4):513-8.
8. Dertinger SKW, Jiang X, Li Z, Murthy VN, Whitesides GM. Gradients of substrate-bound laminin orient axonal specification of neurons. Proceedings of the National Academy of Sciences. 2002;99(20):12542.
9. Eriksson PS, Perfilieva E, Björk-Eriksson T, et al. Neurogenesis in the adult human hippocampus. Nature medicine. 1998;4(11):1313-7.
10. Fass JN, Odde DJ. Tensile force-dependent neurite elicitation via anti- 1 integrin antibody-coated magnetic beads. Biophysical journal. 2003;85(1):623-36.
11. Feron F, Perry C, Cochrane J, et al. Autologous olfactory ensheathing cell transplantation in human spinal cord injury. Brain. 2005;128(12):2951.
12. Fry EJ. Central nervous system regeneration: Mission impossible? Clinical and Experimental Pharmacology and Physiology. 2001;28(4):253-8.
13. Gage FH. Mammalian neural stem cells. Science. 2000;287(5457):1433.
14. Grimshaw PE, Nussbaum JH, Grodzinsky AJ, Yarmush ML. Kinetics of electrically and chemically induced swelling in polyelectrolyte gels. The Journal of Chemical Physics. 1990;93:4462.
15. Hauben E, Nevo U, Yoles E, et al. Autoimmune T cells as potential neuroprotective therapy for spinal cord injury. The Lancet. 2000;355(9200):286-7.
16. Heidemann SR, Buxbaum RE. Growth cone motility. Current opinion in neurobiology. 1991;1(3):339.
17. Jiang FX, Yurke B, Firestein BL, Langrana NA. Neurite outgrowth on a DNA crosslinked hydrogel with tunable stiffnesses. Annals of Biomedical Engineering. 2008;36(9):1565-79.
18. Kim BG, Hwang DH, Lee SI, Kim EJ, Kim SU. Stem cell-based cell therapy for spinal cord injury. Cell Transplantation. 2007;16(4):355-64.

19.   Kirshblum S, Campagnolo DI, DeLisa JA. Spinal cord medicine: Lippincott Williams & Wilkins; 2001.

20.   Lamoureux P, Ruthel G, Buxbaum RE, Heidemann SR. Mechanical tension can specify axonal fate in hippocampal neurons. Journal of Cell Biology. 2002;159(3):499.

21.   Lin DC, Yurke B, Langrana NA. Inducing reversible stiffness changes in DNA-crosslinked gels. Journal of Materials Research. 2005;20(6):1456-64.

22.   Lin VW, Cardenas DD. Spinal cord medicine: principles and practice: Demos Medical Pub; 2003.

23.   Lindvall O, Kokaia Z. Stem cells for the treatment of neurological disorders. NATURE-LONDON-. 2006;441(7097):1094.

24.   Liu XZ, Xu XM, Hu R, et al. Neuronal and glial apoptosis after traumatic spinal cord injury. Journal of Neuroscience. 1997;17(14):5395.

25.   McDonald JW, Liu XZ, Qu Y, et al. Transplanted embryonic stem cells survive, differentiate and promote recovery in injured rat spinal cord. Nat Med. 1999;5(12):1410-2.

26.   Molloy PJ, Smith MJ, Cowling MJ. The effects of salinity and temperature on the behaviour of polyacrylamide gels. Materials and Design. 2000;21(3):169-74.

27.   Okano H. The application of stem cells in spinal cord injury. New Orleans: Soc Neurosci. 2000.

28.   Osada Y, Ross-Murphy SB. Intelligent gels. Scientific American. 1993;268(5):42-7.

29.   Pointillart V, Petitjean ME, Wiart L, et al. Pharmacological therapy of spinal cord injury during the acute phase. Spinal Cord. 2000;38(2):71-6.

30.   Rafiuddin Ahmed M, Jayakumar R. Peripheral nerve regeneration in RGD peptide incorporated collagen tubes. Brain research. 2003;993(1-2):208-16.

31.   Raisman G. Olfactory ensheathing cells—another miracle cure for spinal cord injury? Nature Reviews Neuroscience. 2001;2(5):369-75.

32.   Rangappa N, Romero A, Nelson KD, Eberhart RC, Smith GM. Laminin-coated poly (L-lactide) filaments induce robust neurite growth while providing directional orientation. Journal of biomedical materials research. 2000;51(4):625-34.

33.   Schultz SS. Adult stem cell application in spinal cord injury. Current Drug Targets. 2005;6(1):63-73.

34.   Smith DH, Wolf JA, Meaney DF. A new strategy to produce sustained growth of central nervous system axons: continuous mechanical tension. Tissue Engineering. 2001;7(2):131-9.

35.   Tanaka T. Gels. Scientific American. 1981;244(1):124.

36.   Thompson DM, Buettner HM. Schwann cell response to micropatterned laminin surfaces. Tissue Engineering. 2001;7(3):247-65.

37.   Tuszynski MH, Weidner N, McCormack M, Miller I, Powell H, Conner J. Grafts of genetically modified Schwann cells to the spinal cord: survival, axon growth, and myelination. Cell Transplantation.7(2):187.

38.   van Praag H, Schinder AF, Christie BR, Toni N, Palmer TD, Gage FH. Functional neurogenesis in the adult hippocampus. Nature. 2002;415(6875):1030-4.

39.	Zheng J, Lamoureux P, Santiago V, Dennerll T, Buxbaum RE, Heidemann SR. Tensile regulation of axonal elongation and initiation. Journal of Neuroscience. 1991;11(4):1117.

CHAPTER 8   Summary and Future Work

8.1   Summary of the dissertation work

The key accomplishments of the dissertation study are presented below:

1) A microscope stage mounted electromagnet system capable of applying either a force or torque on microneedles embedded in hydrogels was developed.

2) A Labview program was developed which controls the magnitude and direction of either the force or the torque applied by the magnet system.

3) A procedure to obtain the force and torque being applied on the microneedles is described which relies on calibration of the particle's magnetic moment by using gels of known elastic modulus.

4) Analytical expressions for the force-displacement and the torque-rotation for non-spherical rods placed in a soft, homogeneous, elastic and isotropic medium were obtained. These expressions were verified using finite element package ANSYS$^{\circledR}$ Workbench™.

5) Young's modulus, Poisson's ratio and shear modulus of bis-crosslinked polyacrylamide gels were evaluated for three different concentration gels using the developed magnet setup. The results were found to be consistent with the values obtained using rheometry and bead experiments.

6) A design space for DNA-crosslinked polyacrylamide gels was created by varying the side-chain lengths, crosslinker lengths, side-chain concentration and crosslinker concentration.

7) Mechanical properties of these DNA gels were characterized using bead experiments and the four magnet setup.

8) Two techniques to measure the contracting force generated by DNA gels are presented and utilized to evaluate the force generating potential of D-14 and D-20 hydrogels.

8.2   Limitations and Future Work

Some of the limitations of the current study and prospective applications to future work are detailed below.

1) One of the limitations of the current study is that the space between the four magnets is limited to a 1x1 cm^2 area. This severely limits the sample size that can be utilized to measure the mechanical properties. The distance between the poles can be increased, but then the force applied on the embedded particles decreases rapidly as the distance from the magnet increases. This can be resolved by using larger coils and applying larger coil currents to generate a stronger magnetic field.

2) In Section 3.4.1, we have shown that the nickel needles were biocompatible and can be utilized in conjunction with cells. Measuring the mechanical properties of the substrates in the presence of cells would allow us to better understand the cell-ECM interactions. Previous researchers have demonstrated that hydrogels tend to swell and change mechanical properties over time. Microneedles can be randomly dispersed in the substrate and cells plated on top of the substrate. Needles in close proximity of the cells can be isolated, and their deflection can be measured using time lapse studies under the application of the magnetic field.

3) Microneedles used in the present study were manufactured at NJNC (New Jersey Nanotechnology Consortium LLC, a wholly owned subsidiary of Alcatel-Lucent). For future studies more readily and commercially available solutions should be pursued. Amblard et al.[1] have utilized a set of five M280 (Dynal, Norway) beads aligned in a row for measuring the local rheological and micromechanical properties of biological systems. Such beads are commercially available and are used in protein extraction systems. However care should be taken to calibrate the magnet system before utilizing the beads. Also since these rows of beads are not perfect cylindrical rods, the equations derived in this study might have to be modified to suit the needs.

4) The displacement of the needles is measured using an image analysis technique. The maximum resolution that can be obtained by this system using a 50X objective lens is around 0.2 microns per pixel. This sets the smallest measurable displacement of the needles that can be achieved with our system. The image resolution could be increased by using an expensive frame grabber card.

5) Currently our group is pursuing the design of a DNA-crosslinked bi-functional construct that exerts traction on adjacent constructs. The force generated by introducing additional DNA crosslinks can be quantified. Figure 8-1 shows a schematic of the design with 3 distinct gels (A, B and C) connected as 5 units in series. Gel A is intended to mimic the mechanics of a healthy spinal cord which is significantly stiffer than single neurites. Gel B serves as the primary substrate for neurite ingrowth. Gel C is the actuating portion of the system. As Gel C contracts, it will induce a traction force on Gel B and this traction will drive the neurites to grow towards each other.
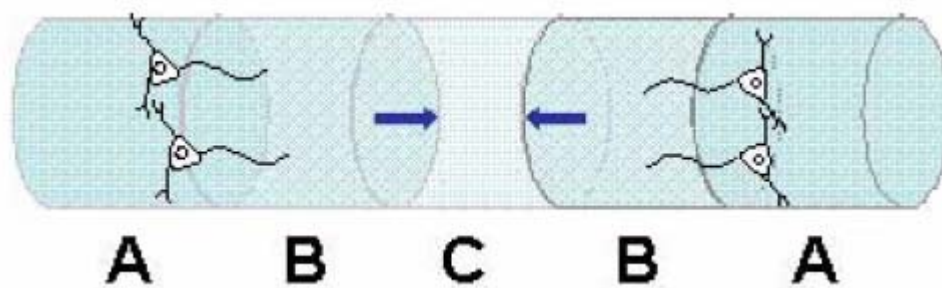
Figure 8-1. Force conditions for bi-functional assays

References

1.	Amblard F, Yurke B, Pargellis A, Leibler S. A magnetic manipulator for studying local rheology and micromechanical properties of biological systems. Review of Scientific Instruments. 1996;67:818.

Curriculum Vita

Uday Chippada

2000   B.S., Mechanical Engineering

Osmania University, Hyderabad, India

2003   M.S., Mechanical Engineering

University of Cincinnati, Cincinnati, OH

2004   Graduate Research Assistant

Bone Mechanics Laboratory

Department of Mechanical and Aerospace Engineering

Rutgers University, New Brunswick, NJ

2006   Graduate Research Assistant

Biomechanics Group

Department of Mechanical and Aerospace Engineering

Rutgers University, New Brunswick, NJ

2010   Ph.D., Mechanical Engineering

Rutgers University, New Brunswick, NJ

Publications

2007   Chippada U, Jordan K, Zhang D. Effect of the Structural Water on the Mechanical Properties of Collagen-like Microfibrils: A Molecular Dynamics Study. Annals of Biomedical Engineering. 2007:35(7)

2008   Li L, Sharma N, Chippada U, et al. Functional modulation of ES-derived hepatocyte lineage cells via substrate compliance alteration. Annals of Biomedical Engineering. 2008;36(5):865-76.

2009   Chippada U, Yurke B, Georges PC, Langrana NA. A Nonintrusive Method of Measuring the Local Mechanical Properties of Soft Hydrogels Using Magnetic Microneedles. Journal of Biomechanical Engineering. 2009;131:021014

2009   Chippada U, Yurke B, Langrana NA. Complete Mechanical Characterization of Soft Media Using Non-Spherical Rods. Journal of Applied Physics. 2009;106(6)

2010   Chippada U, Yurke B, Langrana NA. Simultaneous determination of Young's modulus, shear modulus and Poisson's ratio of soft hydrogels. Journal of Materials Research. *Accepted for publication*.